Proteome and metabolome changes associated with mitochondrial diseases

Inaugural-Dissertation
to obtain the academic degree
Doctor rerum naturalium (Dr. rer. nat.)
submitted to the Department of Biology, Chemistry and Pharmacy
of Freie Universität Berlin

by
Ina Aretz (nee Gielisch)
from Quedlinburg

Berlin, 2016

The present work was carried out from April 2012 until February 2016 at the Max Planck Institute for Molecular Genetics under the supervision of Dr. David Meierhofer.

1st Reviewer: Prof. Dr. Hans Lehrach
2nd Reviewer: Prof. Dr. Christian Freund

Date of Defence: 07.06.2016

Für Zwicki.

Acknowledgements

I would like to thank my PhD advisor Dr. David Meierhofer for giving me the opportunity to work in his lab and on this exciting project. David provided me with guidance and support, but also gave me the freedom to develop and follow own research ideas. I also want to thank Prof. Dr. Hans Lehrach and Prof. Dr. Christian Freund for reviewing this PhD thesis.

Many thanks go to my colleagues in the lab: Beata Lukaszewska-McGreal and Yang Ni, you guys provided such a friendly and helpful working environment that enabled me to finish this PhD work.

Also, this work would never have been possible without the help of my co-authors from the Max Planck Institute and in Frankfurt. Therefore I would like to thank Christopher Hardt and Ilka Wittig.

I also want to thank Jonas and Robin for proofreading this thesis and your useful comments.

Besonders dankbar bin ich meinen Eltern, für die dauerhaft Unterstützung und Ermutigung, ohne die meine schulische und universitäre Ausbildung nicht möglich gewesen wäre.

Finally, I would like to endlessly thank my love and best friend Jonas!

Contents

Abstract

Mitochondrial diseases are a group of metabolic disorders with heterogeneous phenotypes that are frequently characterized by anomalies of oxidative phosphorylation (OXPHOS). To date, hundreds of mutations affecting the nuclear and mitochondrial DNA (mtDNA) have been associated with mitochondrial disease, but with little investigation of the underlying pathogenic mechanisms. This thesis presents a holistic view of regulatory mechanisms in mitochondrial diseases by integrating quantitative metabolome and proteome data derived from a cell line with a complex I deficiency induced by rotenone and a cell line lacking mtDNA (ρ^0 cells). In rotenone treated cells, energy producing pathways such as the respiratory chain, glycolysis, the pentose phosphate pathway (PPP), the galactose metabolism and the tricarboxylic acid (TCA) cycle were down-regulated. A protein-protein interaction (PPI) and pathway analysis revealed that proteins involved in cell division processes were increased, while proteins related to the cytoskeleton were decreased. Furthermore, a deficiency of complex I causes a disruption in the iron-sulfur (Fe-S) cluster assembly, resulting in an impairment of redox reactions. In cells lacking mtDNA, mitochondrial energy pathways were down-regulated as well, but data integration revealed that ρ^0 cells perform anaerobic glycolysis for sufficient energy supply. Furthermore, a remarkable de-ubiquitination was observed, especially of proteins involved in the cytoskeleton, cytosolic ribosomal proteins and solute carrier (SLC) amino acid transporters. Signaling pathways were significantly up-regulated on the proteome level, which was further supported by a dephosphorylation of proteins involved in GTPase signaling and the cytoskeleton organization. Perturbation of the mitochondrial energy metabolism could cause an activation of the mitochondrial retrograde response, as observed by proteome data and phosphorylation patterns of GTPase signaling pathways in ρ^0 cells. In conclusion, the integrated omics approach revealed possible regulatory mechanisms and features of mitochondrial diseases in order to adapt to the changed energy metabolism.

Zusammenfassung

Mitochondriale Erkrankungen sind heterogene metabolische Erkrankungen, welche häufig durch Anomalien der oxidativen Phosphorylierung (OXPHOS) charakterisiert werden. Bisher konnten hunderte Mutationen der nukleären und mitochondrialen DNA (mtDNA) mit ihnen in Verbindung gebracht werden, jedoch ist wenig über zu Grunde liegende pathogene Mechanismen bekannt. Um ein einheitliches Bild regulatorischer Mechanismen in mitochondrialen Erkrankungen zu erhalten, wurden quantitative Daten aus Metabolom- und Proteomexperimenten integriert. Hierfür wurden eine Zelllinie mit einer Rotenon-induzierten Komplex I-Defizienz und eine Zelllinie ohne mtDNA (ρ^0 cells) untersucht. In mit Rotenon behandelten Zellen waren Energie produzierende Stoffwechselwege wie die Atmungskette, die Glykolyse, der Pentosephosphatweg, der Galaktosestoffwechsel und der Citratzyklus runterreguliert. Eine Analyse der Protein-Protein Interaktionen (PPI) und Stoffwechselwege offenbarte niedrigere Zytoskelettproteinkonzentrationen, wohingegen an Zellteilungsprozessen beteiligte Proteine abundanter in Komplex I defizienten Zellen waren. Weiterhin führte eine Komplex I-Defizienz zu einer Synthesestörung der Eisen-Schwefel (Fe-S) Cluster, welche wiederum Redoxreaktionen beeinträchtigen könnte. Zellen ohne mtDNA wiesen ebenfalls einen verminderten Energiestoffwechsel auf. Jedoch zeigte die Datenintegration, dass ρ^0 Zellen anaerobe Glykolyse betreiben um ihren Energiebedarf zu decken. Weiterhin wurde eine auffallende De-Ubiquitinylierung von Zytoskelettproteinen, zytosolischen ribosomalen Proteinen und *solute carrier* (SLC) Aminosäuretransportern beobachtet. Signalwege waren in ρ^0 Zellen signifikant hochreguliert, was durch die Dephosphorylierung von Proteinen, beteiligt an GTPase Signalwegen und der Organisation des Zytoskeletts, unterstützt wurde. Störungen des mitochondrialen Energiestoffwechsels könnten die Aktivierung der mitochondrialen retrograden Antwort begünstigen. Diese Hypothese wird weiterhin durch Proteomdaten und Phosphorylierungsmuster von GTPase Signalwegen in ρ^0 Zellen unterstützt.

Diese Arbeit präsentiert mögliche regulatorische Mechanismen und Eigenschaften mitochondrialer Erkrankungen, um sich an den veränderten Energiestoffwechsel anzupassen.

1 Introduction

1.1 Mitochondria and disease

Mitochondria are a sub-compartment and the power plant of the cell, breaking down nutrients and generating energy. Typically, mitochondria form a budding and fusing network similar to the endoplasmatic reticulum (ER). They play a leading role in many cellular processes, including energy and fatty acid metabolism, pyrimidine biosynthesis, the modulation of ionic homeostasis and cell signaling.

To date, more than 300 pathogenic mutations in the mitochondrial DNA (mtDNA) are known to cause a spectrum of mitochondrial diseases, while the list of nuclear DNA mutations is still growing (Marín-García 2012). Mitochondrial diseases are a clinically heterogeneous group of disorders with multi-systemic involvement (Chinnery 2014; Bannwarth et al. 2013). Epidemiological studies suggest that at least 1 in 5000 individuals is affected by mitochondrial dysfunction and disease (Schaefer et al. 2008; Marín-García 2012). Molecular defects affecting the mitochondrial oxidative phosphorylation (OXPHOS) system are called respiratory chain disorders (Berardo, Musumeci, and Toscano 2011). At present, there is no explicit, detailed pathological mechanism for any mitochondrial disease and no approved or effective therapy has been developed (Hayashi and Cortopassi 2015; Querec et al. 2009; Viscomi, Bottani, and Zeviani 2015). Therapeutic options for mitochondrial diseases remain focused on supportive interventions aimed at relieving complications (Viscomi, Bottani, and Zeviani 2015).

The mitochondrial structure and genetics, the tricarboxylic acid (TCA) cycle, the electron transport chain and the OXPHOS system are described in the following subsections, some of them in regard to mitochondrial diseases.

1.1.1 Mitochondrial structure

Mitochondria consist of two membranes, the outer and the inner membrane. The aqueous compartments between these two membranes and the one that is delimited by the inner membrane are called intermembrane space and matrix, respectively (Krawetz 2008). Both membranes are composed of phospholipid bilayers and proteins. The outer membrane contains porins that act as a pore through which molecules of 5000 or

10,000 Daltons can, driven by concentration gradients, freely diffuse. Larger molecules enter the mitochondrion if an N-terminal signaling sequence (mitochondrial targeting sequence) binds to the multisubunit protein translocase. Translocases are actively transporting those proteins across the outer membrane. Furthermore, the mitochondrial membrane can associate with the ER, in a structure called mitochondria-associated ER-membrane (MAM). The MAM regulates calcium homeostasis, mitochondrial function, autophagy and apoptosis and it is responsible for the import of some lipids into the mitochondrion (Vance 2014). The inner mitochondrial membrane, which has a larger surface area than the outer membrane, contains features referred to as cristae (Mannella 2006). This membrane contains a variety of transport proteins that make it selectively permeable to small molecules that are metabolized or required by mitochondrial enzymes concentrated in the matrix (Alberts et al. 2002).

The major working part of the mitochondrion is the matrix and the inner membrane that surrounds it. The inner mitochondrial membrane contains proteins with various functions: those that carry out the OXPHOS and specific transport proteins. The electron transport chains are embedded in the inner mitochondrial membrane. They are essential for the process of OXPHOS, which generates most of the animal cells ATP. The matrix plays a critical role in energy production, because it's where the TCA cycle and β-oxidation are taking place. Furthermore, it contains mtDNA molecules, ribosomes and enzymes that catalyze the oxidation of pyruvate and other small molecules.

1.1.2 Mitochondrial genetics

Mitochondria possess their own, maternally inherited, DNA (mtDNA) of 16,569 base pairs in size, while each mitochondrion contains two to ten mtDNA molecules (Wiesner, Rüegg, and Morano 1992; Sylvester et al. 2004). The mtDNA encodes for 13 proteins of the electron transport chain as well as for two rRNA and 22 tRNA genes for mitochondrial protein synthesis (Figure 1). The remaining ~80 respiratory chain subunits are nuclear encoded, as are all proteins required for transcription, translation, modification and protein assembly (Calvo and Mootha 2010; Lightowlers, Taylor, and Turnbull 2015).

There are hundreds of mitochondria and thousands of mtDNA molecules within each human cell, while the mutation rate of mtDNA is much higher than for nuclear DNA, because of very few non-coding regions and the ROS rich environment in the inner mitochondrial membrane (Richter 1992; Brown, George, and Wilson 1979). When a mutation arises in an mtDNA molecule, it generates a mixed population, a state that is called heteroplasmy (Tsang and Lemire 2002). When such a cell divides, mtDNA molecules are randomly distributed between daughter cells, resulting in a genetic drift toward either pure mutant or wild type (Douglas C Wallace 2010). The decline of mitochondrial energy functions can be a result of an increased amount of mutated mtDNA within a cell. When the energy production is insufficient for normal cell functions, a threshold is exceeded (~70-90% of total mtDNA (Seo et al. 2010)), symptoms appear, and apoptosis or necrosis may be initiated (Douglas C Wallace 2005).

A broad spectrum of clinical phenotypes has been linked to mutations in mtDNA and nuclear DNA of mitochondrial genes. But the categorization is difficult, because mutations in different mitochondrial genes can give similar phenotypes, mutations in the same gene can give different phenotypes and the same mtDNA mutation at different levels of heteroplasmy can result in very different phenotypes (Douglas C Wallace 2010).

Pathogenic mutations in the mtDNA are associated with involvement of many organs like muscle, heart, liver and CNS (DiMauro 2004; Zeviani and Di Donato 2004). Depending on which cell type or tissue is affected, symptoms may include loss of motor control, muscle weakness and pain, seizures and many more (Chinnery 2014). Mitochondrial defects have been implicated in all the major neurodegenerative diseases, such as Alzheimer’s disease (AD), Parkinson’s disease (PD) and familial amyotrophic lateral sclerosis (ALS) (Gillardon 2006; Atamna and Frey 2007). Examples of diseases that are caused by mtDNA mutations are Leber's hereditary optic neuropathy (LHON) and mitochondrial myopathy, encephalomyopathy, lactic acidosis, stroke-like symptoms (MELAS) (Figure 1).

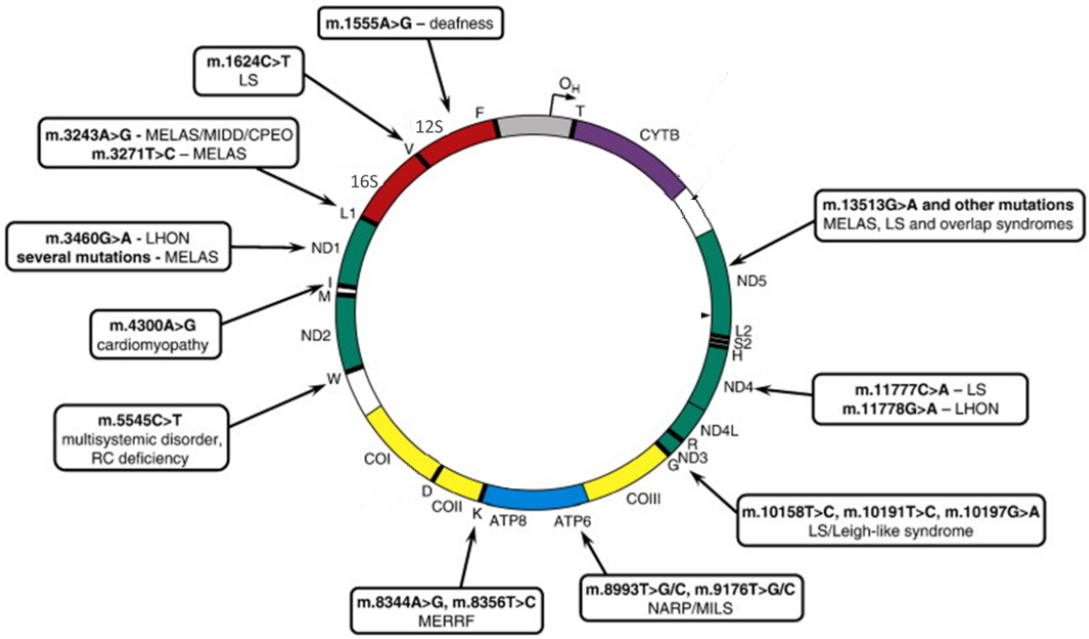

Figure 1: Map of the mtDNA and sites of common mtDNA mutations are highlighted (modified from: Tuppen et al. 2010). MELAS, mitochondrial myopathy, encephalopathy, lactic acidosis, and stroke-like episodes; CPEO, chronic progressive external ophthalmoplegia; LS, Leigh syndrome; LHON, Leber's hereditary optic neuropathy; MERRF, myoclonic epilepsy and ragged red fibers; MILS, maternally inherited Leigh syndrome; NARP, neurogenic weakness, ataxia, and retinitis pigmentosa; PS, Pearson syndrome.

1.1.3 The tricarboxylic acid cycle

The TCA cycle is an important source of precursors, such as amino acids, nucleotide bases, cholesterol, and porphyrin (the organic component of heme) (Berg, Tymoczko, and Stryer 2002b).

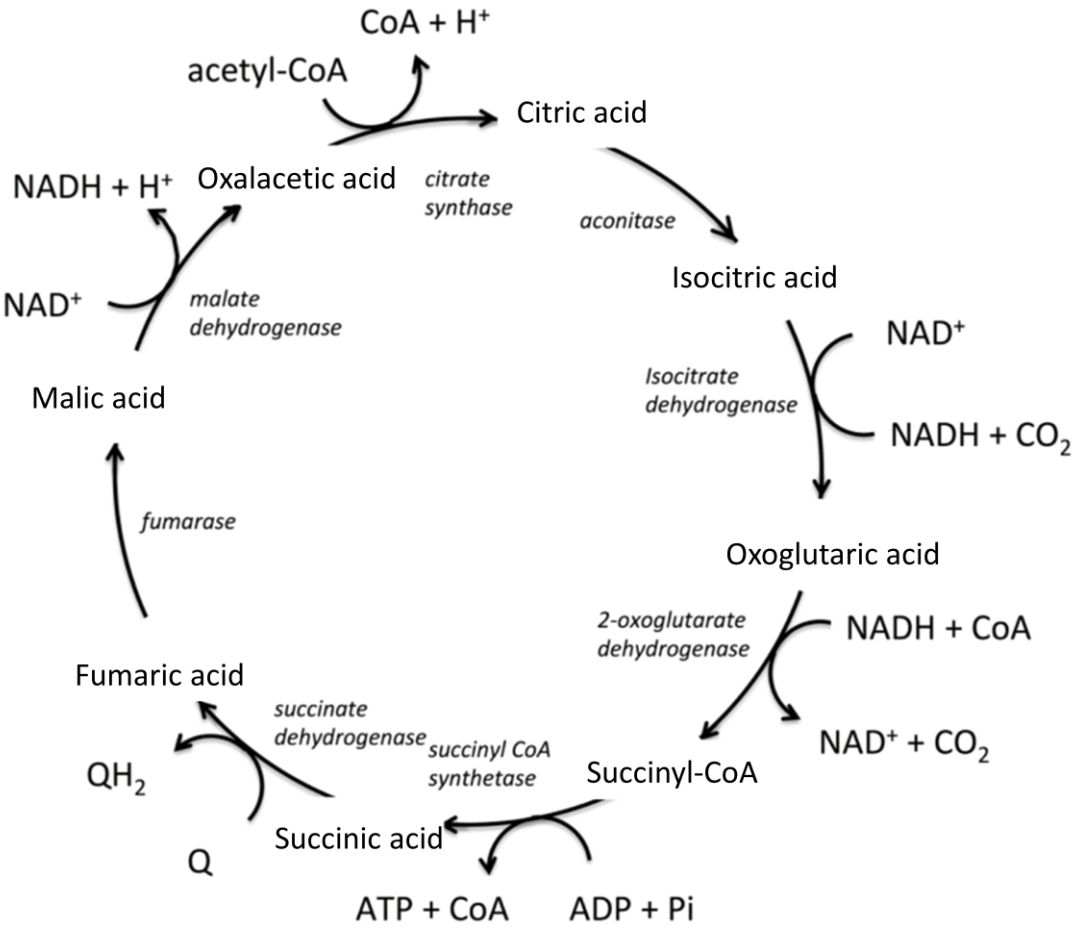

Figure 2: Shown is the TCA cycle, including enzymes, co-factors and metabolites. The enzymes of the TCA cycle catalyzing the reactions are shown in italics, the co-factors are shown to each respective reaction and the TCA cycle intermediates are shown in line with the direction of the cycle. Q and QH_2 are electron acceptor/donator pairs and are entry points to the electron transport chain (modified from: Cannon 2014).

Pyruvate is oxidized to acetyl-CoA and enters the TCA cycle, where it is metabolized to NADH, $FADH_2$ and carbon dioxide (Figure 2). The reducing equivalents NADH and $FADH_2$ are fed into the electron transport chain, where they act as electron donors. Fatty acids are oxidized by β-oxidation to generate acetyl CoA, NADH and $FADH_2$.

The eight reactions of the TCA cycle use oxalacetic acid as a catalyst. The circle starts when a two-carbon acetyl group from acetyl-CoA is transferred to four-carbon oxalacetic acid by citrate synthase to form the six-carbon compound citric acid. In the next step, aconitase in assistance with an iron-sulfur (Fe-S) cluster performs an isomerization reaction to create isocitric acid. Isocitrate dehydrogenase removes one carbon from isocitric acid, forming carbon dioxide, and reduces NAD^+ to NADH. The resulting five-carbon oxoglutaric acid is metabolized by 2-oxoglutarate dehydrogenase complex to succinyl-CoA by releasing another carbon atom as carbon dioxide and electrons are transferred to NADH. The enzyme succinyl-CoA ligase catalyzes the reversible reaction of the four-carbon molecule succinyl-CoA to succinic acid. This reaction is coupled to the formation of GTP or ATP from a phosphate molecule and a nucleoside diphosphate (GDP, ADP). The next step is performed by the membrane bound succinate dehydrogenase that extracts hydrogen atoms from succinic acid and transferring them to the carrier FAD, by generating fumaric acid. In parallel ubiquinone (Q) is reduced to ubiquinol (QH_2). The resulting fumaric acid is further modified by fumarase driven addition of a water molecule, to create malic acid. Malate dehydrogenase is reducing NAD^+ with electrons derived from malic acid and by this recreates oxalacetic acid.

The TCA cycle is of central importance for metabolism, since energy in form of ATP or GTP is generated, precursors of several amino acids and the reducing equivalent NADH are provided.

1.1.4 The electron transport chain and oxidative phosphorylation

The electron transport chain builds a proton gradient across the inner mitochondrial membrane, which is mandatory for OXPHOS, performed by the ATP synthase.

In general, the electron transport chain consists of four complexes: NADH dehydrogenase (complex I), succinate dehydrogenase (complex II), cytochrome c oxidoreductase (complex III) and cytochrome c oxidase (complex IV) (Figure 3). The electron transport chain carries out redox reactions and this energy release is in turn used to transport protons across the inner mitochondrial membrane. Complex II is embedded in the inner mitochondrial membrane and it is the only enzyme that participates in the

TCA cycle and the electron transport chain. Furthermore, it is not a transmembrane protein and therefore not pumping protons. The resulting electrochemical proton gradient, a capacitor that is acidic in the intermembrane space and alkaline in the matrix, is mandatory for the function of the ATP synthase (complex V) (Douglas C Wallace 2010).

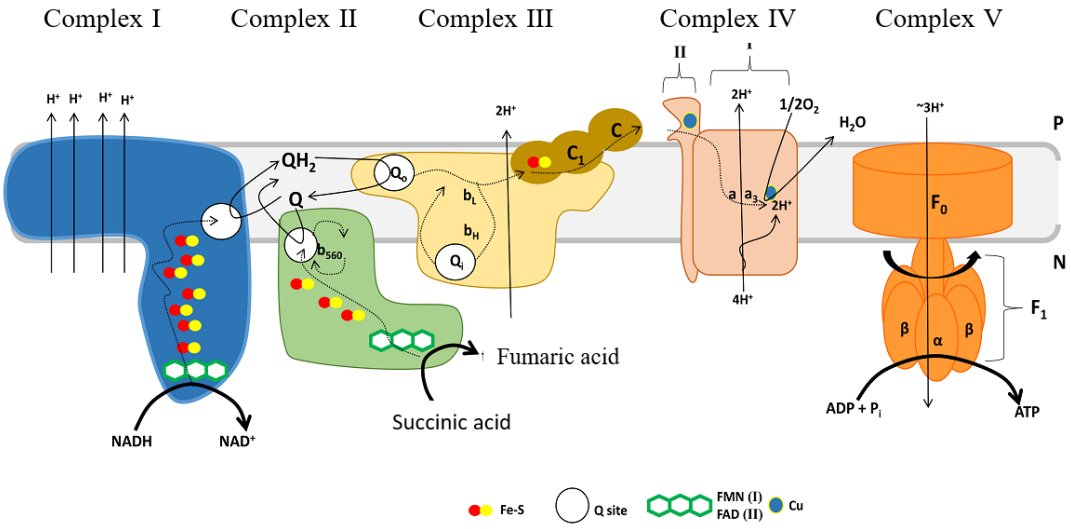

Figure 3: Shown is the respiratory chain and OXPHOS with its five complexes (NADH dehydrogenase (Complex I), succinate dehydrogenase (Complex II), cytochrome c oxidoreductase (Complex III), cytochrome c oxidase (Complex IV) and the ATP synthase (Complex V). P; positive side; IMS and N; negative side; matrix (modified from: Mailloux 2015).

Complex I oxidizes NADH and two electrons are passed to flavin mononucleotide (FMN) and via a chain of Fe-S clusters to Q, which is reduced to QH_2. The energy generated by the series of electron transfer reactions is transduced to pump four protons into the intermembrane space. These four protons contribute ~40% of the electrochemical gradient that drives ATP synthesis (Fassone and Rahman 2012). The respiratory chain disorder LHON is caused by point mutations in the mtDNA, most commonly in the complex I subunits ND1, ND4 and ND6 (Figure 1) and thus reduces the functional capacity of complex I (Huoponen et al. 1991; D C Wallace et al. 1988; Johns, Neufeld, and Park 1992).

Similarly complex II oxidizes succinate to fumaric acid and the two liberated electrons are passed through FAD and three Fe-S clusters reducing Q to QH_2. Subunits of complex II are nuclear encoded and rare mutations can lead to LS, mitochondrial encepha-

lopathy, optic atrophy or they can lead to decreased life-span and an increased production of superoxide ions, depending on which subunit is affected (Wojtovich et al. 2013; Chinnery 2014; Schapira 2012).

QH_2 is oxidized by complex III in the Q_0 (quinone outer membrane) binding site resulting in the transfer of one electron via a Fe-S cluster and cytochrome c1 to cytochrome c. Cytochrome c1 and c can only accept one electron at a time. The second electron is passed through the bL and bH heme groups and utilized to re-reduce Q in Q_i (quinone inner membrane) binding site. The electron transmission from QH_2 is coupled to the transfer of two protons into the intermembrane space. Defects of complex III are rare either alone or in combination, but mutations of the mtDNA gene encoding cytochrome b or the nuclear chaperone BCS1 account for most described to date (Schapira 2012). Mutations in complex III subunits can result in hypokalemia, lactic acidosis, myopathy, encephalopathy and liver disease (Chinnery 2014; Schapira 2012).

Subsequent, cytochrome c binds to subunit II of complex IV where electrons are passed systematically through two heme groups and two copper moieties. This results in the reduction of oxygen to water at subunit I. Simultaneously, two additional protons are pumped into the intermembrane space. The resulting transmembrane potential (proton motive force, pmf) is mandatory for the function of complex V. Defects of complex IV are common and can be caused by mutations of the COX mtDNA genes, cytochrome oxidase assembly, nuclear genes of cytochrome oxidase subunits or maintenance proteins (Schapira 2012). The clinical presentation can vary from LS, encephalopathy to liver failure (Schapira 2012).

Complex V uses the potential difference to generate ATP from ADP and a phosphate group, a process which is called chemiosmosis. Matrix ATP is exchanged for cytosolic ADP by the inner membrane adenine nucleotide translocators (ANTs) (Douglas C Wallace 2010). Mutations of complex V genes in the mitochondrial or nuclear genome are known (Figure 1), with clinical effects, like encephalopathy, of varying severity (Schapira 2012).

An impaired OXPHOS that leads to a decrease in ATP production is the most important cause underlying respiratory chain disorders (Khan et al. 2015).

1.2 Approaches to mimic mitochondrial diseases

Very little is known about the molecular mechanisms leading to human diseases as a result of damages in mtDNA (Kukat et al. 2008). To study those processes it is necessary to develop models to examine regulatory and developmental mitochondrial processes under experimental conditions.

In order to mimic a defect of the OXPHOS system, drugs and toxins are available that can be used to specifically inhibit complexes. The pesticide rotenone for example specifically inhibits the NADH dehydrogenase by binding to the ubiquinone-binding site and thus preventing electron transfer from FMN to ubiquinone (Lambert and Brand 2004; Orr et al. 2013). The enzyme complex succinate dehydrogenase possesses two binding sites, one for succinate and one for ubiquinone and thus two possible sites of action for inhibitors are present. Succinate analogs such as malonate, malic acid and oxalacetic acid or ubiquinone analogs such as thenoyltrifluoroacetone and carboxin cause the inhibition of complex II (Dervartanian and Veeger 1964; Muller et al. 2008). The electron flow in the cytochrome c oxidoreductase can either be inhibited at site Q_i or Q_0 (Section 1.1.4) by antimycin A or myxothiazol and stigmatellin (Lambert and Brand 2004; Orr et al. 2015; Ouchane, Agalidis, and Astier 2002). The four gases, nitric oxide, carbon monoxide, hydrogen sulfide and hydrogen cyanide are known to competitively inhibit oxygen consumption by mitochondrial cytochrome oxidase (Cooper and Brown 2008). For the ATP synthase several inhibitors have been described in the literature, including efrapeptin, oligomycin, aurovertin B and azide (Linnett and Beechey 1979; Zheng and Ramirez 2000).

Cell lines lacking mtDNA (ρ^0 cells) are a very effective tool to study the consequences of the impaired OXPHOS system (Hashiguchi and Zhang-Akiyama 2009). The first mtDNA depleted cell line was derived from the human osteosarcoma cell line 143B.TK$^-$ (thymidine kinase deficient) by chronic exposure to ethidium bromide (King and Attardi 1996). Since then, ρ^0 cells have been established from different species and tissues applying methods like mitochondria targeting restriction enzymes or the application of ditercalinium (Inoue et al. 1997; Schubert et al. 2015; King and Attardi 1996).

1.3 Posttranslational modifications

Posttranslational modifications (PTMs) increase the functional diversity of proteins and ensure efficient signal transduction, rapid adaption to environmental changes or respond to changes in internal state (Hennrich and Gavin 2015; Doll and Burlingame 2015). To date more than 200 different PTMs have been reported that modulate protein functions, with phosphorylation, ubiquitination and acetylation as the most studied ones (Humphrey, James, and Mann 2015). The importance of these modifications is evident from the number of diseases that arise from their deregulation (Hennrich and Gavin 2015).

Phosphorylation is the most pervasive and best-studied PTM, while it is intimately involved in almost every cellular process (Humphrey, James, and Mann 2015). Phosphorylation is the reversible addition of phosphate to serine, threonine or tyrosine residues, catalyzed by kinases and phosphatases (Humphrey, James, and Mann 2015; Komander 2009). In this way, phosphorylation is a rapid molecular switch, with a timescale of milliseconds to seconds, capable of altering the behavior of its targets either directly or indirectly by PTM crosstalk (Humphrey, James, and Mann 2015).

Protein ubiquitination is a PTM in which lysine residues are modified with the 76 amino acid polypeptide ubiquitin. The ubiquitin system is more complex compared to phosphorylation, because ubiquitin is able to form polymers of at least eight different linkages (Komander 2009). The linkage type determines whether a protein is degraded by the proteasome or serves to attract proteins to initiate signaling cascades or be internalized (Komander 2009).

Lysine acetylation is a reversible PTM involved in multiple cellular processes, which occurs on cytoplasmic and mitochondrial proteins and has a role in signaling, metabolism and immunity (Svinkina et al. 2015). In addition to the few actively studied acetylation sites, several studies report acetylation sites on proteins that are involved in diverse biological processes, suggesting that this PTM has broad regulatory functions (Choudhary et al. 2009).

1.4 Mass spectrometry

Mass spectrometry (MS) is an analytical technique to identify the type and amount of compounds in a sample by measuring the mass/charge ratio (m/z) and the abundance of ions. The m/z is a dimensionless notation formed by dividing the mass number of an ion by its charge number. The ratio eases data interpretation since it is numerically more related to the unit dalton (Da) (A. D. McNaught and Wilkinson 1997). Using MS the mass of peptides or small molecules can be determined, as well as structure, amino acid sequences and PTMs. A typical workflow in MS includes sample acquisition and preparation, analysis, data evaluation and result reporting steps. In general, mass spectrometers consist of several components, an inlet system for introducing the sample, an ionization source for creating ions, a mass analyzer for separating ions based upon on their m/z and an ion detector.

The inlet system can be a port through which the sample is injected directly, as well as chromatographic systems (liquid or gas chromatography; LC or GC) and capillary electrophoretic units in order to allow separation and identification of compound mixtures. Liquid chromatography-MS/MS (LC-MS/MS) is commonly used in many clinical specialties such as endocrinology, immunosuppressant and therapeutic drug monitoring, small molecule and peptide and protein marker analysis (Y. V. Zhang and Rockwood 2015). The success of the LC-MS/MS technique arises from its ability to give 3D-data (Kruve et al. 2015). First, the analytes are separated in time by LC, followed by ion generation in the ion source and fragmentation of precursor ions and followed by a separation step in the mass analyzer according their m/z. Finally, the detector determines the abundance of each ion.

To connect LC and MS continuously, ionization has to be applied to a liquid phase. For this purpose, atmospheric pressure ionization (API) sources form gas-phase ions directly from a liquid flow. The most common API applications are electron spray (ESI), atmospheric pressure chemical (APCI) and atmospheric pressure photo (APPI) ionization which can yield positively or negatively charged ions. Furthermore, ions in API sources are formed with little excess energy and therefore undergo little or no fragmentation (Kruve et al. 2015).

After ions are generated in the ion source, they are transferred to mass analyzers like quadrupole, ion trap and time-of-flight (TOF) devices. A quadrupole consist of four cylindrical rods that are set parallel to each other. Controlled by oscillating electric fields (direct current and radio frequency; DC and RF) that are applied to the rods, ions are filtered based on their m/z. By applying this mass filter, all ions that have a stable trajectory will reach the detector.

Ion trap mass analyzers have electrodes like a single quadrupole, but arranged into a circle. The only stable point in this field is in the middle, where the potential never moves up or down as the electric field oscillates. Ion trap mass analyzers store and manipulate ions by DC and RF electric field in a series of carefully timed events. An orbitrap is a modified ion trap, consisting of a barrel-like outer electrode and spindle-like central electrode that traps ions in an orbital motion around the central electrode (Perry, Cooks, and Noll 2008). TOF mass analyzers determine the m/z of ions via a time measurement. Ions are accelerated by an electric field of known strength, which means all ions with the same charge have the same kinetic energy (Wolff and Stephens 1953). But their velocity depends on the m/z, the time that is takes for the ions to reach the detector. The function of a TOF mass analyzer consists of measuring the mass-dependent time that it takes ions of different masses to move from the ion source to the detector.

For sequence or structure analysis of compounds it is necessary to fragment precursor ions, a process called tandem MS. Tandem MS (MS/MS or MS^n) involves multiple steps of MS selection, with some form of fragmentation occurring between the stages. This fragmentation of precursor ions is necessary to identify peptides based on their amino acid sequence and small molecules based on specific fragment ions. The structural analysis of small molecules is more complex, since they consist of a very large set of diverse scaffolds. The most common fragmentation method in MS is collision-induced dissociation (CID) (Eng et al. 2011). CID involves the collision of an ion with an inert gas molecule, followed by a dissociation of the ion (Wells and McLuckey 2005). Higher-energy collisional dissociation (HCD) is a CID technique specific to the orbitrap mass analyzer. The dissociation takes place in the HCD cell by increased radiofrequency voltage and then ions are transferred back through the C-trap for analysis

at high resolution in the orbitrap (Olsen et al. 2007; Jedrychowski et al. 2011). An advantage of HCD is that the low mass region is well represented in the MS^2 spectra when compared with CID (Jedrychowski et al. 2011). Electron capture dissociation (ECD) is a method where an electron is added to a positively charged ion, resulting in its fragmentation (Zubarev, Kelleher, and McLafferty 1998). Another similar approach is called electron transfer dissociation (ETD). Here, free radical anions and not electrons are used to fragment ions randomly along the peptide backbone, while side chains and modifications are left intact (Syka et al. 2004). In the case of ECD and ETD the released energy, when an electron is captured or transferred to a multiply charged ion, can induce fragmentation. Due to this "soft" fragmentation, both methods are effective approaches to study PTMs.

1.5 Mass spectrometry based proteomics

In proteomic studies the abundance of proteins, from tissue or primary cells, cell culture or purified organelles, is determined. Proteomics is used to identify components of small protein complexes and large organelles, to determine PTMs and to reveal how protein levels change (Steen and Mann 2004; Walther and Mann 2010). Several techniques exist to quantify protein concentrations by quantitative proteomics.

It is known that RNA levels do not correlate with the protein content, because mRNA is not always translated into protein. Proteomics validates the presence of the protein and provides a direct measure of the present quantity. Two quantification approaches can be performed: relative and absolute quantification and among those label-based and label-free methods are available.

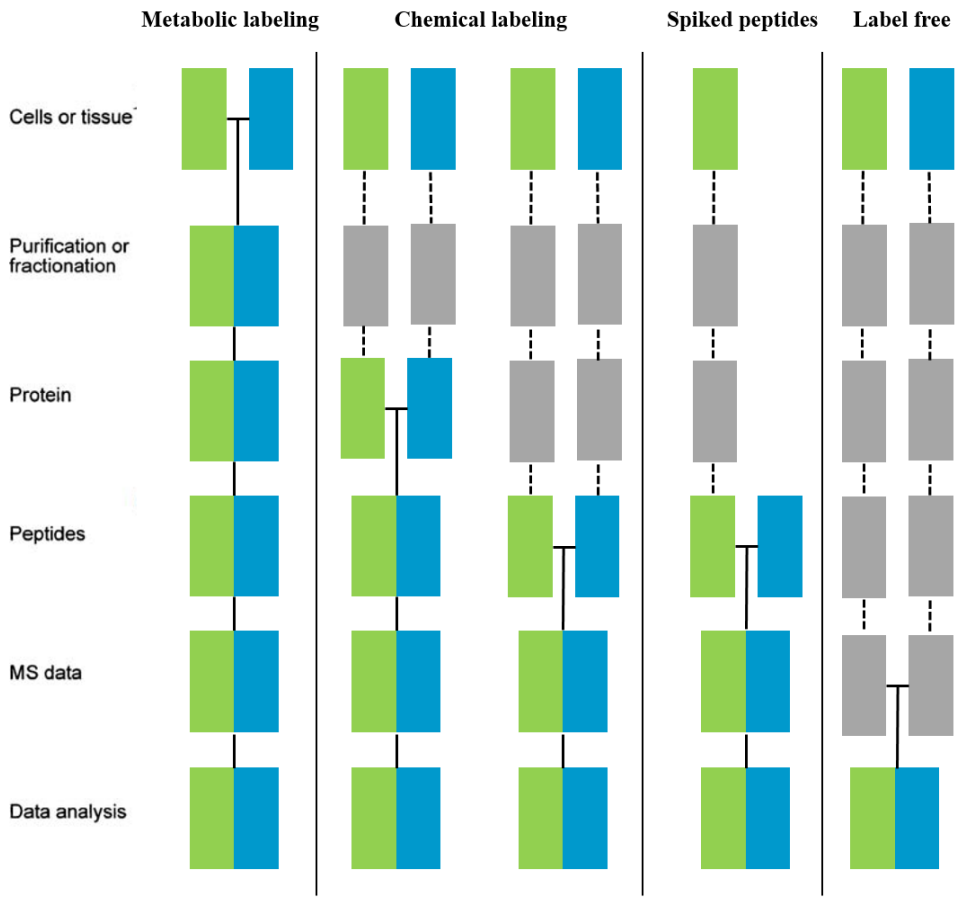

Figure 4: Common quantitative mass spectrometry workflows (modified from: Bantscheff et al. 2007). Boxes in green and blue represent two experimental conditions, horizontal lines indicate when samples are combined and dashed lines show points where experimental variation and quantification errors could occur.

By performing relative quantification, a ratio or relative change of a protein between samples is determined. Examples for label-based relative quantification are SILAC (stable isotope labeling by amino acids in cell culture), ^{15}N-labeling, ICAT (isotope-coded affinity tag), iTRAQ (isobaric tags for relative and absolute quantification) and dimethyl-labeling (Bantscheff et al. 2007). SILAC is a metabolic labeling approach, in which essential amino acids labelled with stable isotopes are added to amino acid deficient cell culture media and are incorporated into all proteins as they are synthesized (Ong 2002; Walther and Mann 2010). Amino acids used for SILAC experiments usually contain carbon-13 (^{13}C) and/or nitrogen-15 (^{15}N), while physicochemical properties of labeled and natural peptides are not changing. The main advantage of SILAC is that differentially labeled samples can be combined at the level of cells or directly after lysis (Walther and Mann 2010), which reduces the risk of introducing biases while

subsequent sample preparation. ICAT, iTRAQ and dimethyl-labeling are chemical labeling reagents, which tag reactive side chains or protein/peptide termini. ICAT probes consist of three elements: a biotin affinity tag, a mass encoded linker and a thiol specific group, which reacts with cysteine (Gygi et al. 1999). ICAT-labeled peptides are isolated utilizing the biotin tag, since reducing the sample complexity is, depending on the scientific issue, advantageous. Using iTRAQ, up to eight tags that react with primary amine groups of peptides can be utilized (Ross et al. 2004). When performing dimethyl labeling all primary amines are converted to dimethylamines (Boersema et al. 2009), but small isotope effects in LC separation can occur. Label-free relative quantification (LFQ), does not use a stable isotope containing compound to label the protein, instead precursor ion intensities are compared or derived spectra are counted. For ion intensity based approaches, peptide signals on the MS^1 level are extracted and compared. The spectral counting method counts the number of identified spectra for a specific peptide and integrates the results for all measured peptides of a protein. The limiting step for both applications is the reproducibility, since the approaches are not suitable for multi-stage sample preparation protocols and the HPLC-MS setup needs to be robust. But the MaxLFQ algorithm implemented in the publicly available software MaxQuant is fully compatible with any protein or peptide separation prior to LC-MS (J. Cox et al. 2014; Jürgen Cox and Mann 2008). Additionally, there is no limit on the number of samples that can be compared (J. Cox et al. 2014).

By performing absolute quantification, a copy number or concentration of a protein within a sample is determined. In the simplest case, absolute quantification can be achieved by the addition of a known quantity of a stable isotope-labeled standard peptide to a protein digest and subsequent comparison of the mass spectrometric signal to the endogenous peptide in the sample (Bantscheff et al. 2007). Several label-free approaches for absolute quantification exist, which make use of the correlation between the amount of protein and number of derived tandem mass spectra (Bantscheff et al. 2007). A protein abundance index (PAI) can be computed, by dividing the number of observed peptides by the number of all possible tryptic peptides from a particular protein that are within the mass range of the employed mass spectrometer (Bantscheff et

al. 2007; Rappsilber et al. 2002). To sum up, proteomics allows an unbiased identification, characterization and quantification of proteins under changing conditions.

1.6 Mass spectrometry based metabolomics

Metabolites are small molecules that participate in metabolic reactions, are required for maintenance, growth and normal function of a cell (Harrigan and Goodacre 2003). Metabolites range from 50 Da to 1500 Da, while their concentrations span several orders of magnitude. The metabolome is highly dynamic, time-dependent and metabolites are sensitive to many environmental conditions. In metabolomic studies the abundance of metabolites, from tissue, primary cells, cell culture or bio fluids, is determined (Forcisi et al. 2013). Unlike DNA, RNA or proteins, metabolites are chemically very diverse (polarity, charge, solubility, stability, volatility and reactivity), thus no single method can capture and analyze the entire metabolome at once yet. The contextual and chemical diversity makes the detection of a whole set of metabolites present in a biological sample an ambitious goal (Veuthey et al. 2013; Wang et al. 2015). Metabolomics offers a framework for analyzing individuals with a specific phenotype at a molecular level that is needed in cell biology, personalized medicine and systems biology (Kuehnbaum and Britz-McKibbin 2013; Johnson and Gonzalez 2012; Patti, Yanes, and Siuzdak 2012). Metabolic profiling studies are mostly performed using chromatography coupled to mass spectrometers, usually gas chromatography (GC)-MS and liquid chromatography (LC)-MS, as well as nuclear magnetic resonance (NMR) spectroscopy (Contrepois, Jiang, and Snyder 2015).

1.6.1 Metabolomic approaches

Nowadays, the combination of chromatography and MS devices has proven to be most suitable for metabolite quantification (Noack and Wiechert 2014). The metabolomics field has a key role in screening small molecules, where two different approaches are distinguished: untargeted and targeted. An untargeted metabolomics approach is data-driven and applied to analyze the widest possible range of compounds in a sample without *a priori* knowledge of the metabolites (Naz et al. 2014; Veuthey et al. 2013). To ease data interpretation, those complex analyses require data-processing tools. Those tools were designed to automatically extract relevant data from batches of crude

chromatographic data, which allow the rapid processing of thousands of data points (Commisso et al. 2013). Data-processing tools, like MetAlign and XCMS, have to deal with challenges, like background subtraction, signal recognition, signal quantification and signal alignment (Lommen 2009; C. A. Smith et al. 2006; Commisso et al. 2013). The output of a batch of LC-MS chromatograms is a table listing the amount of each signal in all samples (Commisso et al. 2013).

The targeted approach is applied when the study aims to detect and quantify a specific class of compounds in a known metabolic pathway, like the TCA, or with a specific biological activity (Naz et al. 2014; Veuthey et al. 2013). This requires the ability to differentiate the targeted analytes from other interfering compounds, which may be achieved based on a chemical shift in a m/z on a mass spectrometer or retention time in chromatography, or a combination thereof (Lu, Bennett, and Rabinowitz 2008). When performing targeted metabolomics the identities of metabolites are initially established based on available libraries or by using standard compounds**.** Electronic libraries of metabolomic analyses by GC-MS or LC-MS, such as METLIN, Human Metabolome Database (HMDB) or ChemSpider, list characteristic ions and retention times of hundreds of compounds (G.-F. Zhang et al. 2011; C. A. Smith et al. 2005; Wishart et al. 2013; Pence and Williams 2010). Molecules that have under gone thorough characterization may be detected with enhanced specificity and sensitivity using ion monitoring techniques, like selective ion monitoring (Kitteringham et al. 2009). During these processes, the analysis is focused only on one molecule with a specific mass, while all others are excluded (Kitteringham et al. 2009). The specificity is mostly enhanced by monitoring the parent and one or more specific fragment ions (Kitteringham et al. 2009). This process is known as multiple reaction monitoring (MRM), it is not the only approach for targeted quantification, but it is the most sensitive (Figure 5) (Kitteringham et al. 2009; Anderson and Hunter 2006). Due to the development of the triple quadrupole (QQQ) technology, MRM has become the method of choice for the analysis of low molecular weight chemicals (Kitteringham et al. 2009). Performing MRM, two stages of mass filtering are employed on a QQQ. In the first stage, the targeted precursor ion is preselected in Q1 and induced to fragment by CID

in a collision cell (Q2). In the second stage, instead of obtaining full scan MS/MS spectra of all possible fragment ions derived from the precursor, only a small number of m/z based, predefined fragment ions (transition ions) are analyzed in Q3 (Figure 5).

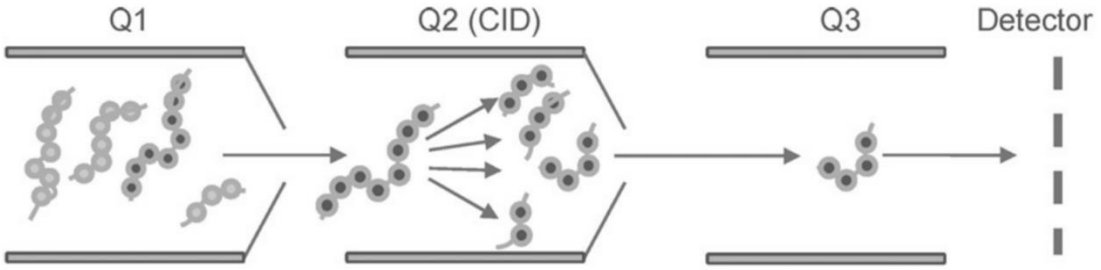

Figure 5: Schematic of multiple reaction monitoring (MRM) scanning technique on a triple quadrupole (QQQ) mass spectrometer. The targeted precursor ion is selected in the first quadrupole (Q1) and enters the second quadrupole (Q2) where it undergoes collision-induced dissociation (CID). One or more fragment ions are selected according to the predefined transitions and the ensuing signal provides the spectral counts for quantification (modified from: Kitteringham et al. 2009).

1.6.1.1 Quantitative metabolomics

Dependent on the scientific question, metabolites can be quantified relatively or absolutely. The major barrier in metabolite quantification is that the signal intensity of a metabolite not only depends on its concentration, but also on its chemical structure and the matrix. Ion enhancement or suppression can be caused by matrix-dependent effect and will result in inaccurate quantification (Lei, Huhman, and Sumner 2011).

Relative quantification is applied by normalizing the metabolite signal intensity (or the peak area) to an internal standard (IS) or a known metabolite considering to have a constant concentration (Lei, Huhman, and Sumner 2011; Rojo, Barbas, and Rupérez 2012). On the other hand, absolute quantification, mostly used in targeted metabolomics, uses external standards or internal isotopically labeled standards to determine the metabolite quantity (Lei, Huhman, and Sumner 2011).

In order to overcome the matrix-dependent effects of MS based metabolomics, heavy atom-labeled isotopologues of metabolites can be used as IS (Chokkathukalam et al. 2014). But this approach is limited to the availability and cost of ^{13}C-labeled standards (Chokkathukalam et al. 2014). Instead, a fully labeled metabolite extract can be generated. In this experimental design, the cells are grown in the presence of a fully labeled stable isotope carbon source (Chokkathukalam et al. 2014). An alternative approach to

absolute quantification for LC–MS based metabolomics is post-extraction derivatization with differentially labeled derivatizing agents (Chokkathukalam et al. 2014).

For a comprehensive and functional characterization of metabolic networks the quantitative knowledge of intracellular fluxes is required. Intracellular fluxes cannot be detected directly, but they can be estimated through interpretation of stable isotope patterns in metabolites and computational modeling (Cascante and Marin 2008; Mendes, Camacho, and de la Fuente 2005).

1.7 Omics technologies as a key to understand systems biology

Systems biology is a novel subject in the field of life science, which aims to understand biological organization as a whole under a variety of conditions (Lee 2015). The availability of huge amounts of quantitative data and the development of computational methodologies are the main reasons for the emergence of systems biology (Lee 2015). An important step in the workflow is that each data type has to be evaluated before the integration to avoid downstream problems with the analysis (Ritchie et al. 2015). The complete biological model can only be discovered if different levels of genomics, proteomics (including PTMs) and metabolomics are considered in an analysis (Ritchie et al. 2015).

Technological advances in whole-genome sequencing, extensive transcriptomics, proteomics and metabolomics, have expanded the breadth of available “omics” data. Computational studies such as bioinformatics, data mining and machine learning have enabled the community to understand and predict interactions and patterns of biological systems (Barabási, Gulbahce, and Loscalzo 2011). Multi-omics data are combined as predictor variables in order to identify effective models that predict phenotypic traits and outcomes, elucidate biomarkers and generate insights into the genetic underpinnings of the heritability of complex traits (Ritchie et al. 2015). In contrast to the genome, the proteome and metabolome are dynamic and much more closer to disease phenotypes (Barallobre-Barreiro, Chung, and Mayr 2013).

Conventional approaches dealt with intracellular signaling cascades as linear models, but today we know that different pathways cross-talk with each other and are organized as networks, including proteins as well as metabolites (Barallobre-Barreiro, Chung, and

Mayr 2013). Network development and graph based analysis are useful to understand the interrelations between different diseases and identification of disease candidates, but it is difficult to understand the dynamic nature of these networks (Kann 2007). Networks are static representations of biological systems and are unable to reveal system states changed by mutations or environmental effects (Ma'ayan 2011). The combination of proteomics and metabolomics, along with new methods for data analysis (e. g. pathway and network analysis), provides a complimentary read-out to improve confidence in data interpretation.

Modeling of disease states is essential for computational analysis of the disease process which involves translating the biological data into quantifiable terms (Cho et al. 2006). Furthermore it permits a more holistic view of biological systems and their alterations in disease (Barallobre-Barreiro, Chung, and Mayr 2013).

1.8 Aim of the thesis

This thesis aims to discover regulatory mechanisms in mitochondrial diseases by integrating quantitative metabolome and proteome data. The pesticide rotenone was used to specifically inhibit NADH dehydrogenase (complex I) of the respiratory chain to mimic a complex I deficiency. A label-free quantification method was applied for proteome profiling by LC-MS/MS. Metabolome and proteome profiles of rotenone treated versus control cells were integrated in order to investigate the interplay of proteins and metabolites under a well-defined condition. Furthermore, a cell line lacking mitochondrial DNA (ρ^0 cells) was analyzed in order to study the consequences of a complete deficiency of the respiratory chain. For quantitative proteome profiling, a shotgun LC-MS/MS approach including SILAC labeling was performed. Metabolome and proteome profiles of the parental cell line 143B.TK$^-$ versus ρ^0 were integrated, including PTM analyses of phosphorylation and ubiquitination. For both studies a targeted metabolome profiling based on multiple reaction monitoring (MRM) was applied.

This thesis will lead to a better understanding of regulatory mechanisms and features in mitochondrial diseases.

2 Material and Methods

2.1 List of buffers

10 x Phosphate-buffered saline (PBS)

- 1.37 M sodium chloride
- 27 mM potassium chloride
- 100 mM disodium hydrogen phosphate
- 18 mM potassium dihydrogen phosphate

1x Immunoaffinity purification (IAP) buffer

- 50 mM 4-morpholino propanesulfonic acid/sodium hydroxide, pH 7.2
- 10 mM sodium hydrogen phosphate
- 50 mM sodium chloride

Acetyl coenzyme A (acetyl-CoA) stock

- 15 mM acetyl-CoA

Britton-Robinson universal buffer for strong anion exchange (SAX)-based fractionation of peptides

- solution containing 20 mM acetic acid, 20 mM phosphoric acid and 20 mM boric acid
- pH adjusted with 1 M sodium hydroxide (pH 3, 4, 5, 6, 8 and 11)
- final concentration of sodium chloride 0.25 M, pH 3

Buffers for strong cation exchange (SCX) chromatography (indicated in brackets are the corresponding pump inlets)

- (A1) 2.5 L: 7 mM potassium dihydrogen phosphate, pH 2.65, 30% acetonitrile
- (B1) 2 L: 7 mM potassium dihydrogen phosphate, 350 mM potassium chloride, pH 2.65, 30% acetonitrile
- (A2) 250 mL: 50 mM potassium hydrogen phosphate, 500 mM sodium chloride, pH 7.5
- (B2) water

Cell lysis buffer

- 4% sodium dodecylsulfate
- 0.1 M dithiothreitol
- 0.1 M TRIS, pH 8

Citrate synthase (CS) stock

- 1 M TRIS, pH 8.1
- 10% Triton X-100
- 10% bovine serum albumin (BSA)
- 20 mM dithionitrobenzoic acid (DTNB) (in ethanol)

Digestion buffer

- 8 M urea
- 10 mM TRIS, pH 8

Elution buffer for phosphorylated peptides

- 100 mM triethylammonium bicarbonate, pH 8.5
- 5% ammonium hydroxide, pH 11.5
- 15% ammonium hydroxide, pH 11.5

Isocitrate dehydrogenase (IDH) stock

- 1 M HEPES, pH 7.6
- 200 mM manganese(II) chloride
- 0.1 mM nicotinamide adenine dinucleotide phosphate (NADP)

Isocitric acid stock

- 4 mM isocitric acid

NADH dehydrogenase (complex I) stock

- 1 M sodium phosphate buffer, pH 8.1
- 10% BSA
- 1 M potassium cyanide
- 50 mM decylubiquinone (in ethanol)

NADH stock

- 20 mM reduced nicotinamide adenine dinucleotide (NADH)

Oxalacetic acid stock

- 50 mM oxalacetic acid

Rotenone stock

- 0.5 mg/mL rotenone (in ethanol)

SEKT-buffer

- 250 mM sucrose
- 2 mM ethylene glycol tetraacetic acid (EGTA)
- 40 mM potassium chloride
- 20 mM TRIS, pH 7.4

TBE-buffer

- 89 mM TRIS
- 89 mM boric acid
- 2 mM ethylenediaminetetraacetic acid (EDTA), pH 8

2.2 Cell culture

2.2.1 Rotenone treated HeLa cells

HeLa (human cervical cancer) cells were cultivated in DMEM medium (Invitrogen Corp., Carlsbad, CA) containing 4.5 g/L glucose, supplemented with 10% FBS and 1% Penicillin-Streptomycin-Neomycin antibiotic mixture (Invitrogen Corp., Carlsbad, CA) at 37°C in a humidified atmosphere of 5% carbon dioxide. The cells were grown in 300 cm^2 polystyrene flasks to approximately 90% confluency. 50 mL of fresh medium was supplemented with 1 µM rotenone or DMSO as control and after 38 h of incubation, cells were sampled for proteome and metabolome analysis. The experiments were performed in biological triplicates for rotenone-treated and controls, respectively.

2.2.2 143B.TK$^-$ and ρ^0 cells

The osteosarcoma cell line 143B.TK$^-$ (ATCC-CRL-8303) was obtained from LGC Standards. According to the protocol from (King and Attardi 1996), ρ^0 cells were generated from the parental cell line 143B.TK$^-$ (Wittig et al. 2010). The wild-type cell line 143B.TK$^-$ and the according ρ^0 cells were cultivated in SILAC DMEM (Silantes, Munich, Germany, without L-lysine and L-arginine) containing 4.5 g/L glucose, 1 mM pyruvate, supplemented with 5% dialyzed FBS (Silantes, Munich, Germany), 1% Penicillin-Streptomycin-Neomycin (Invitrogen, Carlsbad, USA), 100 µg/mL bromodeoxyuridine (Sigma-Aldrich, St. Louis, USA) and 50 µg/mL uridine (Sigma-Aldrich, St. Louis, USA) at 37°C in a humidified atmosphere of 5% carbon dioxide. Cells were labeled with light (L) or heavy (H) isotopes of arginine ($^{12}C_6{}^{14}N_4$, $^{13}C_6{}^{15}N_4$; 30 mg/L) and lysine ($^{12}C_6{}^{14}N_2$, $^{13}C_6{}^{15}N_2$; 80 mg/L; both: Silantes, Munich, Germany) and grown to confluency in one 300 cm^2 polystyrene flask per replicate. Proteomic experiments were done in biological quadruplicates, including a label-switch. For metabolome profiling and enzymatic measurements, light SILAC labeled cultures were grown in biological triplicates.

2.3 Verification of rotenone induced complex I deficiency in HeLa cells

1 mM, 100 µM and 10 µM rotenone (MW 394.42 g/mol) stock solutions were prepared in ethanol. HeLa (human cervical cancer) cells were cultivated as described above (2.2.1). The cells were seeded in six-well plates and rotenone or DMSO was added after three hours. After 38 h the cells were harvested by trypsinization, washed with cold PBS, sedimented by centrifugation and the resulting sediment was used for cell counting and enzyme activity measurement of complex I (see 2.14.1 and 2.14.5). All measurements were performed in duplicates and complex I enzyme activity was normalized to protein concentration.

2.4 Verification of the ρ^0 status by PCR

Full depletion of mtDNA was verified by PCR (Wittig et al. 2010). In brief, genomic DNA was isolated using the QIAmp DNA Mini Kit and amplified by PCR. Here, a 399-bp mtDNA product that span a region of nt 3153 – nt 3551 (Primer: 5´TTCACAAAGCGCCTTCCCCCGT and 5´GCGATGGTGAGAGCTAAGGTCGGG) and a 238-bp nuclear DNA product that span a region of exon 5 (nt 55953445 – nt 55953207) of the gene USMG5 (Primer: 5´AGTGTCTTAAGAGTAAAGCTGGCCACA and 5´ TTGCCTTTGTTGCATTTTCTACAG) were analyzed. PCR was performed with 50 ng of genomic DNA as template, 250 µM dNTPs (Invitrogen, Carlsbad, CA), 0.5 µM of each primer and 2.5 U of Taq polymerase (Invitrogen, Carlsbad, CA) were used.

PCR conditions were as following: initial denaturation at 94°C for 2 min, denaturation at 94°C for 30 sec, primer annealing 30 sec at 60°C, elongation 60 sec at 72°C, 30 cycles in a thermocycler (Mastercycler personal 5332, Eppendorf, Hamburg, Germany). PCR products and a 100 bp mass calibration ladder (New England Biolabs, Ipswich, MA) were loaded and separated on a 2% agarose/TBE gel.

2.5 Cell harvesting and sample preparation for proteomics

Cells were harvested in cell lysis buffer.

2.5.1 Rotenone treated HeLa cells

Lysates of 1 mg protein were sonicated on ice for 15 sec and incubated at 95°C for five minutes to reduce disulfide bonds. Lysates were alkylated with a final concentration of 5.5 mM chloroacetamide for 30 min at room temperature. Samples were precipitated overnight with acetone at -20°C. Precipitates were lyophilized and dissolved in digestion buffer. Lys-C digestion (0.8 µg/sample) was performed for four hours at room temperature followed by a trypsin digestion (2 µg/sample) in 2 M urea overnight at 37°C.

Protein concentration was determined by BCA assay (Sigma-Aldrich). Then, peptides were purified with C18 cartridges with a capacity of 100 mg (see 2.11.1) and further separated using strong anion exchange (SAX) chromatography (see 2.12.1). Each sample was fractionated in six aliquots and subsequently purified and concentrated with C18 stage tips (see 2.11.2).

2.5.2 143B.TK$^-$ and ρ^0 cells

After cultivation, equal amounts of differently labeled ρ^0 and parental samples were mixed, approximately 17 mg of protein for each replicate in total. Lysates were sonicated for one minute, boiled at 95°C for five minutes and alkylated with a final concentration of 5.5 mM chloroacetamide for 30 min at room temperature. Samples were precipitated with acetone overnight at -20°C and lyophilized. Pellets were dissolved in digestion buffer and Lys-C digested (1:2000) for four hours at room temperature followed by a trypsin digestion (1:1000) overnight in 2 M urea at 37°C. Peptides were purified with C18 cartridges (see 2.11.1), 10% of each sample was further separated by SAX chromatography (see 2.12.1). The remaining 90% of each purified peptide mixture was used for immunoprecipitation of ubiquitinated peptides using the PTMScan® Ubiquitin Remnant Motif (K-ε-GG) Kit (see 2.13.1). The peptides which did not bind to the immunoaffinity beads were used for subsequent phosphoproteome profiling. Therefore, samples were fractionated by SCX chromatography (see 2.12.2), followed by titanium dioxide (TiO_2) enrichment (see 2.13.2).

2.6 Sample preparation for metabolomics

2.6.1 Cell harvesting for metabolomics

The growth medium was removed and cells were rapidly rinsed by gently dispensing 5 mL ice cold PBS to the growth surface. Then, 1 mL ice cold water was added into the flask and immediately flash-frozen in liquid nitrogen. Cells were detached with a cell scraper and transferred into a 15 mL tube. All cell suspensions were lysed by two rapid freeze and thaw cycles in liquid nitrogen, followed by 30 sec of sonication on ice (Bi et al. 2013).

2.6.2 Metabolite extraction

Metabolites were extracted with a biphasic methanol/chloroform/water system (ratio 2.0:2.0:1.8, (Wu et al. 2008) and samples were continuously prepared on ice. 8 mL/g (extract) cold methanol (-20°C) and 4 mL/g chloroform were added to the homogenates and subsequently vortexed. Afterwards samples were mixed for ten minutes at 4°C and centrifuged for five minutes at 2000 × *g* at 4°C to remove debris and precipitated protein (resulting sediment could be used to determine the protein concentration). The supernatants were transferred to fresh tubes and 4 mL/g chloroform and 4 mL/g water were added. Samples were vortexed for 60 sec, kept on ice for ten minutes for phase separation and centrifuged for ten minutes at 2000 × *g* at 4°C. The resulting upper polar and lower nonpolar fractions were separately transferred and combined in three clean tubes containing the IS (chloramphenicol, adipic acid, TAPS, MOPS, HEPES and antimycin A), dedicated for subsequent analysis by using methanol, acetonitrile and water, respectively, as alternative solvents for LC-MS runs. Samples were lyophilized in a centrifugal concentrator (Thermo Scientific Savant, Waltham, MA). The sediments were dissolved in 500 µL acetonitrile with 0.1% formic acid and 500 µL methanol with 0.1% formic acid for analysis by hydrophilic interaction liquid chromatography (HILIC) and in 500 µL water with 0.1% formic acid for analysis by reversed phase liquid chromatography (RPLC), sonicated for 40 sec and centrifuged at 3200 × *g* for ten minutes at 4°C. To avoid column clogging, samples were purified by

filtration (iso-disc filters PTFE 13 mm x 0.2 mm, Supelco, Bellafonte, PA). After sample filtration, syringe and filter were rinsed with 200 µL of the according buffer. Samples were lyophilized in the centrifugal concentrator.

2.6.2.1 Metabolite sample preparation for rotenone treated HeLa cells

The residuals were dissolved in 35 µL acetonitrile with 0.1% formic acid and 35 µL methanol with 0.1% formic acid for analysis by HILIC and in 20 µL water with 0.1% formic acid for RPLC, centrifuged at 17,500 × *g* for five minutes at 4°C. The supernatants were transferred to microvolume inserts and 5 µL per run were injected for LC-MS/MS analysis.

2.6.2.2 Metabolite sample preparation for 143B.TK$^-$ and ρ^0 cells

Protein containing sediments of the first extraction-step (2.6.2) were used to determine the protein concentration by a BCA assay (Sigma-Aldrich, St. Louis, MO). These protein concentrations were used for sample normalization. Additionally, an IS, containing chloramphenicol and ^{13}C-labeled glutamine, uracil, arginine, proline and valine (3.5 µM final concentration) was added to each sample. Dry residuals were suspended in 50 µL acetonitrile with 0.1% formic acid and 50 µL methanol with 0.1% formic acid for analysis by according HILIC mode, in 50 µL water with 0.1% formic acid for RPLC mode and centrifuged at 17,500 × *g* for five minutes at 4°C. The supernatants were transferred to microvolume inserts, 5 µL per run were injected for LC-MS/MS analysis.

2.7 Cell counting

10 µL of cell suspension were incubated for one minute at room temperature with 0.4% trypan blue. Then, cells were counted using a hemocytometer and viability was calculated as ratio between living and total cells.

Later on, cell counting was performed with an automated cell counter (NANOENTEK, Seoul, Korea).

2.8 Bicinchoninic acid assay

For the determination of protein concentrations by BCA assay, samples were measured undiluted and 1:10 diluted. Protein concentrations were determined according to the manufacturer's protocol (BCA Protein Assay Kit; Thermo Scientific Pierce, Waltham, MA).

2.9 DNA extraction

DNA from mammalian cells was extracted using the QIAamp DNA Mini Kit (Quiagen, Venlo, Netherlands) according to the manufacturer's protocol.

2.10 Gel electrophoresis

1.5% or 2% agarose gels (Biozyme LE Aagarose, St. Joseph, MO) were prepared with TBE-buffer. 1% ethidium bromide (Roth, Karlsruhe, Germany) was added after the agarose solution cooled down. A 100 bp mass calibration ladder (New England Biolabs, Ipswich, MA) was used as marker.

2.11 Sample clean-up

2.11.1 C18 cartridges

Salts and buffers can be removed using reversed phase resins, of which an octadecyl carbon chain (C18)-bonded silica stationary phase is ideal to capture hydrophobic peptides. The peptides bind to the stationary phase in a high-aqueous mobile phase, salts and buffers are washed out and the peptides are eluted using a high-organic mobile phase.

C18 cartridges (Sep-Pak, Waters, Milford, MA) with a capacity of 100 mg and 500 mg and a volume of 1 mL and 5 mL respectively, were used for sample clean-up. The cartridges were washed with 100% acetonitrile, 70% acetonitrile with 0.1% formic acid and 0.1% formic acid. After each step the cartridges were centrifuged at 1200 × g for one minute. The acidified sample with a final concentration of 1% formic acid was applied and centrifuged for three minutes at 150 × g. This procedure was repeated. The bound peptides were washed twice with 0.1% formic acid and centrifuged at

150 × *g* for three minutes. Peptides were eluted by adding 70% acetonitrile at 150 × *g* for three minutes and the eluate was dried in a rotary evaporator.

2.11.2 C18 stage tips

C18 stage tips (Thermo Scientific Pierce, Waltham, MA) with a volume of 100 µL were washed with the solutions as described in 2.11.1. Samples were loaded by pipetting ten times up and down, followed by three washing steps with 100 µL 0.1% formic acid. The peptides were eluted with 100 µL 70% acetonitrile. The eluate was dried in a rotary evaporator.

2.12 Ion exchange chromatography for sample fractionation

Ion-exchange chromatography separates molecules on the basis of their net surface charge, whereby the absorption of molecules to the solid support is driven by ionic interactions. An anion exchanger will bind a molecule with an overall negative charge, whereas a cation exchanger will bind positively charged molecules. By increasing the salt concentration, the molecules with the weakest ionic interactions will elute first.

2.12.1 Strong anion exchange (SAX)-based fractionation of peptides

This workflow was adapted from (Wiśniewski, Zougman, and Mann 2009).

SAX-tips were prepared by stacking two layers of anion exchange SPE disks (Empore^{TM}, Meriden, CT) into a 200 µL pipet tip. For each sample, one SAX-tip was prepared. The SAX-tips were washed with 100 µL methanol, 1 M sodium hydroxide and twice with pH 11 buffer and centrifuged at 2000 × *g* for five minutes. Samples were dissolved in 200 µL of pH 11 buffer. C18-tips were washed as described in 2.11.2. The prepared SAX-tip was placed into one C18-tip. The sample was loaded onto the SAX-tip and centrifuged at 2000 × *g* for ten minutes. 100 µL of the pH 11 buffer was added to the SAX-tip and centrifuged at 2000 × *g* for five minutes. The same SAX-tip was transferred to a new C18-tip for elution with 100 µL of pH 8 buffer. This procedure was repeated for each pH step. The peptides were subsequently eluted onto individual C18-tips. All C18-tips were washed with 0.1% formic acid and peptides were eluted with 100 µL 70% acetonitrile. All eluates were dried in a rotary evaporator.

2.12.2 Strong cation exchange (SCX) chromatography

Before every run, the ÄKTA system (GE Healthcare, Chalfont St Giles, UK) was washed with 20% ethanol for ten minutes at 10 mL/min. Then, a 1 mL loop was connected to the system, which was further washed with water for ten minutes at 10 mL/min. Afterwards, the column (PolySULFOETHYL A; 200x9.4 mm, 5 µM, 200 Å, PolyLC Inc., Columbia, MD) was connected and rinsed with a flow rate of 3 mL/min for ten minutes. To equilibrate the column buffer A1 was injected for one hour. Then, samples were dissolved in 200 µL buffer A1 and injected into the loop. The sample tubes were washed with another 200 µL that were injected in the loop. During the run, 12 mL-fractions were collected automatically.

Wavelength 220 nm for the peptide bond and nonaromatic amino acids and 280 nm for aromatic amino acids were recorded. The gradient (flow rate of 3 mL/min) is shown in Figure 6. A total of 14 fractions were collected that were purified according to 2.11.1.

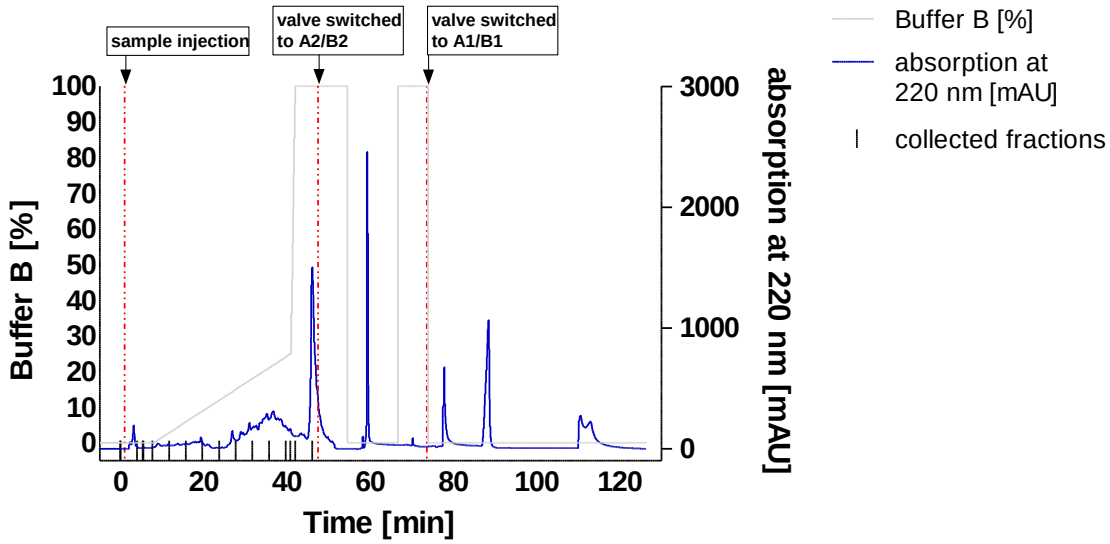

Figure 6: Exemplary spectrum detected at 220 nm showing the gradient, highlighting collected fractions and valve switches. A gradient of the buffers B1/B2 was used to separate peptides (grey). An exemplary spectrum which was detected at 220 nm is shown (blue). Indicated by black ticks are the 14 fractions that were collected, the red dotted line highlights the sample injection and when the valves were switched.

2.13 Analysis of posttranslational modifications (PTMs) by LC-MS

2.13.1 Ubiquitylation

The identification of ubiquitinated peptides by MS relies on the identification of a 114.1 Da diglycine (GG) remnant on lysine residues (K-ε-GG), which is derived from the C-terminus of ubiquitin, following a tryptic digest (Denis et al. 2007). The proteome-wide enrichment of ubiquitination is based on this distinct feature of a K-ε-GG.

The PTMScan® Ubiquitin Remnant Motif (K-ε-GG) Kit (Cell Signaling technology, Danvers, MA) was used for immunopurification of ubiquitinated peptides. A purified peptide mixture (~10-20 mg protein digest/IP) was dissolved in 1-1.2 mL 1x IAP buffer. Care was taken not to introduce bubbles and the pH was always neutral, or no lowers than 6. The peptide solution was centrifuged (five minutes, 10,000 × *g*, 4°C) to remove any precipitates and transferred to a new tube on ice. 40 µL of the antibody-bead suspension was sequentially washed four times with 1 mL PBS. Afterwards, the slurry was suspended in 40 µL PBS and the peptide solution was added on top of the beads to ensure immediate mixing, without bubble formation. The reaction tubes were incubated on a vertical rotator overnight at 4°C. Then, the tubes were centrifuged at 1000 × *g* for 30 sec and the supernatants were removed. All subsequent washing steps were performed at 0-4°C. The beads were washed three times by adding 1 mL IAP buffer, followed by inverting the tube and centrifugation at 1500 × *g* for 30 s. Subsequently, the washing was repeated three times with 1 mL water. The modified peptides were eluted in 100 µL of 0.15% formic acid by incubation at room temperature for ten minutes. The tubes were centrifuged for a few seconds in a table top centrifuge and the supernatant was transferred to a new tube. This elution step was repeated two more times and eluates were combined, concentrated and further purified.

C18 stage tips (Thermo Scientific Pierce, Waltham, MA) with a volume of 100 µL were washed once with 100 µL 50% acetonitrile with 0.1% formic acid and twice with 100 µL 0.1% formic acid. The sample was loaded by pipetting ten times up and down, followed by two washing steps with 100 µL 0.1% formic acid. The peptides were eluted with 20 µL 40% acetonitrile with 0.1% formic acid. The eluate was dried in a rotary evaporator.

2.13.2 Phosphorylation

A global analysis of serine-, threonine- and tyrosine-phosphorylation is achieved by fractionation of tryptic peptides using SCX and subsequent enrichment by titanium dioxide (TiO_2).

The Titansphere™ Phos-TiO Kit (GL Sciences, Torrance, CA) was used for immunopurification of phosphorylated peptides. The peptides which did not bind to the immunoaffinity beads for enrichment of ubiquitinated peptides were used for subsequent phosphoproteome profiling. The samples obtained from the SCX fractionation (2.12.2) were dissolved in 50 µL water. All following steps until the elution of peptides were performed according to the manufactures' protocol. Monophosphorylated peptides were eluted with 100 µL of 100 mM triethylammonium bicarbonate and centrifuged at 1000 × *g* for five minutes at room temperature. Polyphosphorylated peptides were eluted sequentially with 50 µl 5% and 50 µl 15% ammonium hydroxide, followed by centrifugation at 1000 × *g* for five minutes at room temperature. All three elution fractions were combined and dried in a rotary evaporator.

2.14 TCA cycle and OXPHOS enzyme activity measurements

The activity measurements of malate dehydrogenase (MDH) and fumarate dehydrogenase (FH) were monitored with the microplate reader POLARstar Omega (BMG Labtech, Offenburg, Germany). All measurements were performed in biological triplicates from independent culture dishes and normalized for total protein content.

All spectrophotometric measurements were performed at 37°C and supernatants were kept on ice. All other measurements were performed in cuvettes in a spectrophotometer (Ultrospec 3100 pro, GE Healthcare, Chalfont St Giles, UK).

2.14.1 Sample preparation for enzyme activity measurements

Samples were dissolved in cold SEKT-buffer (100 µL for rotenone treated HeLa cells, 30 µL for ρ^0 and 143B.TK$^-$ cells). Cells were disrupted by shear forces by 30 repeated injections through a 26G cannula. The homogenate was centrifuged for ten minutes at 600 × *g* and 4°C. The resulting sediment was used for DNA isolation, while the 600 × *g* supernatant (mitochondrial fraction) was used to measure enzyme activity and to determine the protein concentration via BCA assay (2.8).

2.14.2 Fumarate dehydrogenase and malate dehydrogenase

FH and MDH activities were measured according to the manufactures' protocol (Bio-vision technologies, Golden, CO).

FH catalyzes the reversible reaction of hydration and dehydration of fumaric acid to malic acid. MDH reversibly catalyzes the oxidation of malic acid to oxalacetic acid, by reducing NAD^+ to NADH.

During the reaction, an intermediate is formed while fumaric acid is converted to malic acid. This intermediate reacts with the enzyme mix and the contained developer is reduced to a colored product with absorbance at 450 nm. Similarly, MDH reacts with malic acid to form an intermediate. The intermediate reacts with the MDH developer to form a colored product with absorbance at 450 nm.

2.14.3 Citrate synthase

Citrate synthase (CS) catalyzes the condensation of two-carbon residues from acetyl-CoA and four-carbon oxalacetic acid to form citric acid.

860 µL water at 37°C, 100 µL CS stock, 10 µL acetyl-CoA stock and 20 µL 600 × g supernatant were pipetted in the given order into a pre-warmed cuvette and mixed well. The hydrolysis of the thioester acetyl-CoA results in the formation of CoA with a thiol group. This thiol group reacts with DTNB in the CS stock to form 5-thio-2-nitrobenzoic acid. This yellow product was detected spectrophotometrically at 412 nm.

The reaction kinetic was monitored for 12 min at 412 nm and data points were taken every minute. Four basal turnover points were measured and the enzymatic reaction was started by adding 10 µL of the oxalacetic acid stock. The ΔOD_{412} for each sample after addition of oxalacetic acid was calculated and the averaged value was used to determine the enzyme activity according to the following equation:

$$\mathrm{CS}\left[\frac{\mathrm{mU}}{\mathrm{mg\ protein}}\right] = \frac{\Delta \mathrm{OD}_{412} \times \varepsilon \times 10^6}{\text{sample volume } [\mu\mathrm{L}] \times \text{protein concentration } [\frac{\mathrm{mg}}{\mathrm{mL}}]} \qquad (1)$$

The extinction coefficient (ε) for DTNB at 412 nm was 13.6 M^{-1} cm^{-1} (Ellman 1958).

2.14.4 Isocitrate dehydrogenase

Isocitrate dehydrogenase 1 and 2 (IDH1, 2) are catalyzing the oxidative decarboxylation of isocitric acid to 2-oxoglutaric acid and carbon dioxide while converting $NADP^+$ to NADPH.

875 µL water at 37°C, 100 µL IDH stock and 15 µL 600 × *g* supernatant were pipetted in the given order into a pre-warmed cuvette and mixed well.

IDH activity was measured using a spectrophotometer to monitor the reduction of $NADP^+$ to NADPH at 340 nm, which is the absorption maximum of NADPH.

The kinetic was monitored for 12 min at 340 nm and data points were taken every minute. Five basal turnover points were measured and the reaction was started by adding 10 µl of the isocitric acid stock. The ΔOD_{340} for each sample after addition of isocitric acid was calculated and the averaged value was used to determine the enzyme activity according to the following equation:

$$\text{IDH}\left[\frac{\text{mU}}{\text{mg protein}}\right] = \frac{\Delta \text{OD}_{340} \times \varepsilon \times 10^6}{\text{sample volume [µL]} \times \text{protein concentration}\left[\frac{\text{mg}}{\text{mL}}\right]} \quad (2)$$

The ε for NADP at 340 nm was 6.22 mM^{-1} cm^{-1} (Pandey et al. 2003).

2.14.5 NADH dehydrogenase

NADH dehydrogenase catalyzes the transfer of electrons from NADH to ubiquinone, which is reduced to ubiquinol.

870 µL water at 37°C and 20 µL 600 × *g* supernatant were incubated in a pre-warmed cuvette for three minutes, in order to cause a hypertonic shock of mitochondria. Subsequent, 100 µL complex I stock and 10 µL NADH stock were added and mixed well.

NADH dehydrogenase activity was measured at 340 nm to monitor the oxidation of NADH to NAD^+. NADH has a much higher absorbance at 340 nm than NAD^+. Rotenone is binding to the ubiquinone binding site of complex I and prevents NADH oxidation.

The kinetic was monitored for ten minutes at 340 nm and data points were taken every minute. The enzyme activity was measured for four minutes and stopped with 4 µL rotenone stock. The complex I activity ($\Delta OD_{340\text{-Rotenone}}$) after rotenone addition was

subtracted from the total complex I activity (ΔOD_{340}) in order to derive complex I activity according to the following equation:

$$CI\ [\frac{mU}{mg\ protein}] = \frac{(\Delta OD_{340-Rotenone} - \Delta OD_{340})\ \times \varepsilon \times 10^6}{\text{sample volume } [\mu L] \times \text{protein concentration } [\frac{mg}{mL}]} \quad (3)$$

The ε for NADH at 340 nm was 6.22 mM^{-1} cm^{-1} (Yamada and Carlsson 1975).

2.15 Metabolite tuning and LC-MS/MS optimization for MRM ion ratios

273 target metabolites were selected to cover most of the important metabolic pathways in mammals (Table S1). Pure metabolites were dissolved to a final concentration of 1 µM in methanol with 0.1% formic acid, 10 mM ammonium hydroxide was added and the sample solution was injected with a syringe at a flow rate of 7 µL/min. Precursor ions were fragmented in positive and negative electron spray ionization (ESI) mode. The seven most intense fragment peaks were chosen and optimized for the declustering potential (DP) of precursor ions, collision energy (CE) and collision cell exit potential (CXP) of fragment ions. All seven MRM's in both ionization modes were run on an online coupled LC-MS/MS system (1290 Infinity UHPLC, Agilent, Santa Clara, CA; QTrap 6500, Sciex, Toronto, Canada) featuring a Reprosil-PUR C18-AQ (1.9 µm, 120 Å, 150 x 2 mm ID; Dr. Maisch; Ammerbuch, Germany) column and a zicHILIC (3.5 µm, 100 Å, 150 x 2.1 mm ID; di2chrom; Marl, Germany) column at controlled temperature of 30°C (2.16.1; Figure 7). Transitions were monitored and acquired at low resolution in quadrupole Q1 and unit resolution in Q3.

Data was acquired with an ion spray voltage of 5.5 kV in positive and 4.5 kV in negative mode of the ESI source, nitrogen as collision gas was set to high, curtain gas to 30 psi, ion source gas 1 and 2 to 50 and 70 psi, and an interface heater temperature of 350°C, operated with Sciex Analyst 1.6.1 software with components for 6500 series instruments.

The three most intense peaks of all tested conditions for each metabolite were chosen for the final method. In order to calculate the MRM ion ratios, peaks were normalized to the most intense peak. Three replicates for each metabolite were used to calculate the final MRM ion ratios as reference values. The presence of peaks was compared to the databases Metlin (C. A. Smith et al. 2005) and HMDB (Wishart et al. 2013) in order to confirm the fragment masses. Some metabolites were not available as pure compound. Therefore MS/MS spectra from biological samples were generated, that matched database spectra (three most intense transitions were taken), or transitions from available database resources were used. Instrument settings for these "not tuned" metabolites could not be optimized.

2.15.1 Evaluation of MRMs and MRM ion ratios by amino acid calibration curves

Six amino acid (all from Sigma-Aldrich, St. Louis, MO) stock solutions were prepared at a concentration of 100 mM in different buffers (Table 1).

Table 1: Amino acids that were used to prepare stock solutions in the according buffers.

Amino acid [100 mM]	Buffer
L-isoleucine	water
L-leucine	1 M hydrogen chloride
L-methionine	water
L-phenylalanine	water
L-tryptophan	0.5 M hydrogen chloride
L-valine	0.5 M hydrogen chloride

A 10 mM stock solution containing all six amino acid was prepared and gradually diluted (3 mM, 1 mM, 300 µM, 100 µM, 10 µM, 1 µM, 100 nM, 30 nM, 10 nM, 3 nM, 1 nM and 100 pM). Each sample was measured in triplicates and for correction purposes blank runs were included. To verify the linearity inside this data set, the limit of detection (LOD), the coefficient of variation (% CV) of the technical triplicates, the MRM ion ratios and the Mandel's fitting test at a 95% confidence level were performed.

The LOD is defined as the concentration of analyte that is required to give a signal equal to the background (blank) plus three times the standard deviation of the blank.

The mean and standard deviation (s) of each blank were calculated to determine the LOD.

$$LOD = mean_{blank} + 3s_{blank} \quad (4)$$

Precision is expressed as the coefficient of variation (% CV). The mean and standard deviation (s) of the signal was calculated for each concentration to determine the % CV.

$$\%\ CV = \frac{s}{mean_{signal}} \quad (5)$$

The Mandel's fitting test was used for mathematical verification of linearity (Mandel 2012) at a confidence level of 95%. The test is based on the assumption that relatively large deviations of measured values from a straight line are caused by nonlinearity and may be reduced through the selection of an improved regression model, in this case a second-order function (Funk, Dammann, and Donnevert 2007). For this, the first-order calibration function $y = a + bx$ and the second-order $y = a + bx + cx^2$ calibration function, including the respective residual standard deviations s_y are used (Funk, Dammann, and Donnevert 2007). The difference of the variances DS^2 is calculated using the residual standard deviation s_{y1} (from the first-order calibration function) and s_{y2} (from the second-order calibration function) (Funk, Dammann, and Donnevert 2007):

$$DS^2 = (N-2)s_{y1}^2 - (N-3)s_{y2}^2 \quad (6)$$

The test value (TV) was calculated for the F-test and the result was compared with a value obtained from an F-test table.

$$TV = \frac{DS^2}{s_{y2}^2} \quad (7)$$

2.16 Metabolite profiling by targeted LC-MS/MS

All samples were run as biological triplicates. A total of ten different run conditions (including polarity switches) were necessary to analyze all metabolites. A scheduled

MRM algorithm to monitor transitions 300 sec around the expected retention time was used to decrease the number of concurrent MRMs monitored at any time point.

2.16.1 LC conditions for metabolomics

Two different LC columns have been used for metabolite separation: a Reprosil-PUR C18-AQ (1.9 µm, 120 Å, 150 x 2 mm ID; Dr. Maisch; Ammerbuch, Germany) column and a zicHILIC (3.5 µm, 100 Å, 150 x 2.1 mm ID; di2chrom; Marl, Germany). A 1290 series UHPLC (Agilent, Santa Clara, CA) with four different buffer conditions was used: A1: 10 mM ammonium acetate in LC-MS grade water (adjusted with formic acid to pH 3.5); A2: 10 mM ammonium acetate in LC-MS grade water (adjusted with ammonium hydroxide to pH 7.5); B1: LC-MS grade acetonitrile with 0.1% formic acid B2: LC-MS grade methanol with 0.1% formic acid. Gradients and flow conditions for each column are shown in Figure 7.

The columns had to be equilibrated with a blank run in the according buffer system. In the case of methanol, three blank runs were needed for equilibrating.

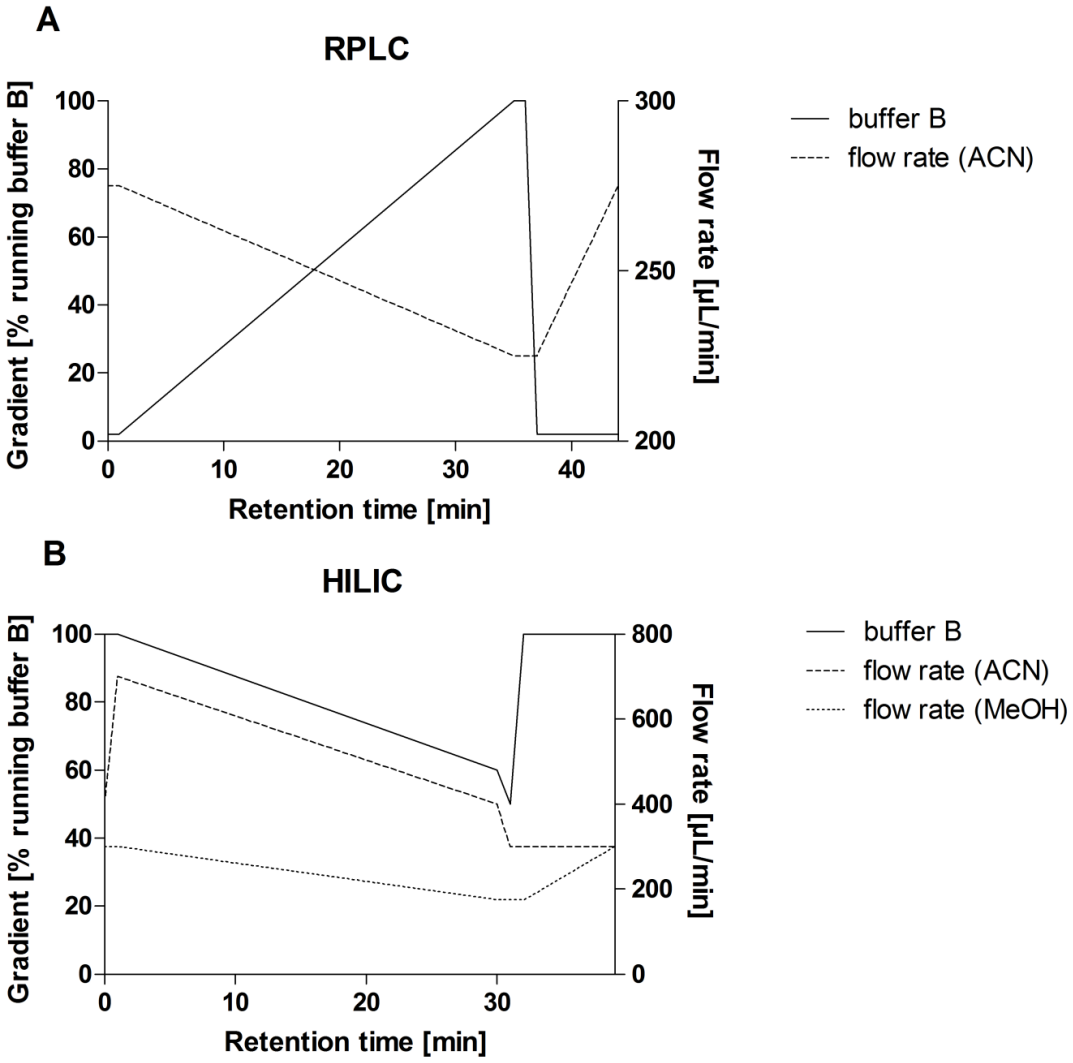

Figure 7: Gradients and flow conditions that have been used for metabolite separation. (A) shows the gradient profile used for RPLC with a run length of 44 min, whereas buffer A2 was used. (B) shows the gradient profile used for HILIC with a run length of 39 min, whereas buffers A1 and A2 were used.

2.17 LC-MS settings for proteomics

LC−MS/MS was carried out by nanoflow RPLC (Dionex Ultimate 3000, Thermo Scientific, Waltham, MA) coupled online to a Q-Exactive Plus Orbitrap mass spectrometer (Thermo Scientific, Waltham, MA). The LC separation was performed using a PicoFrit analytical column (75 µm ID × 25 cm long, 15 µm Tip ID (New Objectives, Woburn, MA) packed in-house with 3 µm C18 resin (Reprosil-AQ Pur, Dr. Maisch, Ammerbuch-Entringen, Germany). Peptides were eluted using the following gradients (solvent A: 0.1% formic acid in water; solvent B: 80% acetonitrile, 0.08% formic acid). For

rotenone treated HeLa cells, the gradient started with 3.8% solvent B to 98% over 192 min at a flow rate of 266 nL/min. For 143B.TK- and ρ^0 cells the gradient started with 2% solvent B to 40% over 210 min at a flow rate of 266 nL/min.

Three kV were applied for nanoelectrospray generation. A cycle of one full Fourier transform scan mass spectrum (300−1700 m/z, resolution of 35,000 at m/z 200) was followed by 12 data-dependent MS/MS scans with normalized collision energy of 25 eV. Target ions for rotenone treated HeLa cells and 143B.TK$^-$ and ρ^0 were excluded for 10 sec and 30 sec, respectively. In addition, only the peptide charge states between two to eight were sequenced, in the case of ubiquitinated peptide samples, only charge states three to eight were allowed.

2.18 Data analysis

2.18.1 Proteomics

2.18.2 Label free quantification - Rotenone treated HeLa cells

Raw MS data were processed with the MaxQuant software (version 1.5.0.0) (Jürgen Cox and Mann 2008) and searched against the human proteome database with 81,213 entries. False discovery rate (FDR) for proteins and peptides was set to 0.01 and a minimum peptide length of seven amino acids was required for identification. For the tryptic digest, a maximum of two missed cleavages was allowed. Cysteine carbamidomethylation was set as fixed modification, while N-terminal acetylation and methionine oxidation were set as variable modifications. The label-free software MaxLFQ (J. Cox et al. 2014), which is integrated in MaxQuant, was used for quantification. Additionally the “match between runs” feature was implemented to increase the number of peptides which can be used for quantification. Data analysis was performed with Perseus (version 1.5.0.8). LFQ intensities (originating of at least two different peptides per protein group) were $\log_2$ transformed and only protein groups with values in every replicate were used for further data evaluation. A t-test with a permutation based FDR was applied (Tusher, Tibshirani, and Chu 2001), while 250 permutations were performed and the FDR was set to 0.05.

2.18.2.1 Pathway and network analysis - Rotenone treated HeLa cells

Gene Set Enrichment Analysis (GSEA, v2.0.14) is a computational method that determines whether an *a priori* defined set of genes shows statistically significant, concordant differences between two biological states (Subramanian et al. 2005). Standard settings and a minimum size of five sets were applied to perform pathway-based analysis upon rotenone treatment. All mean values of the 3424 protein group ratios (Table S2) were used as input for GSEA analysis. To be regarded as significant p- and q-value had to be ≤ 0.05. Significantly regulated as well as more than two-fold regulated proteins were used to generate protein-protein interaction (PPI) networks using STRING 9.1 (search tool for the retrieval of interacting genes) (Franceschini et al. 2013), applying a medium confidence score of 0.4. Protein nodes which were not integrated into a network were removed. Interaction networks were extracted and further analyzed and evaluated using the "network analyzer" plugin (Assenov et al. 2008) for Cytoscape v3.1.1 (Shannon et al. 2003). Network analyzer was used to identify hub proteins, carrying the highest closeness centrality (CC) and betweenness centrality (BC) as key topological parameters. Closeness is regarded as a measure of how fast information's are spread from a given node to other reachable nodes in the network (Newman 2005). Whereas betweenness is a measure of the influence a node has over the spread of information through the network (Newman 2005).

2.18.3 SILAC-based quantification - 143B.TK$^-$ and ρ^0 cells

Raw MS data were processed with MaxQuant (v1.5.0.0) (Jürgen Cox and Mann 2008) using the Andromeda search engine (Jürgen Cox et al. 2011) and searched against the human proteome database UniProtKB with 69,714 entries released in 06/2015. Additionally, the "re-quantify" and "match between runs" features were implemented to increase the number of peptides which can be used for quantification. A FDR of 0.01 for proteins and peptides, a minimum peptide length of seven amino acids, a mass tol-

erance of 4.5 ppm for precursor and 20 ppm for fragment ions were required for identification. A maximum of two and three missed cleavages was allowed for tryptic and ubiquitinated peptides, respectively. Allowed SILAC modifications were $^{13}C_6{}^{15}N_4$-arginine and $^{13}C_6{}^{15}N_2$-lysine. Cysteine carbamidomethylation was set as fixed modification, while N-terminal acetylation, methionine oxidation, diGly modification of lysine and phosphorylation of serine, threonine and tyrosine were set as variable modifications. The two latter PTMs were only used for the according enriched fractions. After processing, MaxQuant output files contained peptide and protein identification, accession numbers, % sequence coverage of the protein, posterior error probability (PEP) values and normalized SILAC ratios. Contaminants as well as proteins identified by site modification and proteins derived from the reversed part of the decoy database were strictly excluded from further analysis. For all PTM analysis, only high confidence sites defined by a localization probability higher than 0.75 for phosphorylation sites and 0.9 for ubiquitination sites, PEP score smaller than 0.01 and Andromeda score difference between the best and second best peptide match larger than five were considered (Iesmantavicius, Weinert, and Choudhary 2014) (Table S3 and S4, respectively).

2.18.3.1 Statistical, pathway and PPI Network analyses - 143B.TK$^-$ and ρ^0 cells

Statistical analysis was performed by a one-sample Student's t-test followed by a Benjamini-Hochberg multiple test correction with a FDR of 0.05. Significantly regulated proteins are marked with a plus sign (Table S5). The cutoff for regulated proteins was set to two standard deviations difference from the median.

To check if an *a priori* defined set of proteins shows statistically significant, concordant differences between ρ^0 and parental state, a comprehensive proteome data analyses by gene set enrichment analysis (GSEA, v2.1.0) was performed (Subramanian et al. 2005). Here, only proteins that were identified in all replicates (Table S5 [4]) were averaged and used for GSEA analysis and $\log_2$ transformation. Standard GSEA settings were applied,

except the minimum size exclusion was set to five and reactome v5.0 was used as gene set database. The cutoff for significantly regulated pathways was set to p-value ≤ 0.05 and q-value≤ 0.25. The average values of L/H and H/L replicates were calculated. Only pathways that were significantly regulated in both merged replicates were extracted (Table 8).

In order to cope with the strong abundance of down-regulated, as compared to up-regulated proteins, additionally a self-contained test was employed. The test was performed on the normalized intensity ratios (or their inverse for the label-switched experiments, respectively) using the *globaltest* R package (Goeman et al. 2004). Gene symbols were mapped to Entrez Gene IDs using the 'org.Hs.eg.db' annotation package. The Broad gene sets (msigdb_v5.0.xml) were downloaded from http://www.broadinstitute.org/gsea/downloads.jsp and filtered for the subset of 509 Reactome pathway annotations that have at least five gene members. After performing the global test, the p-values were corrected for multiple testing using the Benjamini-Hochberg method and are displayed additionally in Table 8.

For PPI network analyses the software tool String v.10 was used to visualize networks of significantly down-regulated proteins of the entire proteome with a confidence level of 0.7 (Franceschini et al. 2013). Protein nodes which were not integrated into a network were removed. Further data analyses were performed using Perseus (v1.5.1.6), a post data acquisition package of MaxQuant.

For PTM analyses, regulated phosphorylation and ubiquitination sites were defined by two standard deviations from the median of unmodified peptides. Resulting protein lists were subjected to the gene set enrichment analysis tool of the DAVID Bioinformatics Resources (D. W. Huang, Sherman, and Lempicki 2009b; D. W. Huang, Sherman, and Lempicki 2009a), and analyzed by gene ontology (GO) “biological process” (GOTERM_BP_FAT), or “molecular function” (GOTERM_MF_FAT), respectively. For the analysis, lists of all phosphorylated or ubiquitinated sites were used as background sets.

Multiple datasets and software tools were used in order to elucidate as much information as possible, as every database has another focus and sets of pathways defined.

2.18.4 Metabolomics

Metabolites were quantified relatively with MultiQuantTM v.2.1.1 (Sciex, Foster City, CA). Manual peak integration was performed by a Gaussian smooth width of 2 points and a peak splitting factor of 2 which was reviewed manually. To unambiguously identify analytes, the ratio between transitions was calculated, which had to match to MRM ion ratios of tuned metabolites. The transitions were normalized to the largest peak area. A shift of ± 10% of the peak area was allowed for MRM ion ratios, compared to the tuned value of the largest peak. All three transitions had to co-occur at the expected retention time and feature the same peak shape. Peak areas in blank runs had to be at least < 90% smaller compared to the biological sample. The signal/noise ratio had to be above ten, at least for one transition. Transitions with a signal/noise ratio below 10 were only used for identification and not for quantification.

For rotenone treated cells, the samples were normalized to an IS mix, containing chloramphenicol, adipic acid, TAPS, MOPS, HEPES and antimycin A. The average ratio from all MRMs of one metabolite was used to calculate the $\log_2$ fold change between treated and control samples. Statistically significant differences in metabolite levels between treated and control samples were evaluated using the two-sample Student's t-test with a significance threshold of p-value < 0.05.

For ρ^0 and 143B.TK$^-$, the samples were normalized according to the protein content and subsequently by an IS mix, containing ^{13}C-labeled glutamine, uracil, arginine, proline and valine. The transition with the largest peak area of one metabolite was used to calculate the $\log_2$ fold change between treated and control samples. Statistically significant differences in metabolite levels between treated and control samples were evaluated using the two-sample Student's t-test. The p-values were corrected for multiple testing using the Benjamini-Hochberg method with a FDR of 0.05.

Significantly regulated metabolites are marked with a plus sign (Table S6 and S7 for rotenone treated and ρ^0/143B.TK$^-$ cells respectively).

3 Results

Parts of this thesis have been published as:

3.1 Evaluation of MRMs and MRM ion ratios by amino acid calibration curves

Metabolomes consist of many thousand different metabolites that are chemically very diverse and their concentration ranges from pM to mM. Thus, profiling an entire metabolome is a major challenge. Due to the high selectivity and low-detection limits, as well as the compatibility with separation techniques mass spectrometry is an ideal tool for metabolome profiling (Dettmer, Aronov, and Hammock 2007). Commonly, small molecules are identified by only one MRM, but this carries a high risk of false-positive identifications. While performing targeted metabolomics with a complex sample it can happen that two or more peaks are detected close to the expected retention time of the target molecule. A relative retention time of a compound can be calculated (Ettre 1980), which gives information about the peak, independent from column length, flow or other parameters. But in case two molecules are indistinguishable based on peaks and retention time, just an alteration in the MRM ion ratio would help to identify the target molecule. Ion ratio calculations are part of most software packages and have been used in clinical, pharmaceutical and forensic laboratories for many years, but the application in the biological field is quite low. This section presents the accuracy and robustness that can be derived for metabolome profiling by using three MRMs per target molecule. Additionally, an example is given, in order to show how the use of ion ratios helps to correctly identify compounds.

In principle, metabolomics focuses on the analysis of a large number of different molecules in a wide concentration range. In order to test the linear range of the mass spectrometer and the robustness of MRM ion ratios, an amino acid mixture containing pure leucine, isoleucine, valine, phenylalanine, tryptophan and methionine was examined in technical triplicates. The concentrations of the amino acids ranged from 100 pM to 3 mM. The verification of linearity was determined by the limit of detection (LOD), the coefficient of variation (% CV) of the technical triplicates, the MRM ion ratios and the Mandel's fitting test performed at 95% confidence level. The linear range of the amino acid set was determined to be below 15% CV (for MRMs and MRM ion ratios) (Gielisch and Meierhofer 2015).

Applying these criteria, the linear range spanned three orders of magnitude, while the calculated LODs were below the linear range of each transition (Table 8, Figure 8). This study presents the

accuracy and robustness that can be derived for metabolome profiling by using three MRMs per target molecule.

Table 2: Single amino acids contained within the mixture with their averaged limit of detection (LOD) and linear range.

Amino acid	Mean LOD [peak area]	Linear range
L-isoleucine	$1.12 \cdot 10^5$	100 nM – 100 µM
L-leucine	$1.14 \cdot 10^5$	30 nM – 10 µM
L-methionine	$2.79 \cdot 10^4$	100 nM – 100 µM
L-phenylalanine	$1.49 \cdot 10^5$	10 nM – 1 µM
L-tryptophan	$3.07 \cdot 10^4$	10 nM – 10 µM
L-valine	$1.56 \cdot 10^5$	100 nM – 300 µM

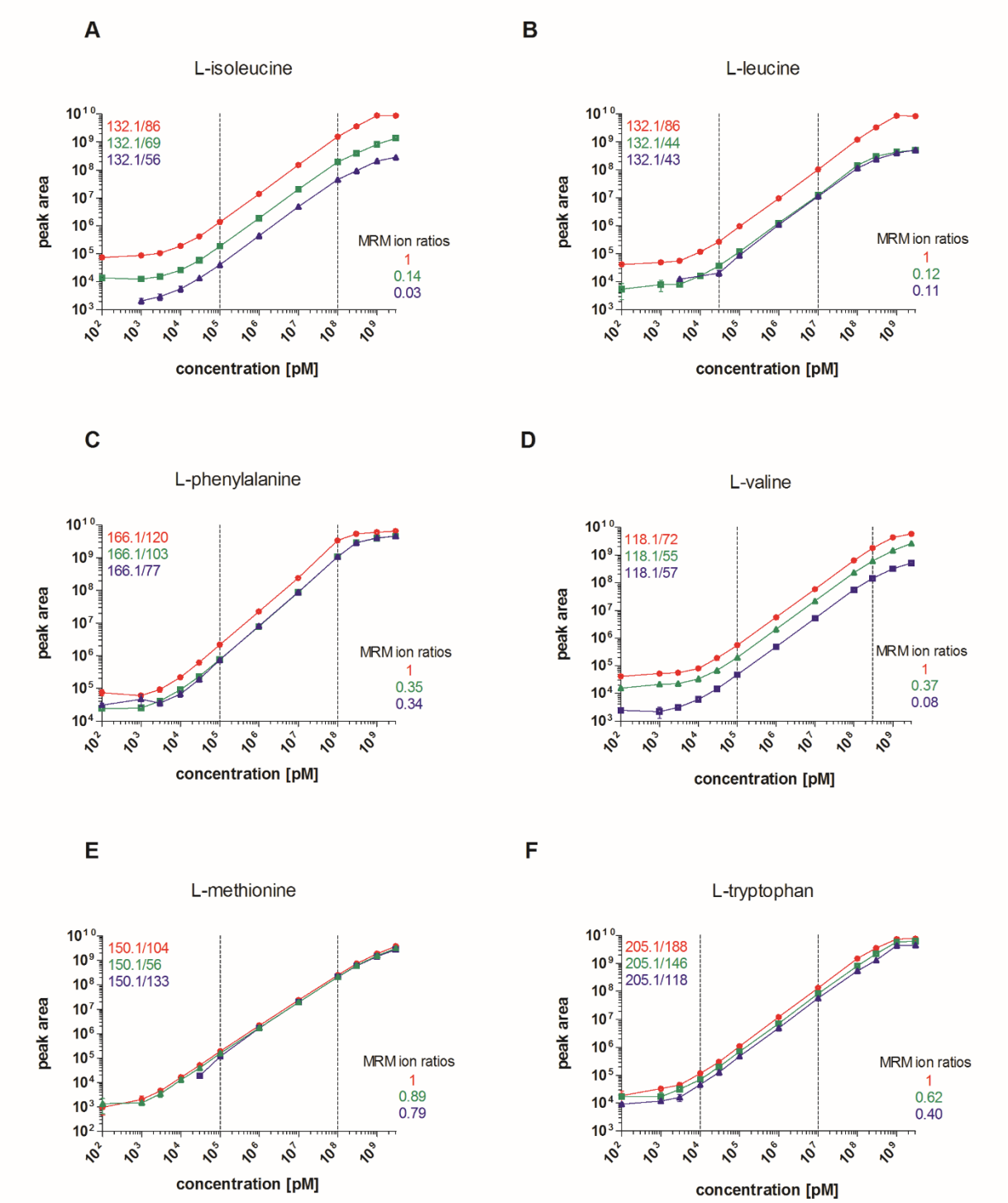

Figure 8: The linear range of six amino acids featuring three specific MRMs and their MRM ion ratios (Gielisch and Meierhofer 2015). Data are means ± S.D., n = 3. The MRM ion ratios within the linear range (between dotted lines) are shown in brackets; transition – % CV. (A) L-isoleucine (86/69 – 2.96%; 86/56 – 4.35%), (B) L-leucine (86/44 – 5.06%; 86/43 – 16.02%), (C) L-phenylalanine (120/103 – 7.05%; 120/77 – 7.68%), (D) L-valine (72/55 – 3.05%; 72/57 – 3.3%), (E) L-methionine (104/56 – 1.81%; 104/133 – 11.75%) and (F) L-tryptophan (188/146 – 3.6%; 188/118 – 3.25%).

3.1.1 Identifying inosine 5'-monophosphate by applying MRM ion ratios

Inosine 5'-monophosphate (IMP) is used as an example, in order to show how the use of ion ratios helps to correctly identify compounds from a complex biological sample. The monoisotopic molecular weight of IMP is 348.05 Da. IMP was detected in the positive ion mode, with a precursor ion mass of 349.05 Da and the fragment masses 137 Da, 119 Da and 110 Da. The targeted LC-MS/MS run for IMP detected two peaks around the retention time (2.62 min), whereas each peak showed all three MRMs, as indicated by the different colors (Figure 9). There are no obvious criteria to assign the correct peak to IMP. The 17-fold more intense peak shown on the right side of the spectrum is most likely selected as the IMP specific peak (Figure 9 A). But, zooming into the left peak shows (Figure 9 B) that the MRM ion ratios (ion ratio: 1/0.13/0.15) are clearly different from those of the peak on the right side (ion ratio: 1/0.28/0.02). Comparing these MRM ion ratios with the tuned values for IMP 1/0.13/0.12 it becomes clear that the peak on the left represents the correct MRMs derived from IMP. To validate the left peak as the correct one, the original sample was run again and after 2.52 min and 2.92 min MS^2 spectra were obtained (time points are indicated in Figure 9 B by dotted lines). The resulting MS^2 spectra are shown in Figure 9 C and D, respectively. Additionally, the reference MS^2 spectrum of pure IMP is shown in Figure 9 E. Differences are noticed when the MS^2 spectrum from the right peak (Figure 9 D) is compared to the reference spectrum (Figure 9 E), since four IMP-specific fragments are missing (indicated in red). This spectrum was searched against the MassBank (Horai et al. 2010) database, but no match was assigned to a metabolite. Whereas the MS^2 spectrum of the left and correct IMP-peak is identical with the reference spectrum (Figure 9 E). Just one peak at 80.9 Da was not matching to the reference spectrum (font color black).

In sum, the use of three MRMs and their MRM ion ratios is essential for robust and unambiguous identification and quantification of metabolites originating from complex biological samples.

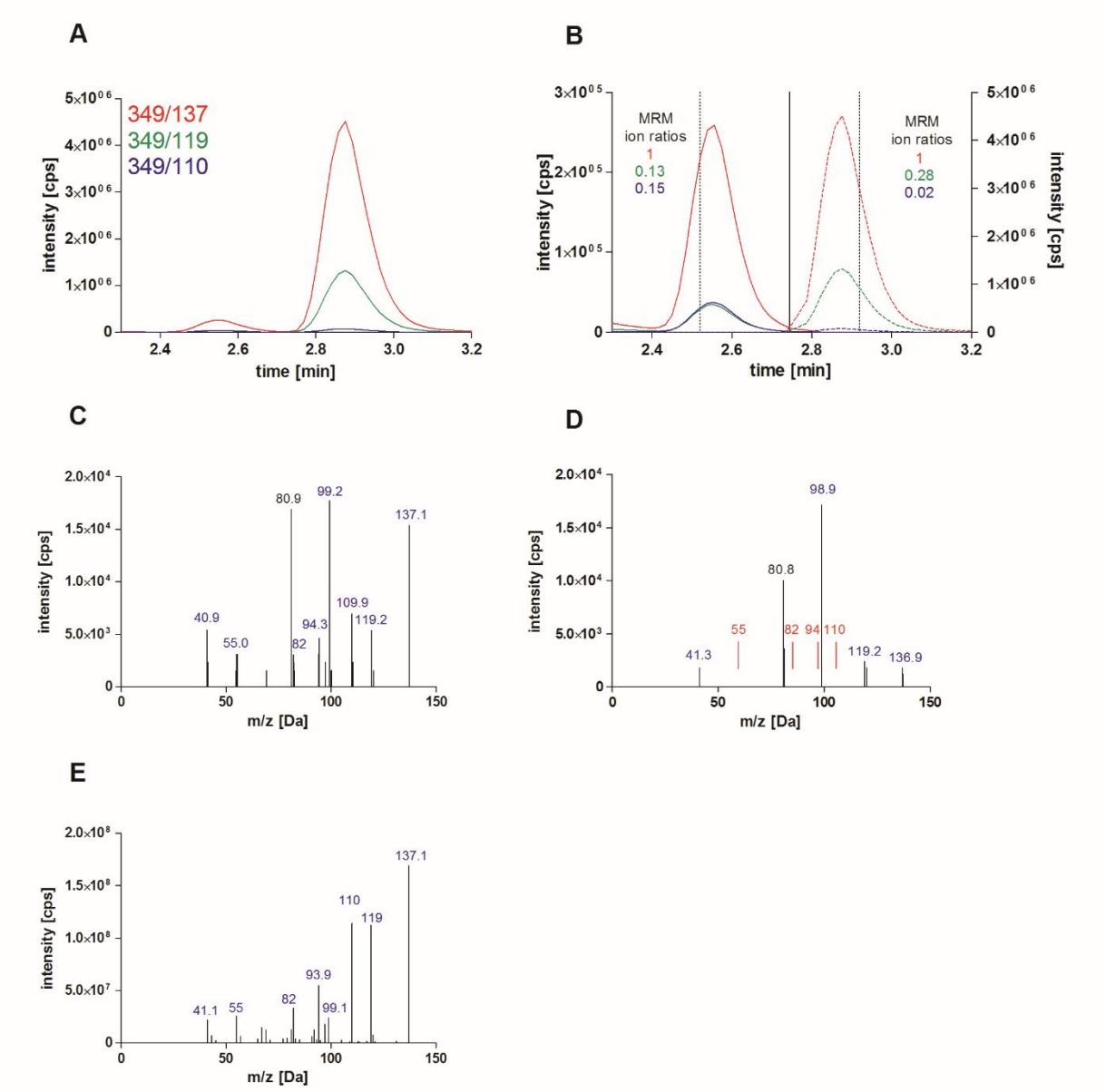

Figure 9: An example for identifying the correct peak based on MRM ion ratios (Gielisch and Meierhofer 2015). Inosine 5'-monophosphate (IMP) with a monoisotopic precursor molecular weight of 348.05 Da and three specific MRM transitions were detected in positive ionization mode: 137 Da, 119 Da and 110 Da. (A) Solely illustrating IMP specific MRMs in a time frame of the expected retention time. Both peaks show all three MRMs and could be identified as correct, but the mean area of the right peak is 17 times larger than the left peak. (B) Only MRM ion ratios identify the left peak as truly to be IMP (zoomed Y-axis), matching the tuned IMP ratios of: 1/0.13/0.12. The peak on the right side has different MRM ion ratios: 1/0.28/0.02, which are not matching to IMP. Dotted lines at minutes 2.52 and 2.92 mark the time points were MS^2 spectra were taken. (C) MS^2 spectrum to verify the left peak to be IMP, (D) the peak on the right side could not be assigned to any metabolite. (E) Tuned IMP spectra as a reference, all MS^2 spectra were taken with a CE of 73 V. Fragment masses shown in blue are identical to tuned IMP, while missing fragment masses are shown in red.

3.2 Rotenone induced complex I deficiency in HeLa cells

Rotenone is frequently used to study complex I dysfunctions (Li et al. 2003; Han et al. 2014; Scola et al. 2014). It inhibits the ubiquinone binding site of complex I and prevents the electron transfer via flavin mononucleotide (FMN) to ubiquinone. The repercussion is the interruption of the entire oxidative phosphorylation chain, simulating the features of a complex I deficiency (Gielisch and Meierhofer 2015).

3.2.1 Verification of rotenone induced complex I deficiency in HeLa cells

Five rotenone concentrations (10 nM, 30 nM, 100 nM, 300 nM and 1 µM) were tested in HeLa cells concerning their inhibition efficiency on complex I enzyme activity, their influence on cell viability and induction of apoptosis, whereas DMSO was used as control. Complex I activity was spectrophotometrically measured, by monitoring the oxidation of NADH to NAD^+.

Table 3: Measured complex I enzyme activity [U/g protein] and cell viability [%] of duplicates after 38 h induction with different concentrations of rotenone or DMSO.

	Complex I enzyme activity [U/g protein]		cell viability [%]	
10 nM Rotenone	76	100	89	99
30 nM Rotenone	52	97	90	95
100 nM Rotenone	23	45	100	100
300 nM Rotenone	13	17	91	83
1 µM Rotenone	11	-11	92	77
DMSO	58	115	94	96

Complex I enzyme activity of HeLa cells was entirely inhibited at a concentration of 1 µM rotenone, while lower rotenone concentrations did not completely inhibit complex I (Figure 10). Cell viability was between 85% and 100% and did not differ considerably from the DMSO control (Figure 10). In addition, no apoptosis specific DNA laddering could be detected for any tested concentration (Figure 10).

Thus, a rotenone concentration of 1 µM is suitable to mimic a complex I deficiency *in vitro*.

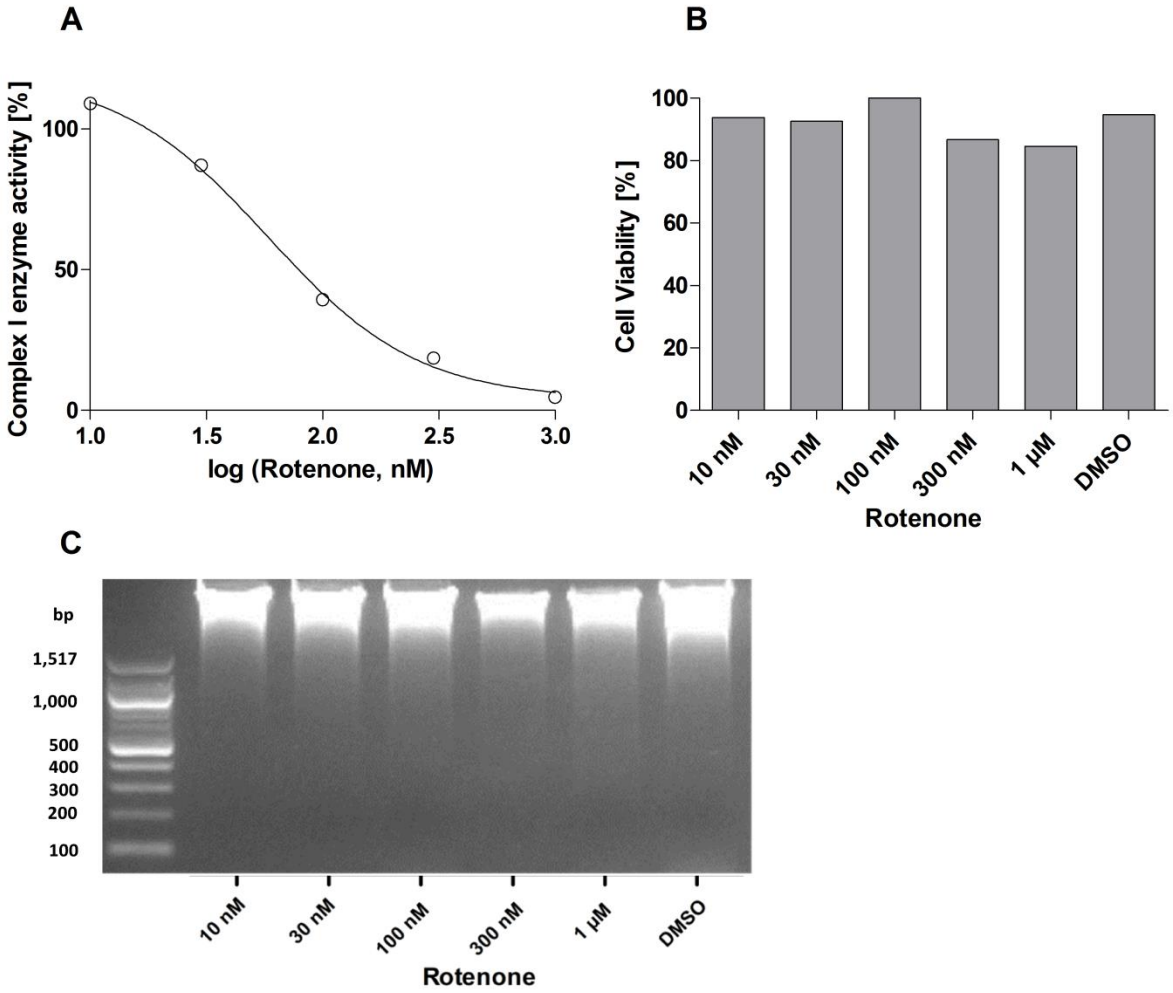

Figure 10: Determination of the complex I enzyme activity, viability and apoptosis rate of HeLa cells treated with different concentrations of rotenone. (A) Dose-response curve of complex I enzyme activity in % (based on DMSO control) versus logarithmized rotenone concentrations. (B) Cell viability of HeLa cells in % after treatment with different rotenone concentrations. (C) Agarose gel loaded with nuclear DNA showed no evidence of apoptosis specific DNA laddering.

3.2.2 Metabolome profiling of rotenone treated HeLa cells

Targeted metabolome profiling of control and rotenone treated HeLa cells was performed, in order to reveal differences in metabolite abundances in rotenone treated cells. As an additional quality criterion for metabolite identification and relative quantification, the MRM ion ratio method was applied.

142 out of 273 metabolites were detected with at least two transitions and three measured values per condition. From these, 23 metabolites were significantly (two-sample Student's t-test; p-value < 0.05) altered between control and rotenone treated cells and had at least a two-fold

change (Figure 11). Overall, three metabolites were up- and 20 were down-regulated. Metabolites belonging to the purine, pyrimidine, nicotinate and nicotinamide, riboflavin and other metabolic pathways were color coded (Figure 11).

Components of the purine and pyrimidine metabolism, such as IMP (~7-fold down-regulated in rotenone treated cells), adenosine (2.6-fold down-regulated), hypoxanthine (3.5-fold down-regulated) and xanthosine (2.2-fold down-regulated), uracil (4.3-fold down-regulated) and 5-thymidylic acid (2.2-fold down-regulated) were significantly down-regulated in rotenone treated HeLa cells (Figure 11).

The electron carrier nicotinamide adenine dinucleotide phosphate ($NADP^+$) was down-regulated in the oxidized ($NADP^+$; 2.7-fold down-regulated) and in the reduced (NADPH; 6-fold down-regulated) form (Figure 11). NADPH plays a crucial role in glutathione metabolism, which prevents oxidative stress generated by reactive oxygen species (ROS). Both oxidized and reduced glutathione were down-regulated as well (GSSG and GSH; both 1.8-fold down-regulated; data not shown). Additionally, NAD^+, a compound of the nicotinate and nicotinamide metabolism and required in glycolysis and the TCA cycle, was down-regulated as well (3.6-fold down-regulated) (Figure 11).

Flavoproteins are mainly located in mitochondria because of their redox power. They utilize either covalently linked or tightly bound flavin mononucleotide (FMN; 2.4-fold down-regulated) or flavin adenine dinucleotide (FAD; 2.9-fold down-regulated) (Figure 11). Moreover, FAD is a condensation product of riboflavin and adenosine diphosphate (ADP; 2.4-fold down-regulated) (Figure 11).

CDP-choline (7.7-fold up-regulated) has been shown to restore the activity of mitochondrial ATPase (Cohadon et al. 1979). Bilirubin (3.4-fold down-regulated), a degradation product of heme, was significantly down-regulated.

Many metabolites were highly, but not significantly, regulated. Citric acid was more than 100-fold and cis-aconitic acid was 6-fold decreased in rotenone treated cells (data not shown).

In sum, important metabolites of the OXPHOS system, like FMN, FAD and ADP, were found to be significantly down-regulated upon rotenone treatment. As well as compounds involved in redox reactions, such as $NADP^+$, NAD^+ and NADPH and oxidized and reduced glutathione.

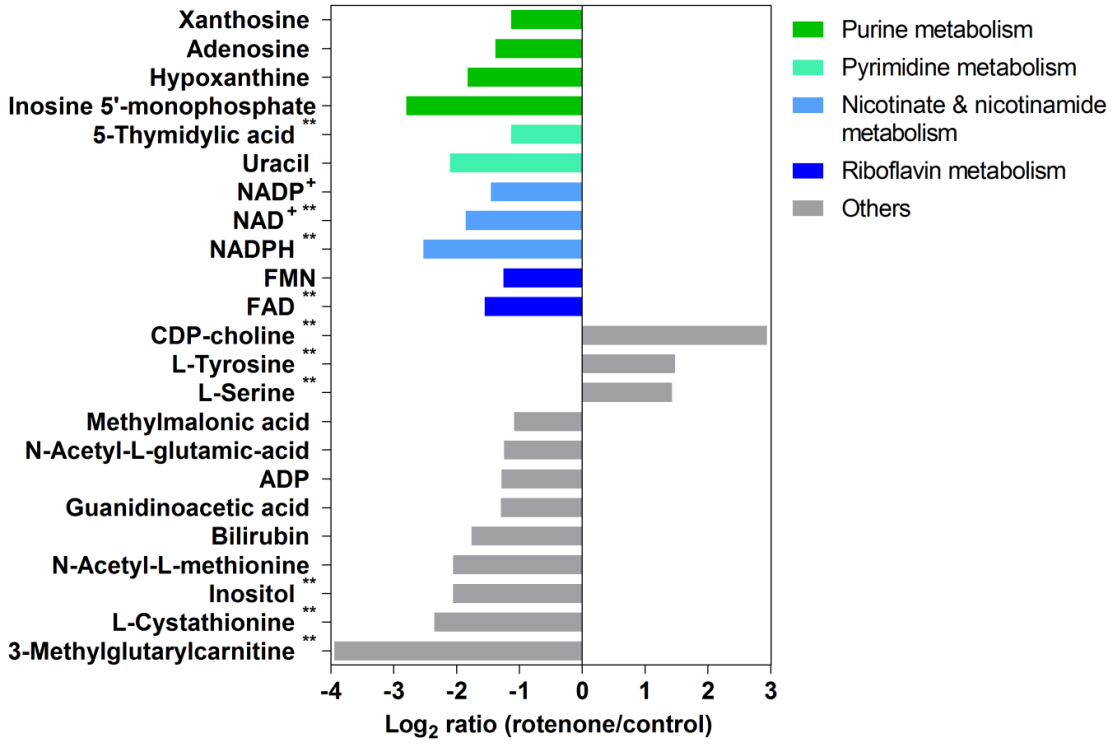

Figure 11: Metabolic profile of significantly regulated metabolites in rotenone-treated versus control cells. Metabolites belonging to the purine, pyrimidine, nicotinate and nicotinamide, riboflavin and other metabolic pathways were color coded. Only significantly (p-value < 0.05) and > 2-fold changed metabolites are shown; ** p-value < 0.01.

3.2.3 Proteome profiling of rotenone treated HeLa cells

Proteome profiling of control and rotenone treated HeLa cells was performed, in order to reveal differences in protein abundances between rotenone treated and control cells. For proteome profiling, six samples (three biological replicates of rotenone and DMSO treated cells) were analyzed in 42 LC-MS/MS runs and quantified label free (LFQ). Around $1.5 \cdot 10^6$ MS^2 spectra were identified that matched to 6,075 protein groups. Only protein groups with LFQ intensities in all replicates were used for further data analysis, which resulted in a protein list with 3,424 entries (Table S2).

3.2.3.1 Reproducibility of the biological replicates

The reproducibility is tested, in order to obtain an assessment of how reliable and valid the methodology and analysis is.

The biological replicates were tested by Pearson correlation and visualized in a multi-scatter plot (Figure 12 A and B). The Pearson correlation of the replicates was consistently > 0.97 for the controls and > 0.94 for the rotenone treated cells, with a p-value < 0.0001 for all correlations. Thus, all experiments show a statistically significant correlation and are reproducible.

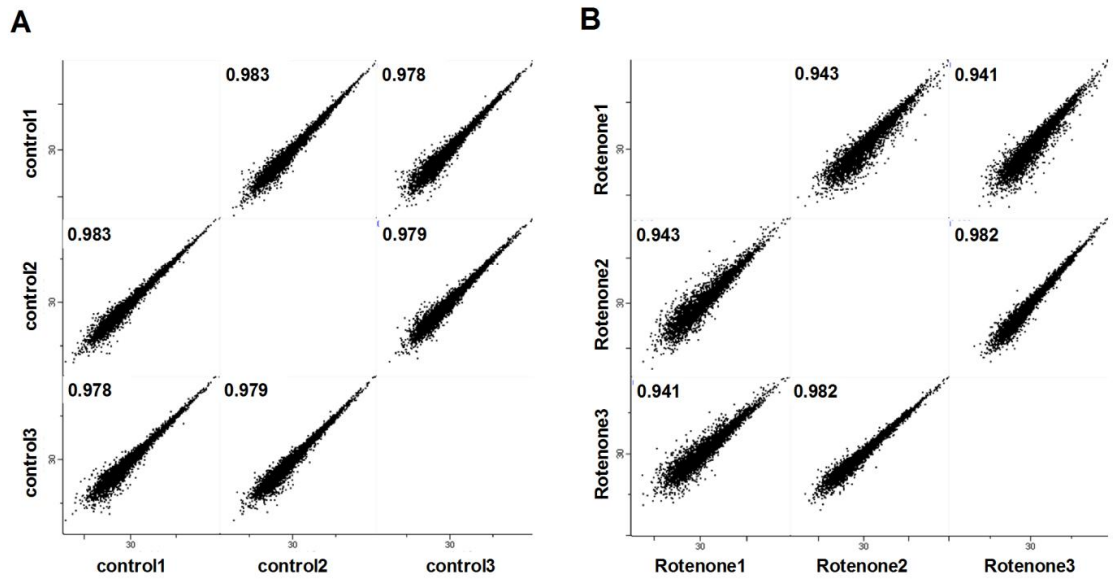

Figure 12: Multi-scatter plot to present the reproducibility of LFQ intensities of all biological replicates. (A) Pearson correlation was > 0.97 for controls and (B) > 0.94 for rotenone treated replicates, with a p-value < 0.0001 for all correlations.

3.2.3.2 Identification of significantly regulated protein groups in rotenone treated HeLa cells

The identification of significantly altered proteins can give a first impression on pathways that are differentially regulated.

To identify significantly altered protein groups a two-sample Student's t-test with a permutation based FDR was applied (Tusher, Tibshirani, and Chu 2001). In total, 250 permutations were performed and the FDR was set to 0.05. The data were visualized in a volcano plot, by plotting the negative $\log_{10}$ of the p-value on the y-axis and the difference of $\log_2$ group means of LFQ intensities of control and rotenone treated cells on the x-axis (Figure 13).

46 protein groups were found to be significantly regulated (26 up, 20 down) in rotenone treated cells. From these regulated proteins, pathways involved in cell division processes, energy metabolism and organization of cytoskeleton appeared to be affected.

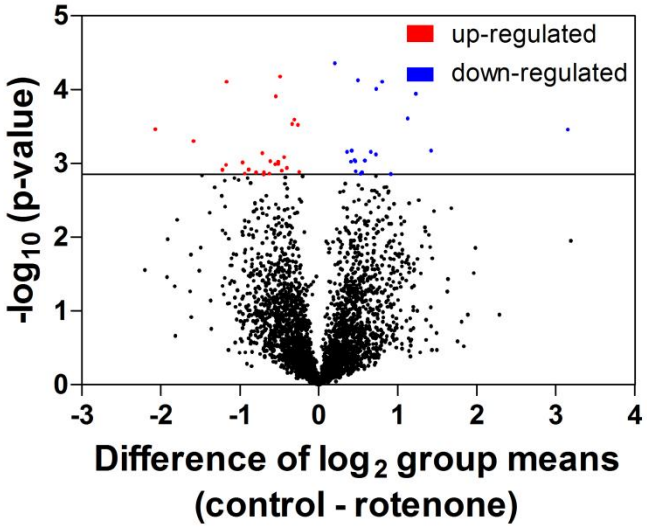

Figure 13: Volcano plot showing the mean difference of LFQ intensities between controls and rotenone treated cells versus statistical significance (-$\log_{10}$ of the p-value). The horizontal line marks where the cutoff was set by applying a FDR of 0.05, resulting in 46 significantly regulated protein groups. 26 proteins were up- (red) and 20 were down-regulated (blue) in rotenone-treated cells.

Table 4: Significantly up- and down-regulated protein groups extracted from Figure 13, indicating the mean $\log_2$ ratio (rotenone/control) and the $-\log_{10}$ (p-value).

Gene names	Protein names	Mean $\log_2$ ratio (rotenone/control)	$-\log_{10}$ (p-value)
Significantly up-regulated proteins in rotenone treated HeLa cells			
ANLN	Actin-binding protein anillin	2.07	3.46
PRC1	Protein regulator of cytokinesis 1	1.58	3.30
HMGA1	High mobility group protein HMG-I/HMG-Y	1.23	2.91
TOP2A	DNA topoisomerase 2-alpha	1.18	2.98
DNAJA1	DnaJ homolog subfamily A member 1	1.17	4.10
NDC80	Kinetochore protein NDC80 homolog	0.96	3.02
ABCF2	ATP-binding cassette sub-family F member 2	0.94	2.87
GNL3L	Guanine nucleotide-binding protein-like 3-like protein	0.90	2.92
EIF4G2	Eukaryotic translation initiation factor 4 gamma 2	0.80	2.88

Continued on next page

Table 4: Continued from previous page.

Gene names	Protein names	Mean log_2 ratio (rotenone/control)	$-log_{10}$ (p-value)
DNAJA2	DnaJ homolog subfamily A member 2	0.72	3.14
DNAJA3	DnaJ homolog subfamily A member 3, mitochondrial	0.70	2.85
TYMS	Thymidylate synthase	0.70	2.88
HDLBP	Vigilin	0.63	2.87
DDX21	Nucleolar RNA helicase 2	0.62	3.03
KPNA6	Importin subunit alpha-7;Importin subunit alpha	0.55	2.99
GNL3	Guanine nucleotide-binding protein-like 3	0.54	3.91
CDK2	Cyclin-dependent kinase 2	0.51	3.02
LRRC59	Leucine-rich repeat-containing protein 59	0.51	3.00
TNS3	Tensin-3	0.49	4.18
TPM1	Tropomyosin alpha-1 chain	0.47	2.90
TSR1	Pre-rRNA-processing protein TSR1 homolog	0.44	3.09
MSH2	DNA mismatch repair protein Msh2	0.40	2.94
TFRC	Transferrin receptor protein 1;Transferrin receptor protein 1	0.34	3.53
UGGT1	UDP-glucose:glycoprotein glucosyltransferase 1	0.31	3.59
SLC9A3R2	Na(+)/H(+) exchange regulatory cofactor NHE-RF2	0.26	3.52
DYNC1H1	Cytoplasmic dynein 1 heavy chain 1	0.25	2.88

Significantly down-regulated proteins in rotenone treated HeLa cells

KTN1	Kinectin	-0.20	4.36
TKT	Transketolase	-0.36	3.16
TALDO1	Transaldolase	-0.40	3.02
TBC1D4	TBC1 domain family member 4	-0.42	3.17
ACTR3	Actin-related protein 3	-0.45	3.04
EIF3D	Eukaryotic translation initiation factor 3 subunit D	-0.47	3.03
PRDX6	Peroxiredoxin-6	-0.47	2.89
ALDOA	Fructose-bisphosphate aldolase A	-0.50	4.13
MSN	Moesin	-0.53	2.86
CAND1	Cullin-associated NEDD8-dissociated protein 1	-0.55	2.88
ST13	Hsc70-interacting protein	-0.58	3.04

Continued on next page

Table 4: Continued from previous page.

Gene names	Protein names	Mean log_2 ratio (rotenone/control)	$-log_{10}$ (p-value)
PARK7	Protein DJ-1	-0.66	3.16
PQBP1	Polyglutamine-binding protein 1	-0.72	3.12
PLIN4	Perilipin-4	-0.73	4.01
CRIP2	Cysteine-rich protein 2	-0.80	4.11
CRABP2	Cellular retinoic acid-binding protein 2	-0.91	2.86
ADD3	Gamma-adducin	-1.12	3.61
CYCS	Cytochrome c	-1.23	3.94
FTH1	Ferritin heavy chain;Ferritin	-1.43	3.17
RBM3	Putative RNA-binding protein 3	-3.15	3.46

The first significantly regulated group of proteins is involved in cell cycle, cytokinesis and spindle formation. Here, seven proteins were up-regulated being PRC1, ANLN, TOP2A, NDC80, TYMS, CDK2 and DYNC1H1. PRC1 (3-fold up-regulated) is a key regulator of cytokinesis, which cross-links antiparallel microtubules and controls the spatiotemporal formation of the midzone. ANLN (4.2-fold up-regulated) is essential for the structural integrity of the cleavage furrow and for completion of cleavage furrow ingression. TOP2A (2.3-fold up-regulated) is involved in processes that occur during DNA transcription and replication, like chromosome condensation and chromatid separation. NDC80 (2-fold up-regulated) is a component of the essential kinetochore-associated NDC80 complex. This complex is required for chromosome segregation and spindle checkpoint activity. TYMS (1.6-fold up-regulated) plays a crucial role, since it catalyzes the methylation of deoxyuridylate (dUMP) to deoxythymidylate (dTMP). This function maintains the dTMP pool that is critical for DNA replication and repair. The serine/threonine-protein kinase CDK2 (1.4-fold up-regulated) is involved in the control of the cell cycle, while the protein DYNC1H1 (1.2-fold up-regulated) acts as a motor for the intracellular retrograde motility of vesicles and organelles along microtubules during G2/M phase of the cell cycle.

The second group of significantly regulated proteins is involved in energy metabolism. Here, three proteins were found to be down-regulated being TKT, TALDO1 and ALDOA. The proteins TKT (1.3-fold down-regulated), TALDO1 (1.3-fold down-regulated) and ALDOA (1.4-fold down-regulated) are involved in the pentose phosphate pathway/glycolysis. TKT and TALDO1 connect pentose phosphate pathway and glycolysis by providing sugar phosphates to

the main carbohydrate metabolic pathways. ALDOA plays a key role in glycolysis and gluconeogenesis by catalyzing the reversible conversion of fructose-1, 6-bisphosphate to glyceraldehyde 3-phosphate and dihydroxyacetone phosphate.

The third group of significantly regulated proteins is involved in organization of the cytoskeleton. Here, four proteins were found to be down-regulated being KTN1, ACTR3, ADD3 and MSN. KTN1 (1.2 -fold down-regulated) is known to be involved in kinesin-driven vesicle transport. ACTR3 (1.4-fold down-regulated) is component of the Arp2/3 complex that participates in the regulation of actin polymerization and mediating the formation of branched actin networks, while ADD3 (2.2-fold down-regulated) promotes the assembly of the spectrin-actin network. The function of MSN (1.4-fold down-regulated) is not yet fully resolved, but it is probably involved in connecting major cytoskeletal structures to the plasma membrane.

Interestingly, two proteins involved in iron homeostasis, TFRC (1.3-fold up-regulated) and FTH1 (2.7-fold down-regulated), were found to be dysregulated. TFRC is a cell surface receptor that is responsible for iron uptake, whereas FTH1 is necessary for iron storage in form of Fe^{3+} within the cell.

In sum, 46 proteins were significantly regulated in rotenone treated cells. Among the up-regulated proteins, several are involved in cell cycle, cytokinesis and spindle formation. Several down-regulated proteins were involved in energy metabolism and the organization of the cytoskeleton.

3.2.3.3 Protein-protein interaction network analysis and hub protein identification of rotenone treated HeLa cells

Protein-protein interaction (PPI) networks are a useful tool to understand the functional organization of the proteome (Chen et al. 2014). Furthermore, PPI networks are important sources of information connected to biological processes and metabolic functions of a cell (Asur, Ucar, and Parthasarathy 2007).

To identify interactions and pathway affiliations, the PPI networks of significant and/or 2-fold up- and down-regulated proteins upon rotenone treatment were analyzed using STRING (Figure 14 A and B). The evaluation of the 46 significantly altered proteins upon rotenone treatment already showed that the proteins are mainly involved in cell division processes, energy metabolism and organization of cytoskeleton (3.2.3.2).

Interestingly, the evaluation of the network build with up-regulated proteins revealed that proteins are mainly involved in cell cycle (Figure 14 C), spindle organization (Figure 14 D) and cytokinesis (Figure 14 E). The PPI network, which was built with down-regulated proteins, was too small to identify meaningful pathway affiliations (Figure 14 B).

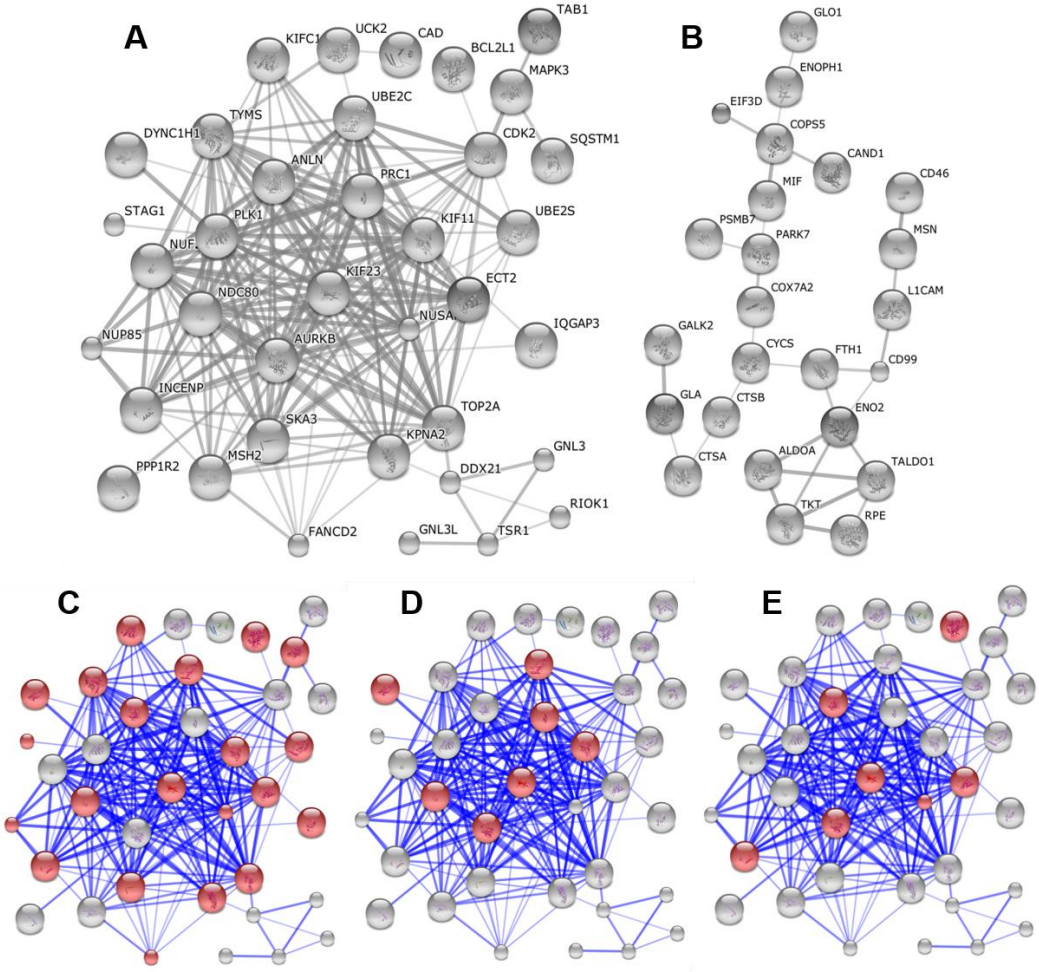

Figure 14: String network and pathway analysis of significant and/or 2-fold regulated proteins upon rotenone treatment (Gielisch and Meierhofer 2015). (A) Up-regulated network, (B) down-regulated network. (C-E) Network from A, highlighted in red: proteins of the GO category "biological process" (C) cell cycle, (D) spindle organization and (E) cytokinesis.

Proteins that interact with multiple partners play central roles in PPI networks and are called hub proteins (Higurashi, Ishida, and Kinoshita 2008). The "network analyzer" plugin for Cytoscape was used to identify hub proteins, based on degree, closeness centrality (CC) and betweenness centrality (BC) as key topological parameters. The degree of a node is defined as the number of connections that are associated with a protein (Azuaje 2014). The CC value is a measure of how fast information is spread from a given node to other reachable nodes in the network (Newman 2005). A node with a high CC value is likely to receive information faster

than others. The BC value is a measure of the influence a node has over the spread of information through the network (Newman 2005). A node with a high BC value has a large influence on the transfer of information through a network, by taking the shortest paths.

Identified hub proteins, derived from the up- or down-regulated PPI network, had to have a degree value of at least nine or three, respectively. Hub proteins extracted from these PPI networks (Figure 14 A and B) are listed in Table 5 with an additional description of their function.

Table 5: Hub proteins based on topological parameters betweenness (BC) and closeness centrality (CC) of the STRING network of differently regulated proteins upon rotenone treatment (Gielisch and Meierhofer 2015).

protein	protein name	degree	closeness centrality	betweenness centrality	function (extracted from uniprot.org)
Significant and or 2-fold up-regulated proteins upon rotenone treatment					
CDK2	cyclin-dependent kinase 2	18	0.6	0.210	cell cycle
TOP2A	DNA topoisomerase 2-alpha	20	0.643	0.135	segregation of daughter chromosomes
KPNA2	importin subunit alpha-1	18	0.621	0.114	functions in nuclear protein import
AURKB	aurora kinas B	22	0.621	0.100	correct chromosome alignment and segregation
PLK1	serine/threonine-proteinkinase	22	0.621	0.100	key regulator of cytokinesis
KIF11	kinesin-like protein KIF11	21	0.61	0.060	required for establishing a bipolar spindle
UBE2C	ubiquitin-conjugating enzyme	18	0.59	0.055	essential factor of the anaphase promoting complex/cyclosome
TYMS	thymidylate synthase	18	0.59	0.055	mitochondrial thymidylate biosynthesis pathway
NUF2	kinetochore protein Nuf2	20	0.6	0.016	required for kinetochore integrity
NDC80	kinetochore protein NDC80 homolog	19	0.59	0.013	chromosome segregation and spindle checkpoint activity
NUSAP1	nucleolar and spindle-associated protein 1	20	0.6	0.012	organization of mitotic spindle microtubules

Continued on next page

Table 5: Continued from previous page.

protein	protein name	degree	closeness centrality	betweenness centrality	function (extracted from uniprot.org)
KIF23	kinesin-like protein KIF23	19	0.59	0.009	component of the centralspindlin complex
MSH2	DNA mismatch repair protein Msh2	14	0.529	0.008	component of the post-replicative DNA mismatch repair system
PRC1	protein regulator of cytokinesis 1	19	0.59	0.008	key regulator of cytokinesis
ANLN	actin-binding protein anillin	18	0.581	0.006	required for cytokinesis
INCENP	inner centromere protein	15	0.522	0.004	key regulator of mitosis
ECT2	protein ECT2	17	0.571	0.002	component of the central spindle in complex
SKA3	spindle and kinetochore-associated protein 3	16	0.529	0.002	essential for proper chromosome segregation
FANCD2	fanconi anemia group D2 protein	9	0.468	0.001	required for maintenance of chromosomal stability
KIFC1	kinesin-like protein KIFC1	9	0.439	0.000	required for bipolar spindle formation
Significant and or 2-fold down-regulated proteins upon rotenone treatment					
CYCS	cytochrome c	3	0.311	0.656	heme carrying key player of the respiratory chain
FTH1	ferritin heavy chain	3	0.295	0.498	important for iron homeostasis
PARK7	parkinson disease protein 7	3	0.261	0.466	plays a significant role in antioxidative defense
COPS5	COP9 signalosome complex subunit 5	4	0.202	0.320	cellular and developmental processes
ENO2	gamma-enolase	5	0.261	0.300	glycolysis and gluconeogenesis

Continued on next page

Table 5: Continued from previous page.

protein	protein name	degree	closeness centrality	betweenness centrality	function (extracted from uniprot.org)
CD99	CD99 antigen	3	0.258	0.237	involved in T-cell adhesion processes
TALDO1	Transaldolase	4	0.217	0.042	balance of metabolites in the pentose-phosphate pathway
TKT	Transketolase	4	0.217	0.042	pentose phosphate pathway

Among the up-regulated hub proteins (Table 5) in rotenone treated cells, CDK2 and TOP2A show the highest BC values being 0.21 and 0.13, respectively, rendering them the main hub proteins in the network (Table 5). Furthermore, three other cell cycle proteins were identified to be hub proteins, being AURKB, PLK1 and NUSAP1. AURKB is a component of the chromosomal passenger complex (CPC), which has essential functions at the centromere, like ensuring correct chromosome alignment and segregation (Capalbo et al. 2012). The serine/threonine-protein kinase PLK1 performs several important functions throughout the M phase of the cell cycle, like regulating the centrosome maturation and spindle assembly (Neef et al. 2003; Yuan et al. 2002; Roshak et al. 2000). The two kinases, AURKB and PLK1, both regulate PRC1 (Glotzer 2009), a key regulator of cytokinesis, controlling the spatiotemporal formation of the midzone during the metaphase to anaphase transition (Hu, Coughlin, and Mitchison 2012). NUSAP1 has the capacity to bundle and stabilize microtubules and it may associate with chromosomes and promote the organization of surrounding mitotic spindle microtubules (Raemaekers et al. 2003).

The down-regulated hub proteins (Table 5) CYCS and FTH1 have the highest BC values being 0.66 and 0.5, respectively. CYCS is a heme carrying key player of the respiratory chain, which transfers electrons from complex III to complex IV. Several proteins involved in glycolysis and the pentose phosphate pathway were also found to be hub proteins among the down-regulated proteins, like TALDO1, ENO2 and TKT. Another hub protein is PARK7, which plays a significant role in antioxidative defense (Lev et al. 2008).

In conclusion, the PPI network of up-regulated proteins revealed that proteins are mainly involved in spindle organization, cell cycle and cytokinesis. The majority of up-regulated hub

proteins are also involved in cell division processes. Whereas many of the down-regulated hub proteins in rotenone treated cells play a role in the energy metabolism.

3.2.3.4 Pathway enrichment analysis of rotenone treated HeLa cells

Pathway analysis is a useful tool for gaining insight into the underlying biology of differentially regulated proteins, since it reduces complexity and increases the explanatory power (Khatri, Sirota, and Butte 2012).

The pathway enrichment tool GSEA was applied to reveal if an *a priori* defined set of proteins shows significant differences between rotenone treated and control cells. To be regarded as significant the p- and q-value of a pathway had to be ≤ 0.05.

While no significantly up-regulated KEGG pathways could be identified, pathways of the energy metabolism, such as glycolysis and gluconeogenesis, pentose phosphate pathway, galactose metabolism and glutathione metabolism were significantly down-regulated in rotenone treated cells (Table 6).

Table 6: GSEA analysis of proteome data, listed are significantly down-regulated KEGG pathways of rotenone treated HeLa cells.

KEGG Pathway	p-value	q-value
ribosome	0.000	0.000
cell adhesion molecules	0.000	0.001
pentose phosphate pathway	0.000	0.001
amino sugar and nucleotide sugar metabolism	0.002	0.009
glycolysis gluconeogenesis	0.000	0.008
galactose metabolism	0.004	0.020
cysteine and methionine metabolism	0.000	0.028
glutathione metabolism	0.007	0.045

To further investigate up-regulated proteins, the dataset was analyzed based on Gene Ontology (Table 7). Here, pathways involved in cell division processes and cytokinesis were significantly up-regulated in rotenone treated cells.

Table 7: GSEA analysis of proteome data, list of significantly up-regulated GO pathways of rotenone treated HeLa cells.

Pathway GO	p-value	q-value
cell division	0.000	0.000
cytokinesis	0.000	0.000
chromosome segregation	0.000	0.002
mitotic cell cycle	0.000	0.009
M phase of mitotic cell cycle	0.000	0.008
M phase	0.000	0.009
mitosis	0.000	0.012
DNA packaging	0.000	0.023
cell cycle process	0.000	0.024
spindle	0.000	0.022
cell cycle	0.000	0.021
peptide binding	0.000	0.028
Sh2 domain binding	0.000	0.032
cell cycle phase	0.000	0.044

Interestingly, the Reactome pathway “Respiratory electron transport” was not significantly (q-value 0.12; down-regulated on pathway level) regulated. In total, 40 of 77 proteins that are assigned to complex I-IV were identified (Figure 15 A). The identified subunits of the complexes I-IV were dysregulated, whereas the majority was down-regulated in rotenone treated cells (Figure 15 A).

Ten proteins were found to belong to the Reactome pathway “Formation of ATP by chemiosmotic coupling” (q-value 0.75; up-regulated on pathway level) (Figure 15 B). The ATP synthase (complex V) uses the proton motive force to generate ATP from ADP and a phosphate group, a process that is called chemiosmosis. Complex V is composed of two linked multisubunit complexes: the soluble catalytic core (F_1) and the membrane-spanning component (F_o), which comprises the proton channel. ATP synthase H^+ transporting subunits of the F_0 and F_1 portion were mainly up-regulated in rotenone treated cells.

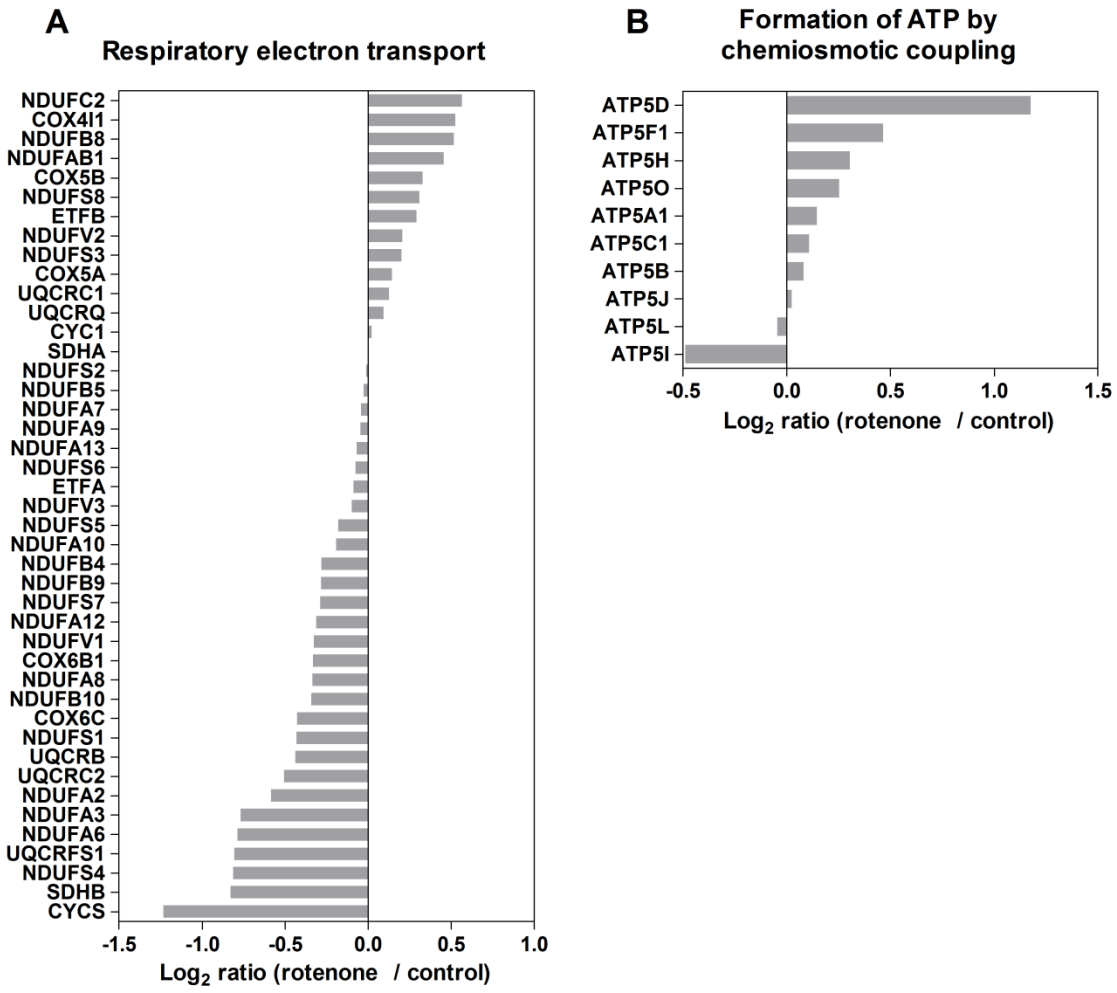

Figure 15: Regulated Reactome pathways and individual protein ratios between rotenone treated and control cells. An uneven regulation of complexes and their subunits is shown in (A) Respiratory electron transport and (B) Formation of ATP by chemiosmotic coupling.

3.3 Human cells lacking mtDNA

Cell lines lacking mtDNA (ρ^0 cells) are a very effective tool to study the consequences of an impaired OXPHOS system (Hashiguchi and Zhang-Akiyama 2009). Thus, a proteome and metabolome analysis of ρ^0 cells will lead to a better understanding of interactions between nuclear and mitochondrial genomes in mitochondrial diseases.

3.3.1 Verification of the mtDNA depletion in ρ^0 cells

Complete mtDNA depletion in ρ^0 cells was verified by PCR of nuclear and mtDNA encoded genes. Nuclear PCR products were detected in 143B.TK$^-$ and ρ^0 cells, but mtDNA derived PCR products were amplified only in 143B.TK$^-$ cells, confirming the mtDNA depletion of ρ^0 cells.

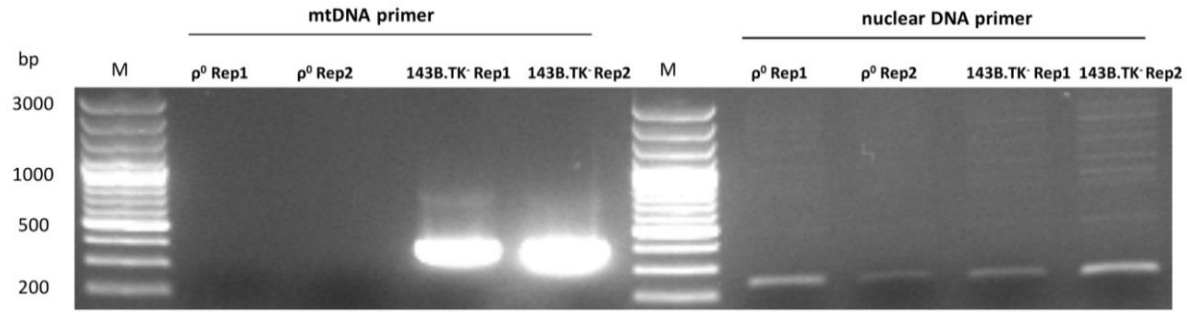

Figure 16: Verification of full mtDNA depletion in ρ⁰ cells by PCR. The mtDNA PCR product (399 bp) could only be amplified in 143B.TK⁻ cells, whereas the nuclear PCR product (238 bp) was detected in all samples. Shown are PCR products of the biological replicates (Rep1, 2) of ρ⁰ and parental cells (143B.TK⁻) (Aretz et al. 2016).

3.3.2 Metabolome profiling of ρ⁰ cells

Targeted metabolome profiling of 143B.TK⁻ and ρ^0 cells was performed, in order to reveal differences in metabolite abundances in mtDNA depleted compared to 143B.TK⁻ cells. As an additional quality criterion for metabolite identification and relative quantification, the MRM ion ratio method was applied.

In total, 103 metabolites in ρ^0 versus 143B.TK⁻ cells were identified with at least two transitions and three measured values per condition. From these, 44 were ≥ 1.5-fold and 20 were significantly (two-sample Student's t-test followed by a Benjamini-Hochberg multiple test correction with FDR < 0.05) altered between 143B.TK⁻ and ρ^0 cells (Figure 17). Metabolites belonging to the pyruvate metabolism and TCA cycle, pyrimidine metabolism and amino acids were color coded (Figure 17).

Components of the pyruvate metabolism and the TCA cycle, such as succinic acid (6-fold up-regulated in ρ^0 cells), oxalacetic acid (2.5-fold up-regulated) and lactic acid (2-fold up-regulated), citric acid (6-fold down-regulated) and cis-aconitic acid (2.5-fold down-regulated) were dysregulated in ρ^0 cells (Figure 17).

Metabolites of the pyrimidine metabolism, such as methylmalonic acid (6.5-fold up-regulated), uracil (5.4-fold up-regulated), thymidine (4.4-fold up-regulated), uridine (4.2-fold up-regulated), ureidopropionic acid (2.4-fold up-regulated), thymine (1.5-fold up-regulated) were up-regulated, whereas uridine monophosphate (1.6-fold down-regulated) and deoxyuridine (1.8-fold down-regulated) were down-regulated in ρ^0 cells (Figure 17).

Most of the detected amino acids were up-regulated, such as L-tryptophan (2.5-fold), L-leucine (2.5-fold), L-phenylalanine (1.9-fold), L-isoleucine (1.9-fold), L-methionine (1.9-fold) and L-valine (1.8-fold), except for the 2-fold down-regulation of proline.

In sum, metabolites of the pyruvate metabolism and TCA cycle, pyrimidine metabolism, as well as amino acids were found to dysregulated in ρ^0 cells.

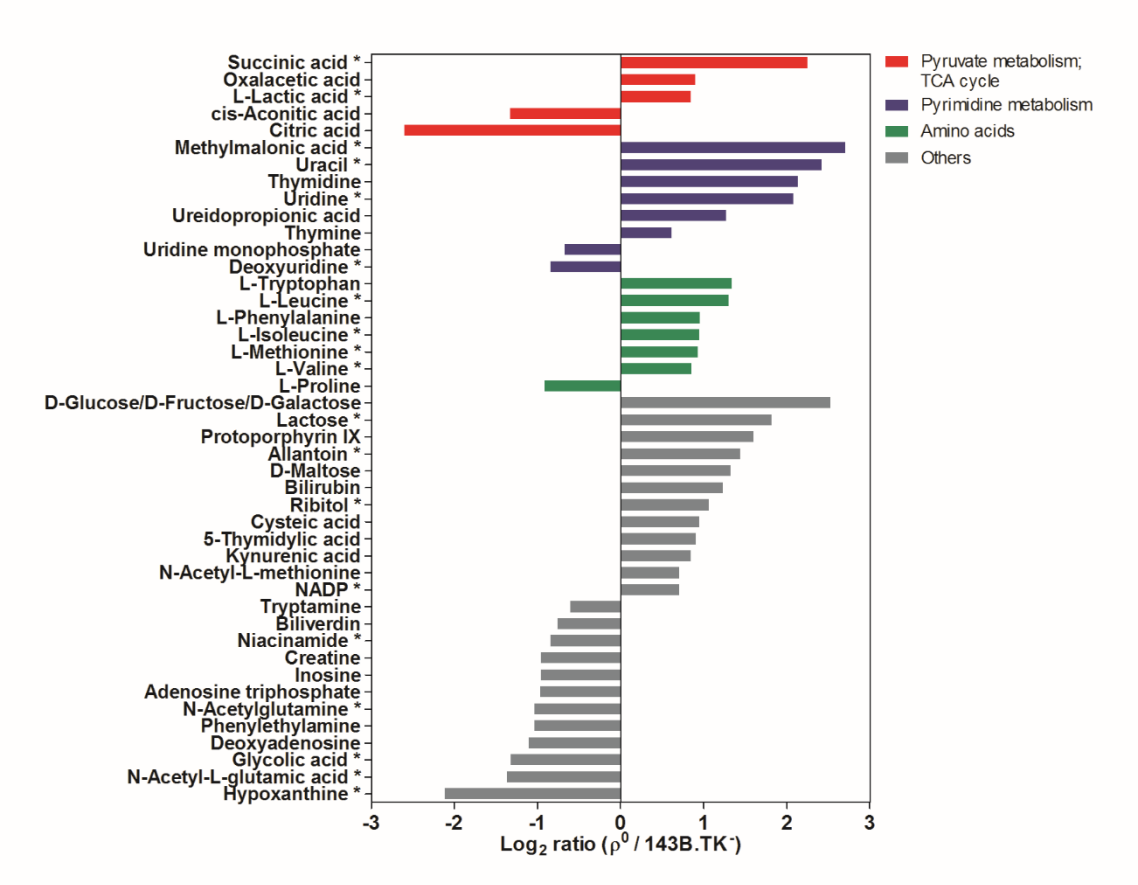

Figure 17: Regulated metabolites in ρ^0 versus parental cells. Shown are 44 ≥ 1.5-fold and/or significantly (adjusted p-value < 0.05; marked with an asterisk) changed metabolites. A grouping of compounds belonging to the pyruvate metabolism/TCA cycle (red), pyrimidine metabolism (blue), of amino acids (green) and other metabolites (grey) is color coded (Aretz et al. 2016).

3.3.3 Proteome profiling of ρ^0 cells

Proteome profiling of ρ^0 and parental cells was performed, in order to reveal differences in protein abundances in ρ^0 cells. For proteome profiling, tryptic peptides were fractionated by strong anion exchange (SAX) and strong cation exchange (SCX) chromatography. In total four biological replicates of ρ^0 and parental cells, including the SILAC label switches were analyzed in 124 LC-MS/MS runs. Around 1.4 million MS^2 spectra were identified, which belong to more than 8,000 protein groups with a least one peptide per protein group. Only peptides with ratios in all replicates were used for further data analysis. This resulted in a final protein group list with 4,815 entries, of which 2,708 were found to be significantly regulated (adjusted p-value < 0.05) (Figure 18, Table S5). The cutoff for significantly up- and down-regulated proteins was determined based on two standard deviations from the median of all proteins (n=4). By applying these criteria, 42 and 154 proteins were found to be significantly up- and down-regulated, respectively (Figure 18).

In order to identify mitochondrial proteins, a curated list of 1,158 genes with high confidence of mitochondrial localization derived from the Human MitoCarta2.0 (Calvo, Clauser, and Mootha 2015) was used. In total, 609 (13%) mitochondrial proteins could be identified in the dataset.

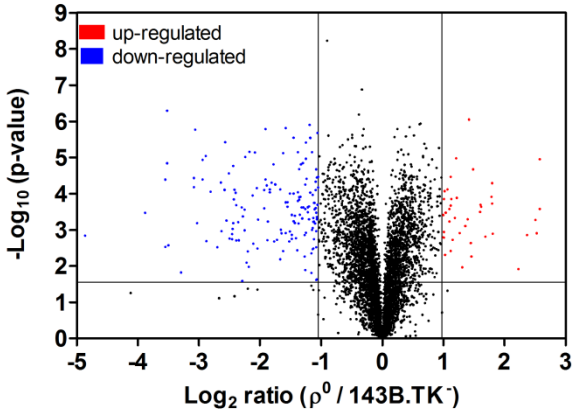

Figure 18: Volcano plot showing log_2 ratios of 4,815 identified proteins against the $–log_{10}$ of the p-value. The horizontal line (at 1.55) indicates the significance cutoff, whereas the vertical lines (-1.05; 0.98) are the cutoffs based on two standard deviations from the median of all (n=4) identified proteins. Highlighted in blue and red are down- or up-regulated proteins in ρ^0 cells, respectively (Aretz et al. 2016).

3.3.3.1 Reproducibility of the biological replicates

The reproducibility is tested, in order to obtain an assessment how reliable and valid the methodology and analysis is.

The biological replicates of the proteome, phosphoproteome and ubiquitylome analysis were tested by Pearson correlation and visualized in a multi-scatter plot (Figure 19 A-C). A statistically significant correlation was observed between the biological replicates of each analysis (Pearson correlation coefficient > 0.8, > -0.68; p-value < 0.0001) (Figure 19 A-C).

Thus, all experiments show a statistically significant correlation and are reproducible.

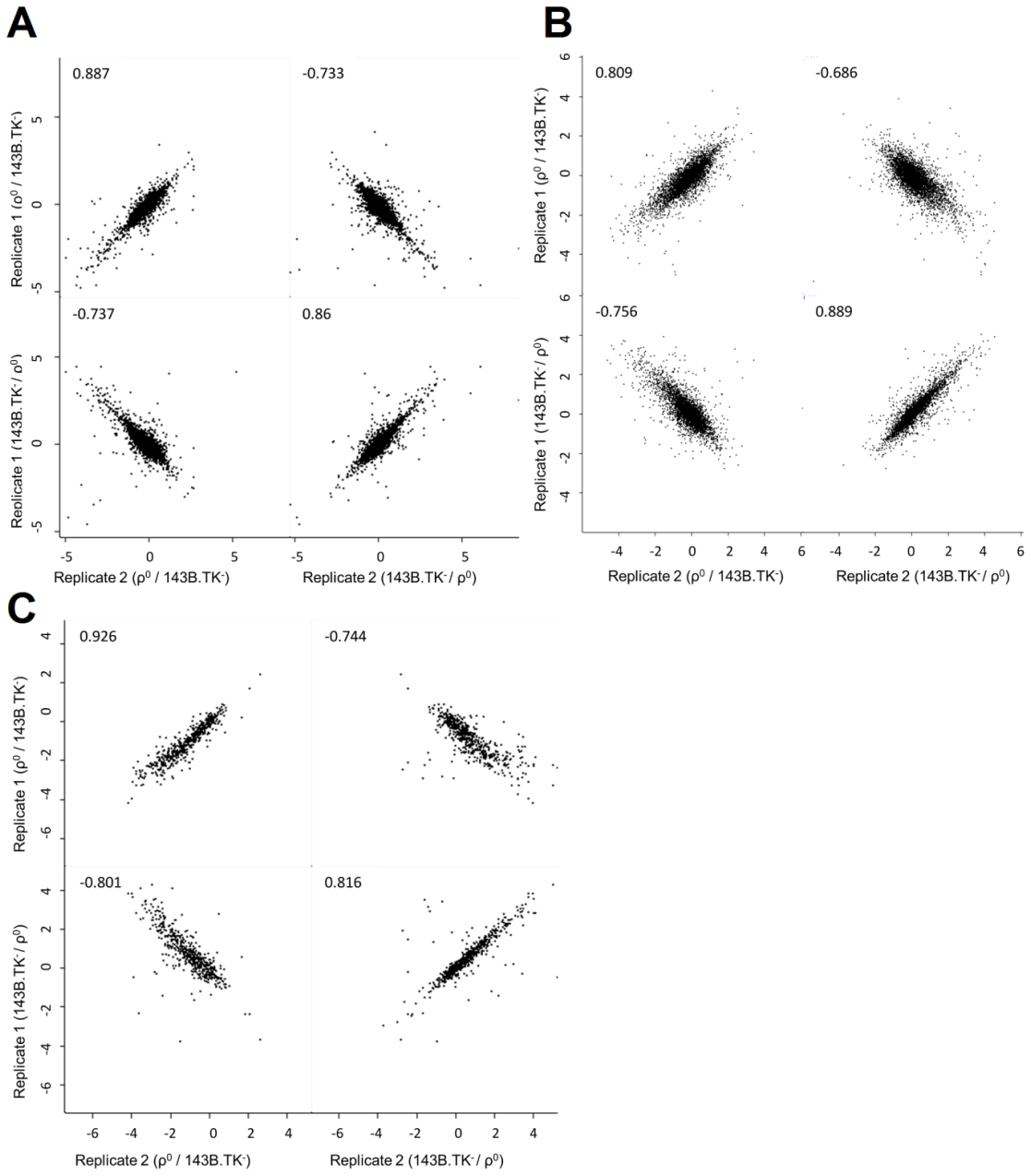

Figure 19: The Pearson correlation between ρ^0 versus 143B.TK$^-$ cells and the label switches are shown in scatter plots. Replicates are shown for the (A) proteome, (B) phosphoproteome and (C) ubiquitylome (Aretz et al. 2016).

3.3.3.2 Pathway enrichment analysis of ρ^0 cells

Pathway analysis is an advantageous tool for gaining insight into the underlying biology of differentially regulated proteins.

The pathway enrichment tool GSEA was applied to reveal if an *a priori* defined set of proteins shows significant differences between ρ^0 and 143B.TK$^-$ cells. Pathways with a p-value ≤ 0.05

and a q-value ≤ 0.25 were considered as significantly regulated (Table 8). Since down-regulated proteins are more abundant than up-regulated ones (Figure 18), a self-contained test for enriched pathways was performed, to confirm the GSEA results. GSEA uses a competitive approach, where the dataset is compared to a background dataset (Rahmatallah, Emmert-Streib, and Glazko 2012). Whereas a self-contained approach compares whether a gene set is differentially regulated between two phenotypes (Rahmatallah, Emmert-Streib, and Glazko 2012). The calculated p- and q-values are slightly different than the ones derived from GSEA, but still significant for all pathways shown in Table 8.

The analysis revealed five significantly down- and 26 significantly up-regulated Reactome pathways in ρ^0 cells (Table 8). Pathways of the energy metabolism, such as the respiratory electron transport, ATP synthesis by chemiosmotic coupling, the pyruvate metabolism and the TCA cycle and were found to be down-regulated in ρ^0 cells. The majority of pathways were up-regulated in ρ^0 cells (Table 8). Several signaling pathways, like $G_{12/13}$ and Rho GTPases and G-protein-coupled receptor (GPCR) mediated events and pathways involved in cell cycle progression, like meiosis, mitotic prometaphase, meiotic synapsis and recombination were found to be up-regulated as well.

Table 8: Significantly regulated Reactome pathways in ρ^0 versus parental cells, analyzed by GSEA (thresholds: p-value ≤ 0.05; q-value ≤ 0.25; average of valid values) (Aretz et al. 2016).

Reactome pathway	GSEA			Global test	
	Protein entries	p-Value	q-Value	p-Value	q-Value
Down-regulated pathways in ρ^0 cells					
respiratory electron transport	41	0.00	0.00	0.00	0.00
TCA cycle and respiratory electron transport	77	0.00	0.00	0.00	0.00
respiratory electron transport ATP synthesis by chemiosmotic coupling and heat production by uncoupling proteins	51	0.00	0.00	0.00	0.00
pyruvate metabolism and citric acid TCA cycle	28	0.00	0.04	0.00	0.00
TCA cycle	17	0.01	0.24	0.00	0.00
Up-regulated pathways in ρ^0 cells					
$G_{12/13}$ α signaling events	24	0.00	0.02	0.02	0.04
deposition of new CENPA containing nucleosomes at the centromere	15	0.00	0.03	0.03	0.06
signaling by Rho GTPases	40	0.00	0.03	0.04	0.07
meiosis	34	0.00	0.03	0.00	0.00
meiotic synapsis	19	0.00	0.05	0.00	0.00
GPCR downstream signaling	46	0.00	0.08	0.00	0.01
chromosome maintenance	53	0.00	0.16	0.00	0.01
signaling by GPCR	74	0.00	0.16	0.00	0.00
mitotic prometaphase	61	0.00	0.19	0.00	0.01
hormone sensitive lipase HSL mediated triacylglycerol hydrolysis	7	0.00	0.14	0.00	0.00
apoptosis induced DNA fragmentation	11	0.00	0.04	0.06	0.10
packaging of telomere ends	7	0.01	0.15	0.00	0.00
cell cell communication	38	0.01	0.19	0.05	0.08
regulation of insulin secretion by acetylcholine	5	0.01	0.18	0.01	0.03
Rap1 signaling	7	0.01	0.15	0.02	0.04
Gap junction trafficking	8	0.01	0.18	0.01	0.02
EGFR downregulation	19	0.01	0.18	0.03	0.05
recycling pathway of L1	19	0.01	0.19	0.01	0.02

Continued on next page

Table 8: Continued from previous page.

Reactome pathway	GSEA			Global test	
	Protein entries	p-Value	q-Value	p-Value	q-Value
gap junction degradation	8	0.01	0.14	0.01	0.02
meiotic recombination	20	0.02	0.14	0.00	0.01
glucagon signaling in metabolic regulation	10	0.02	0.19	0.07	0.10
GPCR ligand binding	7	0.02	0.19	0.00	0.00
regulation of insulin secretion by glucagon like peptide1	14	0.02	0.18	0.07	0.10
factors involved in megakaryocyte development and platelet production	55	0.02	0.23	0.00	0.01
RNA Pol I promoter opening	9	0.03	0.18	0.06	0.10
G_i α signaling events	12	0.04	0.22	0.00	0.00

A detailed view on individual protein ratios of the pathways pyruvate metabolism, TCA cycle and respiratory electron transport reveals an uneven regulation of complexes and their subunits (Figure 20).

Within the pyruvate metabolism an up-regulation of the anaerobic part, the lactate dehydrogenase A (LDHA, 1.2-fold), but an unchanged ratio for lactate dehydrogenase B (LDHB, 1.0-fold), was detected (Figure 20 A). Both proteins catalyze the reversible conversion of pyruvate to lactic acid and simultaneously inter-convert NADH and NAD^+ to restore it for glycolysis. Within the TCA cycle individual enzymes were unregulated such as malate dehydrogenase 2 (MDH2, 1.0-fold) and citrate synthase (CS, 1.0-fold) or showed an up-regulation, like fumarase (FH, 1.1-fold). This dysregulation was also observed within enzyme complexes, like succinate-CoA ligase and isocitrate dehydrogenase, in which some subunits were decreased (IDH3G, 1.4-fold; SUCLA2, 2.6-fold), while others were increased (IDH2, 1.1-fold; SUCLG2, 1.1-fold) in ρ^0 cells.

A significant down-regulation of the entire respiratory electron transport chain was observed (Table 8, Figure 20 B), since all mitochondrial encoded subunits were missing in ρ^0 cells. The majority of subunits were up to 17-fold decreased, but an up-regulation of the complex III subunit cytochrome c1 (CYC1, 1.3-fold) and the electron carrier cytochrome c (CYCS, 2-fold) was observed in ρ^0 cells. Interestingly, subunits of the ATP synthase were unregulated (average 1.0-fold) in ρ^0 cells.

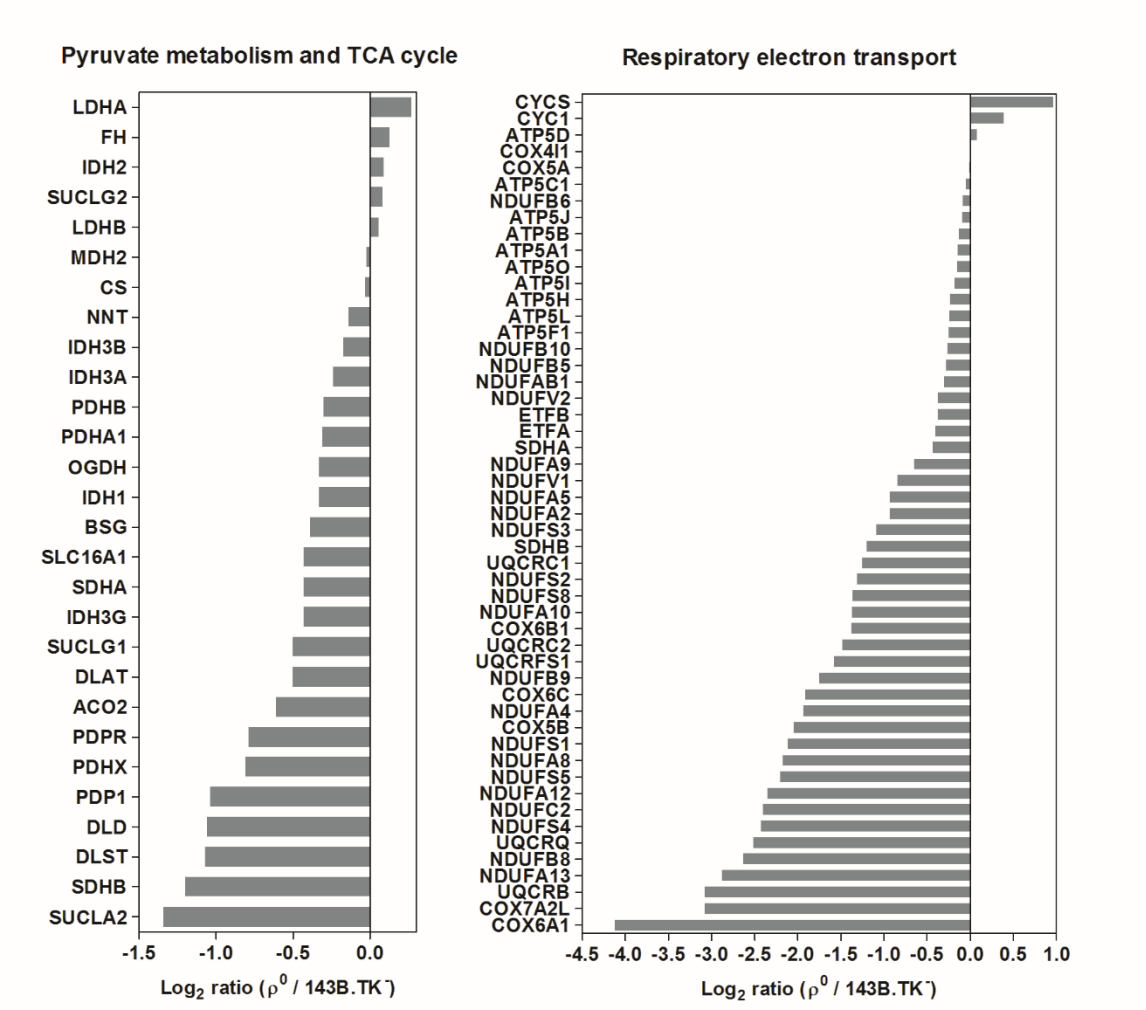

Figure 20: Significantly down-regulated Reactome pathways and individual protein ratios between ρ^0 and parental cells. An uneven regulation of complexes and their subunits is shown in (A) Pyruvate metabolism and TCA cycle and (B) Respiratory electron transport and ATP synthesis by chemiosmotic coupling and heat production by uncoupling (Aretz et al. 2016).

3.3.3.3 Protein-protein interaction network analysis of ρ^0 cells

PPI networks help to understand the functional organization of the proteome and they provide important information connected to biological processes and metabolic functions of a cell (Asur, Ucar, and Parthasarathy 2007).

To identify interactions and pathway affiliations of ρ^0 cells, the PPI networks of significantly down-regulated proteins were analyzed using STRING (Figure 21). The PPI network, which was built with up-regulated proteins, was too small to identify meaningful pathway affiliations (data not shown).

The PPI network features proteins of the respiratory electron transport, the TCA cycle and mitochondrial 55S ribosomal proteins (Figure 21). Mitochondrial 55S ribosomal proteins were on average 3-fold down-regulated in ρ^0 cells, but cytoplasmic 80S ribosomal proteins were unregulated (1.1-fold down-regulated) (Figure 22).

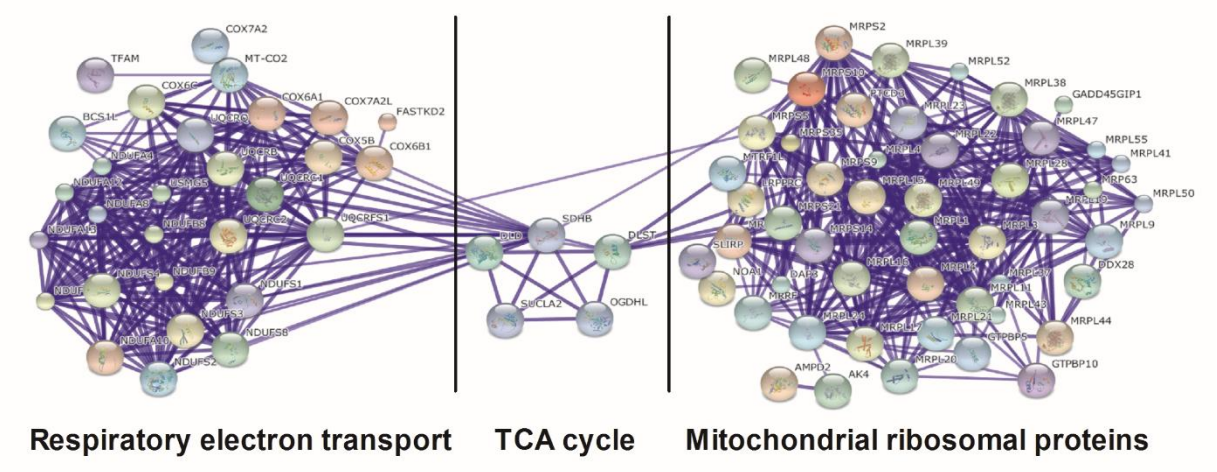

Figure 21: PPI network analysis of significantly down-regulated proteins in ρ^0 cells (average of valid values), featuring subunits of the respiratory electron chain, proteins involved in the TCA cycle and mitochondrial 55S ribosomal proteins. The proteins that are known to interact with each other are linked with a blue line (Aretz et al. 2016).

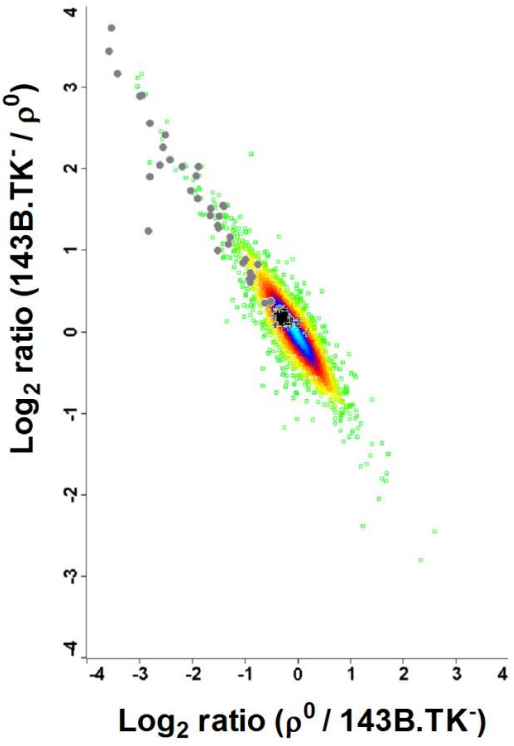

Figure 22: The density scatter plot shows unregulated cytoplasmic 80S ribosomal proteins, indicated by black crosses and mitochondrial 55S ribosomal proteins indicated by grey dots (Aretz et al. 2016).

3.3.3.4 Ubiquitylome profiling of ρ^0 cells

Protein ubiquitination is a PTM in which the polypeptide ubiquitin is covalently attached to lysine residues of the target protein. The ubiquitin system is more complex compared to phosphorylation, because ubiquitin is able to form polymers of at least eight different linkages (Komander and Rape 2012). This linkage type determines whether a protein is degraded by the proteasome or serves to attract proteins to initiate signaling cascades or be internalized (Komander 2009).

The identification of ubiquitinated peptides by MS relies on the identification of a 114.1 Da diglycine (GG) remnant on lysine residues (K-ε-GG), which is derived from the C-terminus of ubiquitin, following a tryptic digest (Denis et al. 2007). The proteome-wide enrichment of ubiquitination is based on this distinct feature of a K-ε-GG.

A specific GG-antibody was used for immunopurification of ubiquitinated peptides. The proteasome inhibitor MG132 could have been used to accumulate ubiquitinated peptides, but was not applied in order to avoid an impact on PTMs and the metabolome and proteome in general. In total, 1,398 ubiquitinated sites, of which 900 were high confidence sites belonging to 551 proteins, were identified (Table S4) (Aretz et al. 2016). 319 ubiquitinated sites were down- and 33 were significantly up-regulated (Figure 23). The applied cutoffs were based on two standard deviations from the median of unmodified peptides (Figure 23, shown in red).

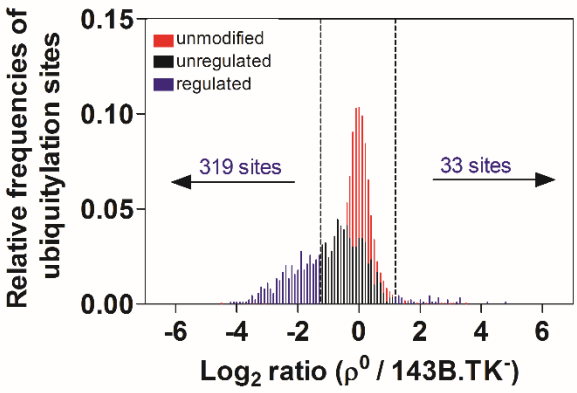

Figure 23: Distribution of relative frequencies of ubiquitination sites in ρ^0 versus parental cells (average of replicates; n=1-4). Log_2 ratios of unmodified peptides (red), unregulated ubiquitination sites (black) and regulated ubiquitination sites (blue). The cutoff value for significantly regulated PTM sites was based on two standard deviations from the median of unmodified peptides (dotted lines: -1.2; 1.2) (Aretz et al. 2016).

The majority of identified peptides were de-ubiquitinated in ρ^0 cells. Thus, the gene list of significantly de-ubiquitinated sites was subjected to the gene set enrichment analysis tool of the DAVID Bioinformatics Resources (D. W. Huang, Sherman, and Lempicki 2009b; D. W. Huang, Sherman, and Lempicki 2009a), and analyzed by gene ontology (GO) "molecular function" (GOTERM_MF_FAT). For the analysis, the list of all ubiquitination sites was used as background set.

The enrichment was computed and the resulting list of de-ubiquitinated proteins of the GO category "molecular function" (GOMF) displayed the following altered pathways, among others: symporter activity, structural constituent of cytoskeleton and ribosomes.

Proteins with a symporter activity, like solute carrier (SLC) proteins were on average 5-fold (Figure 24 A) and 80S ribosomal proteins were on average 3-fold (Figure 24 B) de-ubiquitinated in ρ^0 cells, while the protein abundancies were not altered. Several proteins of the cytoskeleton (GOMF "structural constituent of cytoskeleton"), like tubulin subtypes (TUBB, TUBB4B, TUBB4A, TUBA4A, TUBA1C, TUBB2B, TUBB2A) and vimentin were up to 4-fold de-ubiquitinated in ρ^0 cells.

Table 9: DAVID analysis of de-ubiquitinated sites in ρ^0 cells. Listed are regulated pathways of the GO category "molecular function".

GO category molecular function	p-value	adjusted p-value
symporter activity	0.003	0.357
structural molecule activity	0.003	0.586
actin binding	0.014	0.634
cytoskeletal protein binding	0.013	0.686
solute:cation symporter activity	0.012	0.752
structural constituent of cytoskeleton	0.026	0.774
amine transmembrane transporter activity	0.026	0.774
structural constituent of ribosome	0.036	0.832
anion:cation symporter activity	0.053	0.904
amino acid transmembrane transporter activity	0.053	0.904
GTPase activity	0.084	0.965

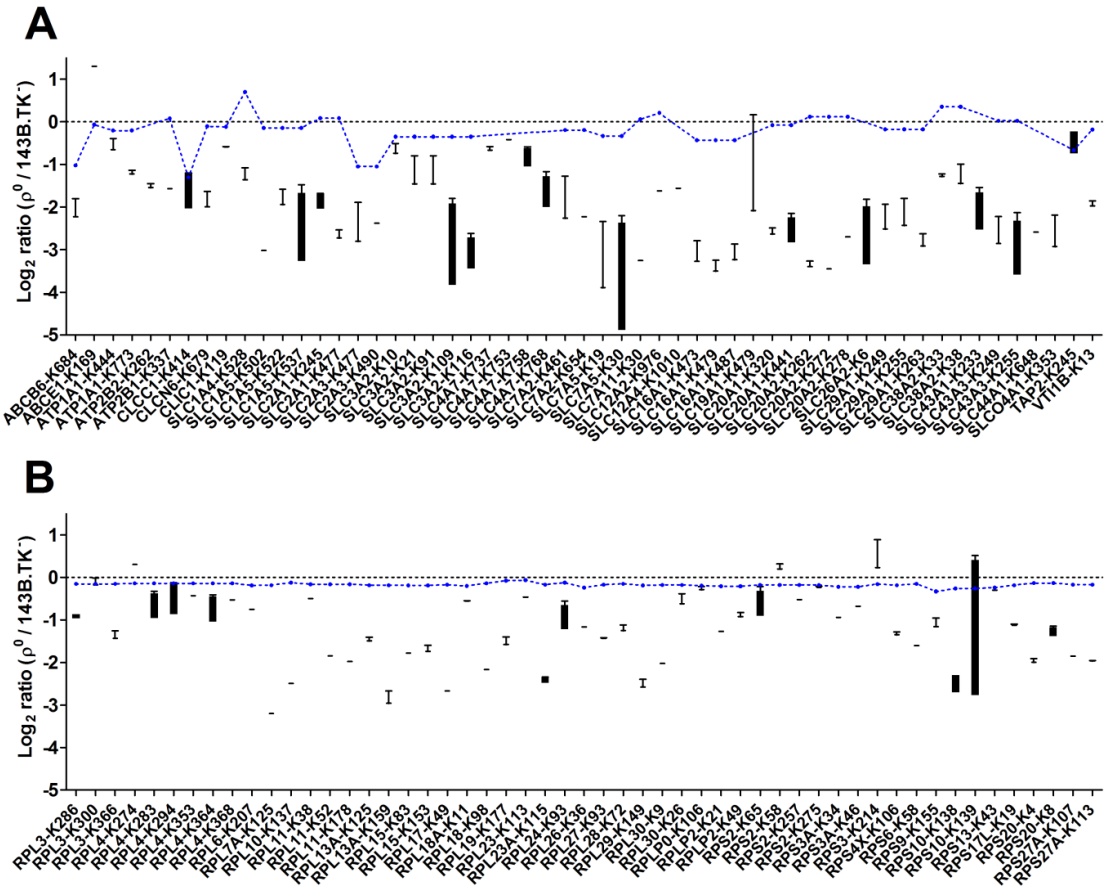

Figure 24: De-ubiquitinated proteins in ρ⁰ cells. Proteins and their specific de-ubiquitination sites are shown for (A) SLC transporter proteins and other transporter or channel proteins and (B) cytosolic ribosomal proteins. The log₂ ratios of all replicates (n=1-4) are shown (or their inverse for the label-switch experiments) in a box plot. For comparison, the mean of according log₂ protein ratios is indicated by connected blue dots (Aretz et al. 2016).

OTU domain-containing protein 7B (OTUD7B) was one of the most de-ubiquitinated proteins (18-fold) in ρ^0 cells. OTUD7B has a de-ubiquitination activity toward 'Lys-11', 'Lys-48' or 'Lys-63'-linked polyubiquitination and mediates de-ubiquitination of epidermal growth factor receptor (EGFR), which can lead to recycling of EGFR to the plasma membrane (Mizuno et al. 2005; Aretz et al. 2016). EGFR itself was 8-fold de-ubiquitinated in ρ^0 cells and is known to activate several signaling cascades, like the mitogen-activated protein kinase (MAPK), Protein kinase B (Akt) and c-Jun N-terminal kinase (JNK) pathways (Avraham and Yarden 2011).

Four mitochondrial ATP synthase subunit beta (ATP5B) sites were found to be more ubiquitinated (average 15-fold) in ρ^0 cells than in the parental cell line. This catalytic subunit of the ATPase (F_1 part) is essential for ATP consumption in ρ^0 cells (Aretz et al. 2016).

Many proteins with increased ubiquitination patterns are involved in cell cycle or DNA replication, such as cancer susceptibility candidate 5 (CASC5), eukaryotic translation elongation factor 1 alpha 1 (EEF1A1), DNA-directed RNA polymerase II subunit RPB1 and 2 (POLR2A, POLR2B), DNA polymerase subunit gamma-1 (POLG), anaphase-promoting complex subunit 1 (ANAPC1) (Aretz et al. 2016).

In sum, the majority of identified peptides were de-ubiquitinated in ρ^0 cells. These were found to be enriched in pathways, such as structural constituent of the cytoskeleton and ribosomes as well as amino acid transporter activities. Among the proteins with increased ubiquitination patterns were the ATP synthase subunit beta and many proteins involved in cell cycle or DNA replication.

3.3.3.5 Phosphoproteome profiling of ρ^0 cells

Phosphorylation is the reversible addition of phosphate to serine, threonine or tyrosine residues, which regulates the majority of all cellular processes, like cell cycle, growth, apoptosis and signal transduction pathways (Humphrey et al. 2015). In order to understand these biological processes on the molecular level, the characterization of phosphorylated proteins is required. Since phosphorylation is a dynamic process, quantification of these phosphorylation events is crucial. Usually, the phosphorylated form of a protein has low stoichiometry relative to its non-phosphorylated counterpart (Beausoleil et al. 2004). A global analysis of serine-, threonine- and tyrosine-phosphorylation is achieved by fractionation of tryptic peptides using SCX and subsequent enrichment by TiO_2. Phosphorylated peptides are separated from non-phosphorylated peptides by SCX at pH 2.7. At this pH lysine, arginine, histidine and the amino terminus of a peptide are positively charged. Thus, most tryptic peptides carry a net solution charge state of 2^+ and since a phosphate group maintains a negative charge at acidic pH values, the net charge state of a phosphorylated peptide is generally 1^+ (Beausoleil et al. 2004). Due to its high affinity for phosphorylated peptides TiO_2 can be used to enrich phosphorylated peptides from complex samples.

The phosphoproteome was analyzed by applying SCX separation followed by TiO_2 enrichment to elucidate the impact of the mtDNA depletion. In total, 14,905 phosphorylation sites were detected, of which 9,051 were high confidence sites and belonged to 3,371 proteins (Table S3)

(Aretz et al. 2016). 918 phosphorylation sites were significantly down- and 236 were significantly up-regulated (Figure 25).

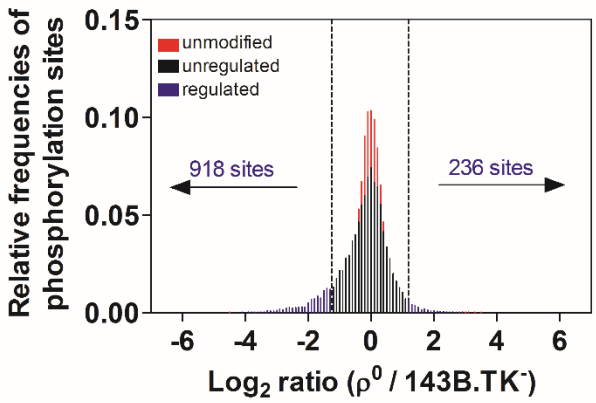

Figure 25: Distribution of relative frequencies of phosphorylation sites in ρ^0 versus parental cells (average of replicates; n=1-4). Log_2 ratios of unmodified peptides (red), unregulated phosphorylation sites (black) and regulated phosphorylation sites (blue). The cutoff value for significantly regulated PTM sites was based on two standard deviations from the median of unmodified peptides (dotted lines: -1.2; 1.2) (Aretz et al. 2016).

Gene lists of significantly up- and down-regulated phosphorylation sites was subjected to the gene set enrichment analysis tool of the DAVID Bioinformatics Resources (D. W. Huang, Sherman, and Lempicki 2009b; D. W. Huang, Sherman, and Lempicki 2009a), and analyzed by gene ontology (GO) “biological process”. For the analysis, the list of all phosphorylation sites was used as background set. The enrichment of up-regulated phosphorylated proteins did not reveal meaningful data, because the dataset was too small.

The enrichment was computed using DAVID, the resulting list of down-regulated phosphorylated proteins of the GO category “biological process” revealed two main processes, GTPase-related signal transduction and cytoskeleton organization (Table 10).

Table 10: DAVID analysis of dephosphorylated proteins in ρ^0 cells. Listed are regulated pathways of the GO category "biological process".

GO category biological process	p-value	adjusted p-value
regulation of small GTPase mediated signal transduction	0	0.001
regulation of Ras protein signal transduction	0	0.001
regulation of Rho protein signal transduction	0	0.026
regulation of microtubule-based process	0.002	0.458
regulation of cytoskeleton organization	0.001	0.523
regulation of Ras GTPase activity	0.004	0.700
regulation of microtubule cytoskeleton organization	0.004	0.705
chemical homeostasis	0.008	0.871

3.3.4 Measurement of TCA cycle enzyme activities of ρ^0 cells

Proteome and metabolome profiling revealed an uneven regulation of metabolites and proteins involved in the TCA cycle (Figure 17, Figure 20) (Aretz et al. 2016). To further investigate on this, enzyme activities of individual TCA cycle enzyme activities were determined, in order to explore how these activities are correlated to according protein abundances and metabolite levels (Table 11).

Enzymatic activities of the TCA cycle proteins citrate synthase (CS), isocitrate dehydrogenase 2 (IDH2), malate dehydrogenase 2 (MDH2) and fumarase (FH) were determined. While the activities of CS and IDH2 did not change significantly between the ρ^0 and parental cell line, the activities of MDH2 and FH varied significantly. The enzyme activities for CS and FH correlated well with the protein abundances (CS, 1.0-fold; FH, 1.1-fold up-regulated in ρ^0 cells), whereas MDH2 and IDH2 did not correlate (MDH2, 1.0-fold; IDH2, 1.1-fold up-regulated in ρ^0 cells).

Table 11: Enzyme activities of TCA cycle proteins in ρ^0 and 143B.TK$^-$.

Enzyme	ρ^0 [mU/mg of protein] ± SD	143B.TK$^-$ [mU/mg of protein] ± SD	p-value
CS	31 ± 3	28 ± 2	0.161
IDH2	13 ± 1	16 ± 2	0.116
MDH2	504 ± 91	161 ± 19	0.003
FH	25 ± 1	13 ± 4	0.011

4 Discussion

4.1 Evaluation of MRMs and MRM ion ratios and identifying inosine 5'-monophosphate by applying MRM ion ratios

Metabolome profiling focuses on the analysis of a large number of different molecules in a wide concentration range. This is challenging since metabolites are chemically very diverse and their concentration ranges from pM to mM. Usually, metabolites are identified by only one MRM, but if an endogenous isobaric compound is present at a high concentration it could produce a variety of product ions at relevant abundances. The signal intensity of the monitored product ions is explained by the too high precursor abundance (Schürmann et al. 2009). Therefore, the calculation of ion ratios is a useful method to reduce the risk of false-positive findings, which can also originate from impure Q1 isolation (Yan and Yan 2015), co-eluting isobaric compounds, wrong database entries or incorrect peak picking.

In this study, the linear range of the mass spectrometer and the robustness of MRM ion ratios were tested by analyzing a mixture containing six amino acids. In order to demonstrate the use of MRM ion ratios to avoid false-positive identifications from a complex biological sample, IMP was used as an example (Figure 9).The results clearly present the accuracy and robustness that can be derived for metabolome profiling by using three MRMs per target molecule, while the linear range spanned three orders of magnitude (Table 2, Figure 8).

To date there is an insufficient discussion about the importance of using multiple transitions for compound identification (Schürmann et al. 2009). The need of a third transition was revealed in a pesticide residue analysis using LC-MS/MS to demonstrate that the identification of sebuthylazine was false-positive (Schürmann et al. 2009). In this study a coeluting interfering matrix compound resulted in product ions that perfectly correspond to the MRM of two sebuthylazine transitions (Schürmann et al. 2009).

In summary, the use of three MRMs and their MRM ion ratios is essential for robust and unambiguous identification and quantification of metabolites originating from complex biological samples (Gielisch and Meierhofer 2015).

4.2 Increase of proteins involved in cell division processes and decrease of cytoskeleton related proteins upon complex I inhibition by rotenone

In order to mimic a complex I deficiency, HeLa cells were treated with the complex I specific inhibitor rotenone. Afterwards, proteome and metabolome analysis was performed. A PPI network and pathway enrichment analysis as well as the evaluation of significantly up-regulated proteins in rotenone treated cells revealed major changes in cell cycle, cytokinesis and spindle formation processes. Significantly down-regulated proteins were found to be involved in the organization of the cytoskeleton.

The observed mechanisms could be caused by complex I independent or dependent effects of rotenone.

Chromosomes, spindle and centriole configurations of rotenone treated mammalian cells have been shown to be grouped in a spherical mass near the cell center (Barham and Brinkley 1976). These results are identical to mitotic cells arrested with colcemid, a microtubule assembly inhibitor (Barham and Brinkley 1976). Furthermore, rotenone depolymerizes spindle microtubules, induced by binding of rotenone to tubulin, and suppresses reassembly of microtubules in living HeLa cells (Srivastava and Panda 2007). Thus, the chromosomes are not properly attaching to the microtubules and this results in a perturbed chromosome alignment at the metaphase plate (Srivastava and Panda 2007). In summary, these results suggest that rotenone arrests mitosis in mammalian cells by inhibition of spindle microtubule assembly (Barham and Brinkley 1976).

A deficiency in the energy converting system and oxidative stress can lead to cytoskeletal changes (Annunen-Rasila et al. 2007). While osteosarcoma cells lacking complex I show minor proteomic and cytoskeletal changes, a lack of mtDNA leads to more dramatic changes like a collapsed vimentin network (Annunen-Rasila et al. 2007). Furthermore, the expression of cell cycle proteins is up-regulated under stress conditions,

like oxidative stress and the presence of DNA damaging agents (Currais, Hortobágyi, and Soriano 2009). In another part of this study, mtDNA depleted cells were analyzed (Aretz et al. 2016). Here, a significant up-regulation of pathways involved in cell cycle progression, like meiosis, mitotic prometaphase, meiotic synapsis and recombination was found as well. The down-regulation of cytoskeleton proteins could result from the induced complex I deficiency and an impaired ROS defense, as indicated by down-regulation of the glutathione metabolism and individual metabolites like NADPH, GSH and GSSG (Table 6, Figure 11, Table S6). Thus, due to similarities in literature and findings from the study investigating ρ^0 cells, a complex I dependent mechanism of rotenone is very likely.

Deficiency of complex I is a common cause for Leber's hereditary optic neuropathy (LHON), a respiratory chain disorder caused by pathogenic mutations in the mtDNA. Histopathologic features of LHON are a disturbed axonal flow, such as clumps of mitochondria in the retrolaminar sections of remaining axons, accumulation of debris or microtubule depletion (Kirches 2011). Furthermore, the microtubule system has an impact on the pathogenesis of neurodegenerative disorders (Cappelletti et al. 2015), such as peripheral neuropathy and loss of axons in many kinds of brain neurons as well as familial amyotrophic lateral sclerosis (ALS) (B. N. Smith et al. 2014; Tischfield et al. 2010).

In conclusion, the increase of cell cycle associated proteins is a side effect of the cytoskeletal changes, caused by the deficiency in the energy converting system. The impaired cytoskeleton arrests cell cycle progression during mitosis and leads to an overexpression of proteins to rescue mitosis. Similar mechanism could be found in respiratory chain diseases, since alterations of the cytoskeleton are a known feature (Annunen-Rasila et al. 2007). Thus, a rotenone induced complex I deficency is a suitable model to study regulatory mechanisms of respiratory chain diseases.

4.3 Respiratory chain and TCA cycle fail to provide ATP for rotenone treated HeLa cells

The metabolome and proteome profiling of rotenone treated cells revealed a down-regulation of the respiratory chain and TCA cycle. Most affected metabolites were FMN, FAD and ADP from the respiratory chain, citric acid and cis-aconitic acid from the TCA cycle and $NADP^+$, NAD^+ and NADPH which are involved in redox reactions. Rotenone is known to block the ubiquinone-binding site within complex I. Consequently, the electron transfer via FMN to ubiquinone is prevented and the respiratory chain is interrupted, explaining the observed down-regulation of FMN upon rotenone treatment (Figure 11).

The respiratory electron transport was found to be down-regulated on pathway level, but the corresponding complexes were dysregulated (Figure 15). Electron transport chain assembly requires the coordination between nuclear and mitochondrial genomes. Thus, after assembly of mtDNA encoded complex I subunits, the nuclear encoded subunits are assembled (Heo et al. 2012). This is a dynamic process in which subunits and subassemblies, respectively, may be differentially regulated or exchanged with pre-existing ones (Lazarou et al. 2009; Fernández-Vizarra and Zeviani 2015; Mick, Fox, and Rehling 2011; Seok et al. 2013). In conclusion, dysregulations within complexes of the respiratory chain can be caused by a stepwise assembly and intermediate complexes might be differentially regulated.

Due to the down-regulation of the respiratory chain and the dysregulation of complexes, the creation of the essential proton gradient across the inner mitochondrial membrane could be impaired. To maintain this gradient the ATP synthase is fully reversible, so a proton gradient can be generated by ATP hydrolysis (Yasuda et al. 1998; C. P. Smith and Thorsness 2005; Adachi et al. 2007). Together with the adenine nucleotide translocator (ANT) that exchanges ATP^{4-} against ATP^{3-}, this pathway contributes to maintain the membrane potential (Buchet and Godinot 1998). Since the F_1 complex of the ATP synthase is the catalytic-domain that synthesizes and hydrolyzes ATP, respectively, it is comprehensible that the vast majority of subunits were up-regulated (Figure 15 B). This mechanism could further explain the 7-fold elevated level of CDP-choline in rotenone treated cells (Figure 11), since CDP-choline is known to restore the

activity of mitochondrial ATP synthase and membrane Na^+/K^+ ATP synthase (Secades 2011). Additionally, a 4-fold up-regulation of choline-phosphate cytidylyltransferase A (PCYT1A), which catalyzes the synthesis of CDP-choline, was detected in the proteome profiling (Table S2). In conclusion, the majority of ATP synthase subunits were up-regulated in rotenone treated cells, in order to maintain an electrochemical gradient across the inner mitochondrial membrane by ATP hydrolysis.

Most of the detected metabolites were not significantly regulated (Table S6), maybe due to a high metabolic flux. Nevertheless, the TCA cycle showed reduced metabolite levels, being the lowest for citric acid and cis-aconitic acid. Furthermore, coenzyme A (CoA), acetyl-CoA, succinic acid and oxalacetic acid were down-regulated in rotenone treated cells. Typically, cancer cell lines compensate an energy lack by up-regulating glycolysis, the pentose phosphate pathway or galactose metabolism, but these pathways were significantly down-regulated upon rotenone treatment (Table 6). Based on a lack of pyruvate that is normally generated via glycolysis, the capacity of the TCA cycle is compromised (Das, Steuerwald, and Illsinger 2010). Thus, rotenone treated cells must have a lack of energy, since important pathways of the energy metabolism fail to provide enough ATP. A study of tissues derived from patients with the mitochondrial disease MELAS revealed that neurons with high energy requirements are selectively lost in MELAS (Tzoulis and Bindoff 2012). While many of the remaining neurons show eosinophilic necrosis, a type of death that is associated with cerebral energy deprivation (Tzoulis and Bindoff 2012).

In conclusion, energy producing pathways such as the respiratory chain, glycolysis, the pentose phosphate pathway, the galactose metabolism and metabolites of the TCA cycle were down-regulated in rotenone treated HeLa cells (Gielisch and Meierhofer 2015). This leads to a lack of energy in cells with a complex I deficiency, which is further caused by ATP hydrolysis to maintain the electrochemical gradient across the inner mitochondrial membrane (Gielisch and Meierhofer 2015). These mechanisms could occur in mitochondrial diseases caused by a complex I deficiency as well, which may lead to necrosis of cells with high energy requirements.

4.4 Decrease of iron-sulfur clusters in rotenone treated HeLa cells

Mitochondria are the cellular compartment for biogenesis of iron-sulfur (Fe-S) clusters since they hold the assembly machinery responsible for their synthesis and incorporation into scaffold proteins (Lill and Mühlenhoff 2006). Fe-S cluster are cofactors that consist of varying proportions of iron and inorganic sulfur atoms (Mayr et al. 2015). While the iron source of Fe-S clusters has not been clearly identified, cysteine is the sulfur source for their biogenesis (Rouault 2012). Protein complexes containing Fe-S clusters within the respiratory chain and TCA cycle are NADH-dehydrogenase, succinate dehydrogenase, cytochrome c oxidoreductase and aconitase 1. An inefficient Fe-S cluster assembly process deregulates the maturation of those Fe-S cluster containing proteins.

In this study, the protein responsible for iron uptake, transferrin receptor 1 (TFRC), was found to be significantly up-regulated, while the iron storage protein ferritin (FTH1), the pathway “cysteine and methionine metabolism” and the metabolite cystathionin were significantly down-regulated (Table 4, Table 6, Figure 11). Furthermore, the protein cysteine desulfurase (NFS1) was found to be down-regulated in rotenone treated cells. NFS1 initiates the formation of Fe-S clusters by mobilizing and transferring the sulfur atom from cysteine.

Although cysteine could not be detected, a decrease in its precursor cystathionin and the pathway “cysteine and methionine metabolism” support the conclusion, that the cellular amount of cysteine is decreased. Furthermore, NFS1 was found to be down-regulated as well, maybe due to reduced levels of cysteine. An infantile deficiency in succinate dehydrogenase and cytochrome c oxidoreductase (IMC23D) was found to be caused by a deficiency in NFS1 (Farhan et al. 2014). This could cause an impaired Fe-S cluster assembly in rotenone treated cells which leads to the loss of Fe-S clusters in NADH-dehydrogenase, succinate dehydrogenase, cytochrome c oxidoreductase and aconitase 1.

Upon the loss of Fe-S clusters, aconitase 1 (ACO1) is transformed into iron regulatory protein 1 (IRP1) which causes an up-regulation of TFRC (Mena et al. 2011). After the transformation, IRP1 binds to iron responsive elements and enhances cellular iron up-

take by increasing the translation of TFRC and transporters, but decreases the iron storage capacity by blocking FTH1 translation (Mena et al. 2011). Normally low iron conditions activate IRP1, but decreased levels of Fe-S clusters may give a false low iron signal (Gielisch and Meierhofer 2015).

In conclusion, Fe-S cluster biosynthesis is impaired due to decreased levels of cysteine and NFS1, since sulfur donation is an indispensable and rate-limiting early event during the Fe-S assembly process (Saha et al. 2015). Consequently, the loss of Fe-S clusters may give a false low iron signal, which results in the activation of IRP1 with subsequent up-regulation of TFRC and down-regulation of FTH1 (Fosset et al. 2006). Thus, a deficiency of complex I causes a disruption in Fe-S cluster assembly. This results in the loss of Fe–S clusters in all iron-sulfur proteins, which leads to an impairment of redox reactions.

4.5 Anaerobic glycolysis and down-regulation of the TCA cycle and respiratory chain in ρ^0 cells

Cells lacking mtDNA (ρ^0 cells) are useful models to study mitochondrial diseases and their contributions to phenotypic alterations. Mitochondrial DNA depleted cells are characterized by major changes in metabolic activities, such as a decreased oxygen consumption and mitochondrial membrane potential as well as an up-regulation of the glycolysis pathway (Rommelaere et al. 2011; von Kleist-Retzow et al. 2007).

In this study already known features of ρ^0 cells as well as the complete depletion of mtDNA were verified, in order to validate this approach. Within the pyruvate metabolism an up-regulation of LDHA (Figure 20 A) as well as its product lactic acid (Figure 17) was observed. This results from a complete dependence of ρ^0 cells on anaerobic glycolysis for ATP production and therefore an acidification by enhanced lactic acid fermentation (Kukat et al. 2008; Chandel and Schumacker 1999). Anaerobic glycolysis allows for sufficient energy supply to keep up with the demands of proliferating cells (von Kleist-Retzow et al. 2007). Patients with the mitochondrial disease MELAS buildup lactic acid in their bodies, a process called lactic acidosis (Goto et al. 1992). The increased acidity of their blood causes symptoms like vomiting, muscle weakness, abdominal pain and extreme tiredness. In conclusion, known features of ρ^0 cells that

also match to MELAS could be identified in both proteome and metabolome data, validating the chosen approach and model.

Beside expected changes in the pyruvate metabolism of ρ^0 cells, the pathway and PPI network analysis revealed significantly down-regulated pathways within the mitochondrial energy metabolism, TCA cycle and the respiratory chain (Table 8, Figure 21A, B). Proteins and metabolites of the TCA cycle were dysregulated and complexes of the respiratory chain were down-regulated, but ATP synthase subunits were unregulated. Furthermore, the PPI network analysis revealed a down-regulation of mitochondrial ribosomal proteins.

Individual enzymes within the TCA cycle were unregulated, such as MDH2 and CS, or up-regulated like IDH2 and FH. The metabolome analysis of ρ^0 cells revealed that citric acid and cis-aconitic acid levels were decreased, while oxalacetic acid and succinic acid were increased in ρ^0 cells (Figure 17). Since proteome and metabolome profiling revealed an uneven regulation of metabolites and proteins involved in the TCA cycle, selected enzyme activities were investigated, in order to explore how these activities may correlate to according protein abundances and metabolite levels. The measured values of CS and FH correlated with the protein abundances, but MDH2 showed an increased and IDH2 an unchanged enzymatic activity in ρ^0 cells, which did not correlate with the unchanged MDH2 abundance as shown in the proteome profiling (Figure 20 A). For a better overview, protein abundances, metabolite levels and enzyme activities of the TCA cycle between ρ^0 and parental cells were integrated (Figure 26). These data demonstrate that the interpretation of dysregulated proteins and metabolites of the TCA cycle is challenging, probably because many other molecules like amino acids, fatty acids and cholesterol are entering and exiting the cycle on different sites. Furthermore the TCA cycle is regulated allosterically by the concentration of ATP and NADH which stimulate or inhibit isocitrate dehydrogenase, 2-oxoglutarate dehydrogenase and pyruvate dehydrogenase (Berg, Tymoczko, and Stryer 2002a).

The pathway gluconeogenesis results in the generation of glucose from non-carbohydrate carbon substrates. First pyruvate is converted into oxalacetic acid, which is reduced to malic acid performed by MDH2. In the cytosol, malic acid is oxidized to oxalacetic acid, which is converted to phosphoenolpyruvate (PEP). PEP can in turn be

reduced to lactic acid, as ρ^0 cells can only rely on anaerobic glycolysis and lactic acid formation. Thus, citric acid levels are decreased, since the majority of oxalacetic acid is used for gluconegenesis. The CS activity was not influenced by this mechanism. Usually high concentrations of NADH are known to inhibit CS activity. Since NADH was identified by just two transitions in two samples, it was not included in data evaluation. Nevertheless, the level of NADH was increased in ρ^0 cells. The maximal reaction rate of CS was measured *in vitro*, but steric effects could considerably decrease the turnover rate of CS *in vivo*. The decreased levels of cis-aconitic acid could result from the decreased citric acid level.

The activity of IDH2 between ρ^0 and parental cells was not changing, but the protein abundance was increased. IDH2 can be inhibited by its products NADPH and oxoglutaric acid or by competitive feedback inhibition by ATP (Maeting et al. 2000). A discussion of the result is difficult, since isocitric acid, oxoglutaric acid and NADPH were not detected in the metabolome profiling. ATP levels were decreased in ρ^0 cells (Figure 17), thus a competitive feedback inhibition is very unlikely.

Succinic acid accumulated, because it cannot be oxidized to fumaric acid, due to a lack of ubiquinone (Q) (Butow and Avadhani 2004). Cells lacking mtDNA contain no functional respiratory chain and thus complex III is failing to oxidize ubiquinol (QH_2).

In conclusion, dysregulation within the TCA cycle could be caused by reactions of gluconeogenesis, steric effect *in vivo* and by missing redox reactions performed by oxidative phosphorylation (Aretz et al. 2016). Lactic acidosis is a common symptom of MELAS that could result from anaerobic glycolysis as an adaptive response to the missing respiratory chain. Thus, the described dysregulation found in this study could also exist in mitochondrial diseases in order to adapt to changing metabolic conditions.

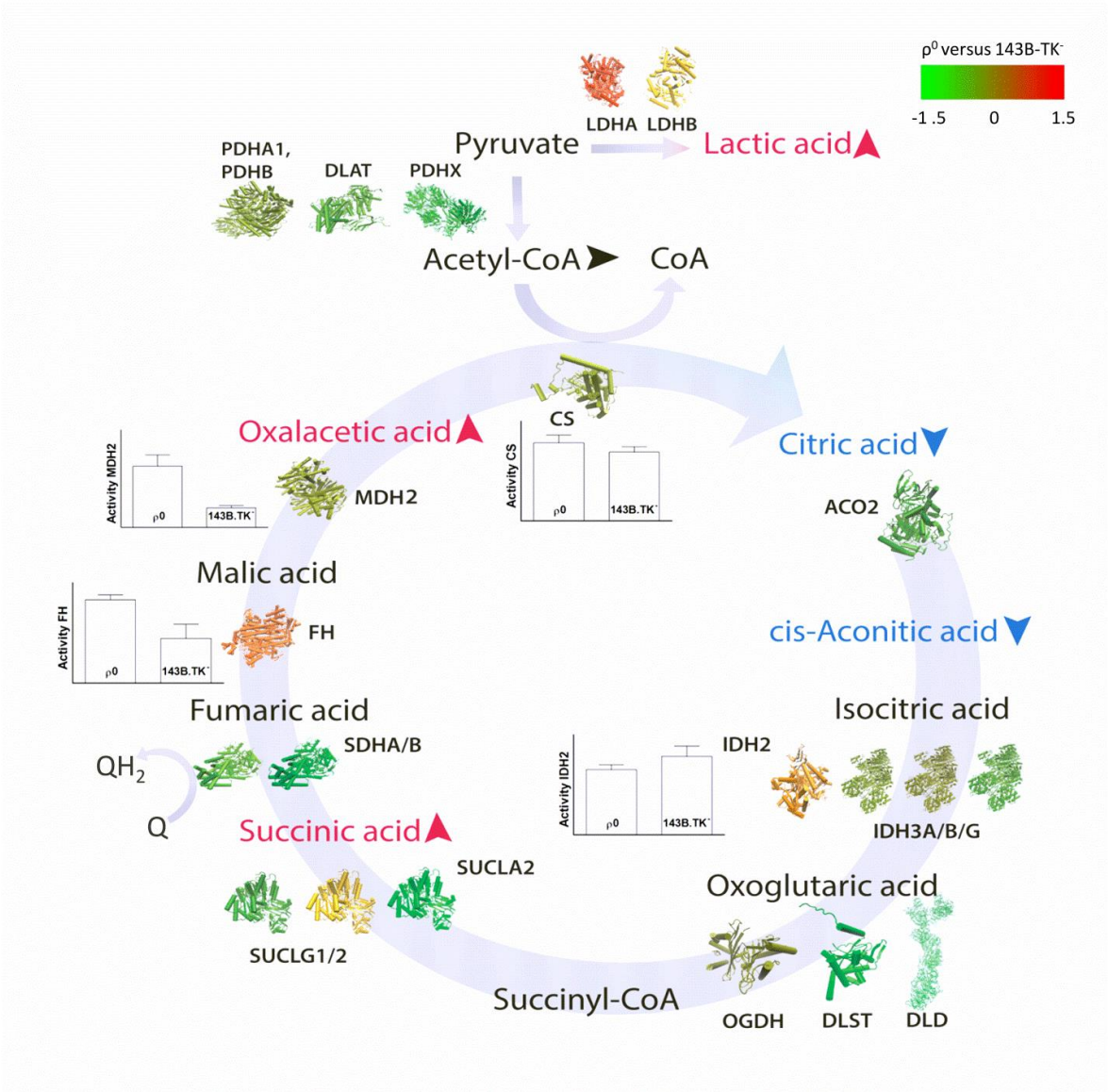

Figure 26: Integration of protein abundances, metabolites and enzyme activities of the TCA cycle between parental and ρ^0 cells. Protein structures of enzymes and their subunits are colored according to the heat map, green = down-regulated and red = up-regulated in ρ^0 cells. Enzyme activities are taken from Table 11. Accumulation or reduction of metabolites is indicated by arrows (Aretz et al. 2016).

The pathway and PPI network analysis revealed the respiratory chain to be significantly down-regulated in ρ^0 cells (Table 8, Figure 21B). Subunits of the complexes I-IV were decreased, but subunits of the ATP synthase were unregulated in ρ^0 cells. Only the heme containing proteins CYCS and CYC1 were up-regulated, as well as metabolites of the heme metabolism, being protoporphyrin IX and bilirubin (Figure 17).

Subunits of complex I were found to be down-regulated in different orders of magnitude, which could be a result of the stepwise assembly to form a functional complex

(Wittig et al. 2010). The assembly of complexes is not a static process in which subassemblies are sequentially combined, but rather a dynamic process in which subunits or subcomplexes may be recycled during assembly (Vogel, Smeitink, and Nijtmans 2007). The proteome profiling disclosed unchanged ratios of ATP synthase subunits. Although ρ^0 cells do not have mtDNA encoded F_o subunits 6 and 8, they possess a functional F_1-ATP synthase and a functional adenine nucleotide translocator (ANT) (Chandel and Schumacker 1999). The discrepancy of up-regulated ATP synthase subunits in rotenone treated cells and unregulated subunits in ρ^0 cells could be explained by the missing F_0-ATP synthase subunits in ρ^0 cells. Due to the down-regulation of the respiratory chain, the creation of a proton gradient could be impaired, but an electrochemical gradient across the inner mitochondrial membrane is essential for cell survival. To maintain this gradient the ATP synthase works in reverse direction, by hydrolyzing ATP^{4-} (Yasuda et al. 1998; C. P. Smith and Thorsness 2005; Adachi et al. 2007). The ATP^{4-} is derived from anaerobic glycolysis and exchanged by ANT against ATP^{3-} (Buchet and Godinot 1998). Thus, a sufficient mitochondrial membrane potential is generated, in order to prevent osmotic swelling of the matrix and subsequent cytochrome c (CYCS) release after rupture of the membrane (Chandel and Schumacker 1999).

The heme containing electron carrier CYCS and CYC1 and compounds of the heme metabolism were up-regulated in ρ^0 cells. CYCS is loosely associated with the inner mitochondrial membrane and it plays a role in apoptosis. Interestingly, it was one of the highest down-regulated proteins in the study, where an artificial complex I deficiency was induced by rotenone (Gielisch and Meierhofer 2015). As CYCS does not need to be assembled into a complex, it is probably not affected by the missing mtDNA. Furthermore, the maintenance of the transmembrane potential by ATP hydrolysis could explain the sensitivity to pro-apoptotic stimuli, since ρ^0 cells have a decreased membrane potential as parental cells (Chandel and Schumacker 1999). In conclusion, ρ^0 cells maintain an increased CYCS distribution in mitochondria, even though the cells were deficient in respiration (Jiang et al. 1999).

The PPI network analysis features mitochondrial 55S ribosomal proteins to be down-regulated in ρ^0 cells, but cytoplasmic 80S ribosomal proteins were unregulated (Figure

22). The mtDNA encodes for two rRNA molecules and because those are missing, a down-regulation of mitochondrial ribosomal proteins was observed in ρ^0 cells. Ribosomal proteins are nuclear encoded and assemble with the two rRNAs to form mitochondrial ribosomes to translate mtDNA encoded proteins. A A1555G mutation in the mitochondrial 12S rRNA is pathogenic in humans, since this mutation causes a decrease in mitochondrial protein synthesis (Sylvester et al. 2004; Guan, Fischel-Ghodsian, and Attardi 1996).

In summary, ρ^0 cells perform anaerobic glycolysis and gluconeogenesis for sufficient energy supply, resulting in production and secretion of lactic acid, which is a common feature of mitochondrial diseases. The TCA cycle and respiratory chain were down-regulated, which results in a lack of ATP, usually derived from these two pathways. The ATP synthase still maintains the mitochondrial membrane potential by hydrolyzing ATP (Aretz et al. 2016). Mitochondrial 55S ribosomal proteins were down-regulated, because the mtDNA was missing. Lactic acidosis is a common symptom, it is likely that mitochondrial diseases have similar characteristics in order to adapt to changing conditions caused by a deficiency within the respiratory chain.

4.6 Mitochondrial retrograde signaling in ρ^0 cells

Mitochondria play a role in signaling, a process that has implications in development, aging, disease and environmental adaption (Butow and Avadhani 2004).

The pathway enrichment analysis revealed a significant up-regulation of cell signaling pathways, such as $G_{12/13}$, Rho GTPases and G-protein-coupled receptor (GPCR) mediated events, as well as cell cycle progression in ρ^0 cells (Table 8).

GPCR-induced signal transduction pathways are able to affect cell cycle progression (New and Wong 2007), whereas the final effect on cellular proliferation is likely to be the result of the combined action of different GPCRs simultaneously regulating different G-proteins. Each G-protein affects the activity of multiple intracellular signaling pathways that modulate the expression, activity and stability of key proteins of the cell cycle machinery (New and Wong 2007). Rho GTPases are G-proteins that are involved in many cell biological processes, such as cell growth control, cytokinesis, cell motility, cell-cell and cell-extracellular matrix adhesion, cell transformation and invasion

(Govek, Newey, and Van Aelst 2005; Bosco, Mulloy, and Zheng 2009; Didsbury et al. 1989; Hall 1990; Kozma et al. 1997; Ridley et al. 1992; Alblas et al. 2001; Worthylake and Burridge 2001). Furthermore, they induce dynamic rearrangements of the plasma membrane-associated actin cytoskeleton (Govek, Newey, and Van Aelst 2005).

The up-regulation of signaling pathways can be explained by mitochondrial retrograde signaling (Aretz et al. 2016). Mitochondrial retrograde signaling is a pathway of communication from mitochondria to the nucleus that influences many cellular and organismal activities under normal and pathophysiological conditions (Butow and Avadhani 2004; Jazwinski 2013). Mitochondrial dysfunctions owing to mtDNA depletion and disruption of the membrane potential, initiate mitochondrial retrograde signaling, which modulates transcription factors and alters nuclear gene expression (Guha et al. 2014). Those signaling mechanisms are used to ensure metabolic control, by balancing cell cycle progression and specific cell fates (Owusu-Ansah et al. 2008). Thus, the alteration of signaling pathways could result in the up-regulation of pathways involved in cell cycle progression.

The observed alteration of signaling pathways confirms described morphological adjustments in ρ^0 cells, because mitochondrial morphology is dependent on the respiration status of the cell (Hackenbrock 1968). Cytoskeletal alterations, like a collapsed vimentin network, a dense accumulation of mitochondria around the nucleus and a few mitochondria distributed throughout the cytoplasm were observed in ρ^0 cells (Annunen-Rasila et al. 2007). Furthermore, the reticulum of ρ^0 cells appears to be disrupted and this yields in a distribution of small individual organelles instead of reticular networks with tubular cristae (Gilkerson et al. 2000; Jazayeri 2003; Garcia 2000).

In summary, morphological adjustments and up-regulation of pathways involved in cell cycle progression in ρ^0 cells are a consequence of mitochondrial retrograde signaling. A similar phenomenon can be expected in patients with a mitochondrial disease, in order to cope with the disrupted respiratory chain.

4.7 De-ubiquitination of ribosomal proteins, SLC transporters and cytoskeleton associated proteins in ρ^0 cells

Ubiquitin is a small protein that can reversibly attach to a target protein. Depending on the linkage type, a protein is degraded by the proteasome, serves to attract proteins to initiate signaling cascades, or it is internalized (Komander 2009). A global ubiquitylome profiling was performed in order to identify regulatory mechanisms in ρ^0 cells.

Ubiquitylome profiling of ρ^0 cells and subsequent gene set enrichment analysis revealed that cytosolic ribosomal proteins, SLC transporters and proteins of the cytoskeleton were significantly de-ubiquitinated in ρ^0 cells (Table 9, Figure 23).

The 60S ribosomal protein L28 (RPL28) is ubiquitinated dependent on the cell cycle, being low in G0 and G1 and high in S phase (Spence et al. 2000). Furthermore, polyubiquitinated RPL28 is able to enhance the translation rate in corresponding ribosomes compared to monoubiquitinated RPL28 (Spence et al. 2000; Xue and Barna 2012). Therefore, ubiquitination may not trigger degradation in ribosomal proteins but rather display a regulatory role (Spence et al. 2000). On the other hand, mature ubiquitinated ribosomes from *Saccharomyces cerevisiae* are rapidly degraded by autophagy upon nutrient starvation while mature ribosomes are very stable (Kraft et al. 2008). Therefore adaptive mechanisms exist to degrade excess ribosomes (Kraft et al. 2008). Dependent on the exact position and chain type of the modification, the ribosomal function can be altered or it comes to an ubiquitin dependent degradation. A degradation of cytosolic ribosomal proteins is unlikely, since their protein abundancies were not altered. Furthermore, cell cycle progression responds to translation capacity and ribosome biogenesis (Thapa et al. 2013) and related pathways were found to be up-regulated in ρ^0 cells (Table 8). Thus, the de-ubiquitination of cytosolic ribosomal proteins seems to have a regulatory function in ρ^0 cells.

Internalization and intracellular sorting of membrane-bound receptors and transporters is regulated by ubiquitin conjugation, which thereby has profound impact on cell signaling and metabolism (Miranda and Sorkin 2007; Hurley and Stenmark 2011). Internalized proteins are either recycled to the plasma membrane or targeted for lysosomal degradation, which often is a response to ligand binding (Hurley and Stenmark 2011).

In this study, a significant de-ubiquitination of SLC transporters was observed, although the protein abundancies were not altered (Table 9, Figure 24). This could indicate a re-localization or higher substrate transport due to less regulation by ubiquitination, which was also demonstrated during ABC transporter (Step6) endocytosis (Kölling and Hollenberg 1994). Similarly, the Na^+-Cl^--dependent co-transporter dopamine transporter (DAT), which belongs to the SLC6 family, is constitutively ubiquitinated upon protein kinase C (PKC) activation (Miranda et al. 2005). Mutating the DAT ubiquitination sites leads to inhibition of its internalization, demonstrating the regulatory function of ubiquitination (Miranda et al. 2007; Sorkina et al. 2005). The major regulator of salt and water reabsorption, the epithelial Na^+ channel (ENaC), is widely expressed in epithelial tissues. Trafficking of ENaC is hormonally controlled and depends on the ubiquitination status (Soundararajan et al. 2010). Ubiquitinated ENaC molecules remain in endosomal membranes and appear to be committed to lysosomal degradation, while de-ubiquitination promotes a recycling of ENaC back to the apical plasma membrane (Butterworth 2010). In this study, most of the SLC transporters were amino acid transporters localized in the plasma membrane. The metabolome profiling of mtDNA depleted cells revealed that the majority of detected amino acids were up-regulated (Figure 17). The amino acid catabolism is linked to the TCA cycle and glucogenic amino acids can form glucose via gluconeogenesis. Thus, in order to compensate for an energy lack caused by missing mtDNA, SLC transporters are most likely de-ubiquitinated to increase their transporter activity (Aretz et al. 2016).

Furthermore, a significant de-ubiquitination of cytoskeleton associated proteins was observed (Table 9). Tubulin and microtubules are major cytoskeletal proteins with functions in cell development, growth, motility, and intracellular trafficking, which need to be controlled accurately by PTMs. Tubulin heterodimers are the target of various ubiquitin ligases, like parkin, ubiquitin C-terminal hydrolase L1 (UCH L1) and the breast cancer susceptibility protein 1 (BRCA1) ubiquitin ligase (Liu et al. 2002; Starita et al. 2004). While ubiquitination is implicated in tubulin turnover and has been observed in various cellular processes (K. Huang, Diener, and Rosenbaum 2009; Thompson, Ramalho-Santos, and Sutovsky 2003; Iqbal and Grundke-Iqbal 1991), its exact physiological role and regulation in microtubule functions is still unclear (Bheda

et al. 2010). Recent data suggest that UCH L1 prevents microtubule formation through ubiquitination of tubulins and microtubule-associated proteins, respectively (Bheda et al. 2010). Mitochondrial morphology is dependent on the respiration status of the cell (Hackenbrock 1968) and cytoskeletal alterations are known features of ρ^0 cells (Annunen-Rasila et al. 2007). Thus, the disruption or the respiratory chain in ρ^0 cells causes cytoskeletal alterations driven by de-ubiquitination.

In summary, the de-ubiquitination of cytosolic ribosomal proteins, SLC transporters and proteins of the cytoskeleton seems to have a regulatory function in ρ^0 cells and probably in mitochondrial diseases. Depending on the genes which are affected by a mutation causing a mitochondrial pathology, not all of the described features of ρ^0 cells will occur in patients. Nevertheless, these results indicate a tight regulation by ubiquitination in response to mitochondrial energy alterations.

4.8 Dephosphorylation of proteins involved in GTPase activity and organization of the cytoskeleton in ρ^0 cells

Phosphorylation is the reversible addition of phosphate to serine, threonine or tyrosine residues catalyzed by kinases and phosphatases (Humphrey, James, and Mann 2015; Komander 2009). Since phosphorylation is a dynamic process, its quantification is crucial in order to obtain a view of a phosphoproteome at a systems level (Olsen et al. 2010). This can be achieved by phosphopeptide-enrichment methods, high accuracy mass spectrometer and bioinformatics tools (Olsen et al. 2010). In this study, a global phosphoproteome profiling was performed in order to identify regulatory mechanisms in ρ^0 cells.

Phosphoproteome profiling of ρ^0 cells and subsequent gene set enrichment analysis revealed GTPase activity, like Ras and Rho protein signal transduction, and cytoskeleton organization pathways as the most dephosphorylated (Table 10).

Ras GTPases and its subfamily Rho GTPases control cell behavior by activating a number of downstream effectors that regulate cell growth, differentiation, cell survival, organelle development, cytoskeletal dynamics and cell movement (Bunda et al. 2014; Van Aelst and D'Souza-Schorey 1997). The non-receptor protein tyrosine kinase Src phosphorylates GTP-, but not GDP-loaded Ras and this Ras-Y32 phosphorylation

markedly reduces the binding to effector Raf and concomitantly increases binding to GTPase-activating proteins and the rate of GTP hydrolysis (Bunda et al. 2014). Additionally, the localization of Ras is determined by phosphorylation of K-Ras4B in its polybasic region which allows it to dissociate from the plasma membrane by a farnesyl-electrostatic switch (Ahearn et al. 2012). Furthermore the phosphorylation of Rho GTPases can affect the activity either by direct activation or through its interaction with downstream effectors (Golen 2010). Thus, GTPase activity in ρ^0 cells is regulated by dephosphorylation, probably in order to regulate and tune mitochondrial retrograde signaling.

Beside the regulation of GTPases, several proteins involved in cytoskeleton organization and microtubule based processes, such as spectrin (SPTBN1), cytoplasmic linker-associated protein 1 (CLASP1) and Rho guanine nucleotide exchange factor 2 (ARHGEF2), were found to be dephosphorylated in ρ^0 cells. Phosphorylation of SPTBN1 is an important mechanism during membrane skeleton remodeling, controlling for example the disassembly of the cytoskeleton during mitosis (Machnicka et al. 2012). Furthermore, SPTBN1 is linked to cell signaling events and it participates in signal transduction pathways (Machnicka et al. 2012). Cytoplasmic linker-associated proteins (CLASPs) are thought to stabilize microtubules after being phosphorylated. The protein ARHGEF2 is a microtubule-regulated exchange factor that activates Rho GTPases during cytokinesis (Birkenfeld et al. 2007). It is phosphorylated by mitotic kinases, which results in an inhibition of the catalytic activity, whereas dephosphorylation occurs prior to cytokinesis and leads to its activation. In conclusion, dephosphorylated proteins involved in cytoskeleton organization and microtubule based processes are associated with cell cycle progression as well as signaling events.

In summary, dephosphorylation regulates mitochondrial retrograde signaling and cytoskeleton rearrangements (Aretz et al. 2016). Both pathways are interconnected and can lead to the known phenotype of ρ^0 cells, a collapsed vimentin network and a dense accumulation of mitochondria around the nucleus.

4.9 Conclusion

Mitochondrial diseases are a heterogeneous class of pathologies caused by a plethora of mutations, which affect the nuclear and mitochondrial DNA (mtDNA). They are often characterized by anomalies of oxidative phosphorylation (OXPHOS), which can cause major changes in metabolic activities. Cells having a deficiency in the OXPHOS system are able to adapt to the changed energy metabolism in order to ensure metabolic control and survival. In this study, the metabolome and proteome of cell lines with a complex I deficiency induced by rotenone and lacking mtDNA (ρ^0 cells) were investigated. Additionally, an ubiquitylome and phosphoproteome profiling was performed for ρ^0 cells. Integrating data from metabolome and proteome profiling enabled a holistic view of cells carrying a deficiency in the respiratory chain in order to reveal possible regulatory mechanisms in mitochondrial diseases. To this end, known features of mitochondrial diseases were disclosed, which validates the chosen approaches and models.

In cells with a mimicked complex I deficiency, proteins involved in cell division processes were increased and cytoskeleton related proteins were decreased. As indicated by an up-regulation of pathways involved in cell signaling, morphological adjustments and up-regulation of pathways involved in cell cycle progression in ρ^0 cells are a consequence of mitochondrial retrograde signaling. Furthermore, PTMs regulate and tune the mitochondrial retrograde response, ribosomal proteins and proteins of the cytoskeleton. The integration of metabolome and proteome data revealed a compromised energy metabolism in cells deficient of the respiratory chain resulting in a lack of ATP. In order to cover the cellular energy demand, cells affected by mitochondrial diseases possibly channel metabolites into gluconeogenesis and lactic acid fermentation. Building blocks for these pathways may be provided by the enhanced uptake of glucogenic amino acids, which were enriched in ρ^0 cells. Furthermore, this hypothesis is supported by the de-ubiquitination of SLC amino acid transporters, which may result in an increased transporter activity. The results indicate a tight regulation by ubiquitination and phosphorylation in response to mitochondrial energy alterations. In order to prove these hypotheses, additional work like studying chain topology in combination with other

factors (e. g. substrate localization) is necessary to determine the consequences of ubiquitination. This study reveals possible regulatory mechanism of mitochondrial diseases, which could be supported and expanded by analyzing patient derived samples carrying a specific disorder. Furthermore, other inhibitors of the OXPHOS system, like antimycin A or oligomycin could be applied. By integrating metabolomics and proteomics data including PTMs, new molecular mechanisms and features of mitochondrial diseases were discovered.

.

References

A. D. McNaught, and A. Wilkinson. 1997. *IUPAC. Compendium of Chemical Terminology*. 2nd ed. Oxford: Blackwell Scientific Publications. http://goldbook.iupac.org.

Adachi, Kengo, Kazuhiro Oiwa, Takayuki Nishizaka, Shou Furuike, Hiroyuki Noji, Hiroyasu Itoh, Masasuke Yoshida, and Kazuhiko Kinosita. 2007. “Coupling of Rotation and Catalysis in F1-ATPase Revealed by Single-Molecule Imaging and Manipulation.” *Cell* 130 (2). Elsevier: 309–21. doi:10.1016/j.cell.2007.05.020.

Ahearn, Ian M, Kevin Haigis, Dafna Bar-Sagi, and Mark R Philips. 2012. “Regulating the Regulator: Post-Translational Modification of RAS.” *Nature Reviews. Molecular Cell Biology* 13 (1). NIH Public Access: 39–51. doi:10.1038/nrm3255.

Alberts, Bruce, Alexander Johnson, Julian Lewis, Martin Raff, Keith Roberts, and Peter Walter. 2002. “The Mitochondrion.” Garland Science. http://www.ncbi.nlm.nih.gov/books/NBK26894/.

Alblas, J, L Ulfman, P Hordijk, and L Koenderman. 2001. “Activation of Rhoa and ROCK Are Essential for Detachment of Migrating Leukocytes.” *Molecular Biology of the Cell* 12 (7): 2137–45. http://www.pubmedcentral.nih.gov/articlerender.fcgi?artid=55668&tool=pmcentrez&rendertype=abstract.

Anderson, Leigh, and Christie L Hunter. 2006. “Quantitative Mass Spectrometric Multiple Reaction Monitoring Assays for Major Plasma Proteins.” *Molecular & Cellular Proteomics : MCP* 5 (4): 573–88. doi:10.1074/mcp.M500331-MCP200.

Annunen-Rasila, Johanna, Steffen Ohlmeier, Hanna Tuokko, Johanna Veijola, and Kari Majamaa. 2007. “Proteome and Cytoskeleton Responses in Osteosarcoma Cells with Reduced OXPHOS Activity.” *Proteomics* 7 (13): 2189–2200. doi:10.1002/pmic.200601031.

Aretz, Ina, Christopher Hardt, Ilka Wittig, and David Meierhofer. 2016. “An Impaired Respiratory Electron Chain Triggers down-Regulation of the Energy Metabolism and de-Ubiquitination of Solute Carrier Amino Acid Transporters.” *Molecular &*

Cellular Proteomics 15 (5): mcp.M115.053181. doi:10.1074/mcp.M115.053181.

Assenov, Yassen, Fidel Ramírez, Sven-Eric Schelhorn, Thomas Lengauer, and Mario Albrecht. 2008. "Computing Topological Parameters of Biological Networks." *Bioinformatics (Oxford, England)* 24 (2): 282–84. doi:10.1093/bioinformatics/btm554.

Asur, Sitaram, Duygu Ucar, and Srinivasan Parthasarathy. 2007. "An Ensemble Framework for Clustering Protein-Protein Interaction Networks." *Bioinformatics (Oxford, England)* 23 (13): i29–40. doi:10.1093/bioinformatics/btm212.

Atamna, Hani, and William H Frey. 2007. "Mechanisms of Mitochondrial Dysfunction and Energy Deficiency in Alzheimer's Disease." *Mitochondrion* 7 (5): 297–310. doi:10.1016/j.mito.2007.06.001.

Avraham, Roi, and Yosef Yarden. 2011. "Feedback Regulation of EGFR Signalling: Decision Making by Early and Delayed Loops." *Nature Reviews. Molecular Cell Biology* 12 (2): 104–17. doi:10.1038/nrm3048.

Azuaje, Francisco J. 2014. "Selecting Biologically Informative Genes in Co-Expression Networks with a Centrality Score." *Biology Direct* 9 (1). BioMed Central Ltd: 12. doi:10.1186/1745-6150-9-12.

Bannwarth, Sylvie, Vincent Procaccio, Anne Sophie Lebre, Claude Jardel, Annabelle Chaussenot, Claire Hoarau, Hassani Maoulida, et al. 2013. "Prevalence of Rare Mitochondrial DNA Mutations in Mitochondrial Disorders." *Journal of Medical Genetics* 50 (10): 704–14. doi:10.1136/jmedgenet-2013-101604.

Bantscheff, Marcus, Markus Schirle, Gavain Sweetman, Jens Rick, and Bernhard Kuster. 2007. "Quantitative Mass Spectrometry in Proteomics: A Critical Review." *Analytical and Bioanalytical Chemistry* 389 (4): 1017–31. doi:10.1007/s00216-007-1486-6.

Barabási, Albert-László, Natali Gulbahce, and Joseph Loscalzo. 2011. "Network Medicine: A Network-Based Approach to Human Disease." *Nature Reviews. Genetics* 12 (1). Nature Publishing Group, a division of Macmillan Publishers Limited. All Rights Reserved.: 56–68. doi:10.1038/nrg2918.

Barallobre-Barreiro, Javier, Yuen-Li Chung, and Manuel Mayr. 2013. “Proteomics and Metabolomics for Mechanistic Insights and Biomarker Discovery in Cardiovascular Disease.” *Revista Española de Cardiología (English Ed.)* 66 (8): 657–61. doi:10.1016/j.rec.2013.04.009.

Barham, S S, and B R Brinkley. 1976. “Action of Rotenone and Related Respiratory Inhibitors on Mammalian Cell Division. 2 Ultrastructural Studies.” *Cytobios* 15 (58-59): 97–109. http://www.ncbi.nlm.nih.gov/pubmed/1001025.

Beausoleil, Sean A, Mark Jedrychowski, Daniel Schwartz, Joshua E Elias, Judit Villén, Jiaxu Li, Martin A Cohn, Lewis C Cantley, and Steven P Gygi. 2004. “Large-Scale Characterization of HeLa Cell Nuclear Phosphoproteins.” *Proceedings of the National Academy of Sciences of the United States of America* 101 (33): 12130–35. doi:10.1073/pnas.0404720101.

Berardo, A, O Musumeci, and A Toscano. 2011. “Cardiological Manifestations of Mitochondrial Respiratory Chain Disorders.” *Acta Myologica : Myopathies and Cardiomyopathies : Official Journal of the Mediterranean Society of Myology / Edited by the Gaetano Conte Academy for the Study of Striated Muscle Diseases* 30 (1): 9–15. http://www.pubmedcentral.nih.gov/articlerender.fcgi?artid=3185833&tool=pmcentrez&rendertype=abstract.

Berg, Jeremy M, John L Tymoczko, and Lubert Stryer. 2002a. “Entry to the Citric Acid Cycle and Metabolism Through It Are Controlled.” W H Freeman. http://www.ncbi.nlm.nih.gov/books/NBK22347/.

———. 2002b. “The Citric Acid Cycle.” W H Freeman. http://www.ncbi.nlm.nih.gov/books/NBK21163/.

Bheda, Anjali, Anuradha Gullapalli, Michael Caplow, Joseph S Pagano, and Julia Shackelford. 2010. “Ubiquitin Editing Enzyme UCH L1 and Microtubule Dynamics: Implication in Mitosis.” *Cell Cycle (Georgetown, Tex.)* 9 (5): 980–94. http://www.pubmedcentral.nih.gov/articlerender.fcgi?artid=4426338&tool=pmcentrez&rendertype=abstract.

Bi, Huichang, Kristopher W Krausz, Soumen K Manna, Fei Li, Caroline H Johnson, and Frank J Gonzalez. 2013. “Optimization of Harvesting, Extraction, and Analytical Protocols for UPLC-ESI-MS-Based Metabolomic Analysis of Adherent Mammalian Cancer Cells.” *Analytical and Bioanalytical Chemistry* 405 (15): 5279–89. doi:10.1007/s00216-013-6927-9.

Birkenfeld, Jörg, Perihan Nalbant, Benjamin P Bohl, Olivier Pertz, Klaus M Hahn, and Gary M Bokoch. 2007. “GEF-H1 Modulates Localized RhoA Activation during Cytokinesis under the Control of Mitotic Kinases.” *Developmental Cell* 12 (5): 699–712. doi:10.1016/j.devcel.2007.03.014.

Boersema, Paul J, Reinout Raijmakers, Simone Lemeer, Shabaz Mohammed, and Albert J R Heck. 2009. “Multiplex Peptide Stable Isotope Dimethyl Labeling for Quantitative Proteomics.” *Nature Protocols* 4 (4). Nature Publishing Group: 484–94. doi:10.1038/nprot.2009.21.

Bosco, E E, J C Mulloy, and Y Zheng. 2009. “Rac1 GTPase: A ‘Rac’ of All Trades.” *Cellular and Molecular Life Sciences : CMLS* 66 (3): 370–74. doi:10.1007/s00018-008-8552-x.

Brown, W M, M George, and A C Wilson. 1979. “Rapid Evolution of Animal Mitochondrial DNA.” *Proceedings of the National Academy of Sciences of the United States of America* 76 (4): 1967–71. http://www.pubmedcentral.nih.gov/articlerender.fcgi?artid=383514&tool=pmcentrez&rendertype=abstract.

Buchet, K, and C Godinot. 1998. “Functional F1-ATPase Essential in Maintaining Growth and Membrane Potential of Human Mitochondrial DNA-Depleted Rho Degrees Cells.” *The Journal of Biological Chemistry* 273 (36): 22983–89. http://www.ncbi.nlm.nih.gov/pubmed/9722521.

Bunda, Severa, Pardeep Heir, Tharan Srikumar, Jonathan D Cook, Kelly Burrell, Yoshihito Kano, Jeffrey E Lee, Gelareh Zadeh, Brian Raught, and Michael Ohh. 2014. “Src Promotes GTPase Activity of Ras via Tyrosine 32 Phosphorylation.” *Proceedings of the National Academy of Sciences of the United States of America* 111 (36). National Academy of Sciences: E3785–94.

doi:10.1073/pnas.1406559111.

Butow, Ronald A, and Narayan G Avadhani. 2004. “Mitochondrial Signaling: The Retrograde Response.” *Molecular Cell* 14 (1): 1–15. http://www.ncbi.nlm.nih.gov/pubmed/15068799.

Butterworth, Michael B. 2010. “Regulation of the Epithelial Sodium Channel (ENaC) by Membrane Trafficking.” *Biochimica et Biophysica Acta* 1802 (12): 1166–77. doi:10.1016/j.bbadis.2010.03.010.

Calvo, Sarah E, and Vamsi K Mootha. 2010. “The Mitochondrial Proteome and Human Disease.” *Annual Review of Genomics and Human Genetics* 11 (September): 25–44. doi:10.1146/annurev-genom-082509-141720.

Calvo, Sarah E., Karl R. Clauser, and Vamsi K. Mootha. 2015. “MitoCarta2.0: An Updated Inventory of Mammalian Mitochondrial Proteins.” *Nucleic Acids Research*, October, gkv1003. doi:10.1093/nar/gkv1003.

Cannon, William R. 2014. “Concepts, Challenges, and Successes in Modeling Thermodynamics of Metabolism.” *Frontiers in Bioengineering and Biotechnology* 2 (January): 53. doi:10.3389/fbioe.2014.00053.

Capalbo, Luisa, Emilie Montembault, Tetsuya Takeda, Zuni I Bassi, David M Glover, and Pier Paolo D’Avino. 2012. “The Chromosomal Passenger Complex Controls the Function of Endosomal Sorting Complex Required for Transport-III Snf7 Proteins during Cytokinesis.” *Open Biology* 2 (5): 120070. doi:10.1098/rsob.120070.

Cappelletti, Graziella, Francesca Casagrande, Alessandra Calogero, Carmelita De Gregorio, Gianni Pezzoli, and Daniele Cartelli. 2015. “Linking Microtubules to Parkinson’s Disease: The Case of Parkin.” *Biochemical Society Transactions* 43 (2). Portland Press Limited: 292–96. doi:10.1042/BST20150007.

Cascante, Marta, and Silvia Marin. 2008. “Metabolomics and Fluxomics Approaches.” *Essays in Biochemistry* 45 (January). Portland Press Limited: 67–81. doi:10.1042/BSE0450067.

Chandel, N S, and P T Schumacker. 1999. “Cells Depleted of Mitochondrial DNA

(rho0) Yield Insight into Physiological Mechanisms." *FEBS Letters* 454 (3): 173–76. http://www.ncbi.nlm.nih.gov/pubmed/10431801.

Chen, Cho-Yi, Andy Ho, Hsin-Yuan Huang, Hsueh-Fen Juan, and Hsuan-Cheng Huang. 2014. "Dissecting the Human Protein-Protein Interaction Network via Phylogenetic Decomposition." *Scientific Reports* 4 (January). Nature Publishing Group: 7153. doi:10.1038/srep07153.

Chinnery, Patrick F. 2014. "Mitochondrial Disorders Overview." University of Washington, Seattle. http://www.ncbi.nlm.nih.gov/books/NBK1224/.

Cho, Carolyn R, Mark Labow, Mischa Reinhardt, Jan van Oostrum, and Manuel C Peitsch. 2006. "The Application of Systems Biology to Drug Discovery." *Current Opinion in Chemical Biology* 10 (4): 294–302. doi:10.1016/j.cbpa.2006.06.025.

Chokkathukalam, Achuthanunni, Dong-Hyun Kim, Michael P Barrett, Rainer Breitling, and Darren J Creek. 2014. "Stable Isotope-Labeling Studies in Metabolomics: New Insights into Structure and Dynamics of Metabolic Networks." *Bioanalysis* 6 (4): 511–24. doi:10.4155/bio.13.348.

Choudhary, Chunaram, Chanchal Kumar, Florian Gnad, Michael L Nielsen, Michael Rehman, Tobias C Walther, Jesper V Olsen, and Matthias Mann. 2009. "Lysine Acetylation Targets Protein Complexes and Co-Regulates Major Cellular Functions." *Science (New York, N.Y.)* 325 (5942): 834–40. doi:10.1126/science.1175371.

Cohadon, F, M Rigoulet, B Guérin, and M Vandendriessche. 1979. "[Vasogenic Cerebral Oedema. Changes in Membrane ATPases. Correction by a Phospholipid Precursor (author's Transl)]." *La Nouvelle Presse Médicale* 8 (19): 1589–91. http://www.ncbi.nlm.nih.gov/pubmed/158743.

Commisso, Mauro, Pamela Strazzer, Ketti Toffali, Matteo Stocchero, and Flavia Guzzo. 2013. "Untargeted Metabolomics: An Emerging Approach to Determine the Composition of Herbal Products." *Computational and Structural Biotechnology Journal* 4 (January): e201301007. doi:10.5936/csbj.201301007.

Contrepois, Kévin, Lihua Jiang, and Michael Snyder. 2015. "Optimized Analytical

Procedures for the Untargeted Metabolomic Profiling of Human Urine and Plasma by Combining Hydrophilic Interaction (HILIC) and Reverse-Phase Liquid Chromatography (RPLC)–Mass Spectrometry." *Molecular & Cellular Proteomics* 14 (6): 1684–95. doi:10.1074/mcp.M114.046508.

Cooper, Chris E, and Guy C Brown. 2008. "The Inhibition of Mitochondrial Cytochrome Oxidase by the Gases Carbon Monoxide, Nitric Oxide, Hydrogen Cyanide and Hydrogen Sulfide: Chemical Mechanism and Physiological Significance." *Journal of Bioenergetics and Biomembranes* 40 (5): 533–39. doi:10.1007/s10863-008-9166-6.

Cox, J., M. Y. Hein, C. A. Luber, I. Paron, N. Nagaraj, and M. Mann. 2014. "MaxLFQ Allows Accurate Proteome-Wide Label-Free Quantification by Delayed Normalization and Maximal Peptide Ratio Extraction." *Molecular & Cellular Proteomics*, June, M113.031591 – . doi:10.1074/mcp.M113.031591.

Cox, Jürgen, and Matthias Mann. 2008. "MaxQuant Enables High Peptide Identification Rates, Individualized P.p.b.-Range Mass Accuracies and Proteome-Wide Protein Quantification." *Nature Biotechnology* 26 (12): 1367–72. doi:10.1038/nbt.1511.

Cox, Jürgen, Nadin Neuhauser, Annette Michalski, Richard a Scheltema, Jesper V Olsen, and Matthias Mann. 2011. "Andromeda: A Peptide Search Engine Integrated into the MaxQuant Environment." *Journal of Proteome Research* 10 (4): 1794–1805. doi:10.1021/pr101065j.

Currais, Antonio, Tibor Hortobágyi, and Salvador Soriano. 2009. "The Neuronal Cell Cycle as a Mechanism of Pathogenesis in Alzheimer's Disease." *Aging* 1 (4): 363–71. http://www.pubmedcentral.nih.gov/articlerender.fcgi?artid=2806021&tool=pmcentrez&rendertype=abstract.

Das, Anibh M, Ulrike Steuerwald, and Sabine Illsinger. 2010. "Inborn Errors of Energy Metabolism Associated with Myopathies." *Journal of Biomedicine & Biotechnology* 2010 (January): 340849. doi:10.1155/2010/340849.

Denis, Nicholas J, Julian Vasilescu, Jean-Philippe Lambert, Jeffrey C Smith, and Daniel Figeys. 2007. “Tryptic Digestion of Ubiquitin Standards Reveals an Improved Strategy for Identifying Ubiquitinated Proteins by Mass Spectrometry.” *Proteomics* 7 (6): 868–74. doi:10.1002/pmic.200600410.

Dervartanian, D.V., and C. Veeger. 1964. “Studies on Succinate Dehydrogenase.” *Biochimica et Biophysica Acta (BBA) - Specialized Section on Enzymological Subjects* 92 (2): 233–47. doi:10.1016/0926-6569(64)90182-8.

Dettmer, Katja, Pavel A Aronov, and Bruce D Hammock. 2007. “Mass Spectrometry-Based Metabolomics.” *Mass Spectrometry Reviews* 26 (1): 51–78. doi:10.1002/mas.20108.

Didsbury, J, RF Weber, GM Bokoch, T Evans, and R Snyderman. 1989. “Rac, a Novel Ras-Related Family of Proteins That Are Botulinum Toxin Substrates.” *J. Biol. Chem.* 264 (28): 16378–82. http://www.jbc.org/content/264/28/16378.abstract?ijkey=5e938b48da77effd16b7fcfa983deb05be334452&keytype2=tf_ipsecsha.

DiMauro, Salvatore. 2004. “The Many Faces of Mitochondrial Diseases.” *Mitochondrion* 4 (5-6): 799–807. doi:10.1016/j.mito.2004.07.032.

Doll, Sophia, and Alma L Burlingame. 2015. “Mass Spectrometry-Based Detection and Assignment of Protein Posttranslational Modifications.” *ACS Chemical Biology* 10 (1): 63–71. doi:10.1021/cb500904b.

Ellman, G L. 1958. “A Colorimetric Method for Determining Low Concentrations of Mercaptans.” *Archives of Biochemistry and Biophysics* 74 (2): 443–50. http://www.ncbi.nlm.nih.gov/pubmed/13534673.

Eng, Jimmy K, Brian C Searle, Karl R Clauser, and David L Tabb. 2011. “A Face in the Crowd: Recognizing Peptides through Database Search.” *Molecular & Cellular Proteomics : MCP* 10 (11): R111.009522. doi:10.1074/mcp.R111.009522.

Ettre, L.S. 1980. “Relative Retention Expressions in Chromatography.” *Journal of Chromatography A* 198 (3): 229–34. doi:10.1016/S0021-9673(00)84761-5.

Farhan, Sali M K, Jian Wang, John F Robinson, Piya Lahiry, Victoria M Siu, Chitra Prasad, Jonathan B Kronick, David A Ramsay, C Anthony Rupar, and Robert A Hegele. 2014. “Exome Sequencing Identifies NFS1 Deficiency in a Novel Fe-S Cluster Disease, Infantile Mitochondrial Complex II/III Deficiency.” *Molecular Genetics & Genomic Medicine* 2 (1): 73–80. doi:10.1002/mgg3.46.

Fassone, Elisa, and Shamima Rahman. 2012. “Complex I Deficiency: Clinical Features, Biochemistry and Molecular Genetics.” *Journal of Medical Genetics* 49 (9): 578–90. doi:10.1136/jmedgenet-2012-101159.

Fernández-Vizarra, Erika, and Massimo Zeviani. 2015. “Nuclear Gene Mutations as the Cause of Mitochondrial Complex III Deficiency.” *Frontiers in Genetics* 6 (January): 134. doi:10.3389/fgene.2015.00134.

Forcisi, Sara, Franco Moritz, Basem Kanawati, Dimitrios Tziotis, Rainer Lehmann, and Philippe Schmitt-Kopplin. 2013. “Liquid Chromatography-Mass Spectrometry in Metabolomics Research: Mass Analyzers in Ultra High Pressure Liquid Chromatography Coupling.” *Journal of Chromatography. A* 1292 (May): 51–65. doi:10.1016/j.chroma.2013.04.017.

Fosset, Cédric, Marie-Jeanne Chauveau, Blanche Guillon, Frédéric Canal, Jean-Claude Drapier, and Cécile Bouton. 2006. “RNA Silencing of Mitochondrial M-Nfs1 Reduces Fe-S Enzyme Activity Both in Mitochondria and Cytosol of Mammalian Cells.” *The Journal of Biological Chemistry* 281 (35): 25398–406. doi:10.1074/jbc.M602979200.

Franceschini, Andrea, Damian Szklarczyk, Sune Frankild, Michael Kuhn, Milan Simonovic, Alexander Roth, Jianyi Lin, et al. 2013. “STRING v9.1: Protein-Protein Interaction Networks, with Increased Coverage and Integration.” *Nucleic Acids Research* 41 (Database issue): D808–15. doi:10.1093/nar/gks1094.

Funk, Werner, Vera Dammann, and Gerhild Donnevert. 2007. *Quality Assurance in Analytical Chemistry: Applications in Environmental, Food and Materials Analysis, Biotechnology, and Medical Engineering*. John Wiley & Sons. https://books.google.com/books?id=evtfXManNAEC&pgis=1.

Garcia, J. J. 2000. “Structure, Functioning, and Assembly of the ATP Synthase in Cells from Patients with the T8993G Mitochondrial DNA Mutation. COMPARISON WITH THE ENZYME IN Rho0 CELLS COMPLETELY LACKING mtDNA.” *Journal of Biological Chemistry* 275 (15): 11075–81. doi:10.1074/jbc.275.15.11075.

Gielisch, Ina, and David Meierhofer. 2015. “Metabolome and Proteome Profiling of Complex I Deficiency Induced by Rotenone.” *Journal of Proteome Research* 14 (1): 224–35. doi:10.1021/pr500894v.

Gilkerson, Robert W, Daciana H Margineantu, Roderick A Capaldi, and Jeanne M.L Selker. 2000. “Mitochondrial DNA Depletion Causes Morphological Changes in the Mitochondrial Reticulum of Cultured Human Cells.” *FEBS Letters* 474 (1): 1–4. doi:10.1016/S0014-5793(00)01527-1.

Gillardon, Frank. 2006. “Differential Mitochondrial Protein Expression Profiling in Neurodegenerative Diseases.” *Electrophoresis* 27 (13): 2814–18. doi:10.1002/elps.200500911.

Glotzer, Michael. 2009. “The 3Ms of Central Spindle Assembly: Microtubules, Motors and MAPs.” *Nature Reviews. Molecular Cell Biology* 10 (1): 9–20. doi:10.1038/nrm2609.

Goeman, Jelle J, Sara A van de Geer, Floor de Kort, and Hans C van Houwelingen. 2004. “A Global Test for Groups of Genes: Testing Association with a Clinical Outcome.” *Bioinformatics (Oxford, England)* 20 (1): 93–99. http://www.ncbi.nlm.nih.gov/pubmed/14693814.

Golen, Kenneth, ed. 2010. *The Rho GTPases in Cancer*. New York, NY: Springer New York. doi:10.1007/978-1-4419-1111-7.

Goto, Y., S. Horai, T. Matsuoka, Y. Koga, K. Nihei, M. Kobayashi, and I. Nonaka. 1992. “Mitochondrial Myopathy, Encephalopathy, Lactic Acidosis, and Stroke-like Episodes (MELAS): A Correlative Study of the Clinical Features and Mitochondrial DNA Mutation.” *Neurology* 42 (3): 545–545. doi:10.1212/WNL.42.3.545.

Govek, Eve-Ellen, Sarah E Newey, and Linda Van Aelst. 2005. “The Role of the Rho GTPases in Neuronal Development.” *Genes & Development* 19 (1): 1–49. doi:10.1101/gad.1256405.

Guan, M X, N Fischel-Ghodsian, and G Attardi. 1996. “Biochemical Evidence for Nuclear Gene Involvement in Phenotype of Non-Syndromic Deafness Associated with Mitochondrial 12S rRNA Mutation.” *Human Molecular Genetics* 5 (7): 963–71. http://www.ncbi.nlm.nih.gov/pubmed/8817331.

Guha, M, S Srinivasan, G Ruthel, A K Kashina, R P Carstens, A Mendoza, C Khanna, T Van Winkle, and N G Avadhani. 2014. “Mitochondrial Retrograde Signaling Induces Epithelial-Mesenchymal Transition and Generates Breast Cancer Stem Cells.” *Oncogene* 33 (45). Macmillan Publishers Limited: 5238–50. doi:10.1038/onc.2013.467.

Gygi, S P, B Rist, S A Gerber, F Turecek, M H Gelb, and R Aebersold. 1999. “Quantitative Analysis of Complex Protein Mixtures Using Isotope-Coded Affinity Tags.” *Nature Biotechnology* 17 (10): 994–99. doi:10.1038/13690.

Hackenbrock, C R. 1968. “Ultrastructural Bases for Metabolically Linked Mechanical Activity in Mitochondria. II. Electron Transport-Linked Ultrastructural Transformations in Mitochondria.” *The Journal of Cell Biology* 37 (2): 345–69. http://www.pubmedcentral.nih.gov/articlerender.fcgi?artid=2107416&tool=pmcentrez&rendertype=abstract.

Hall, A. 1990. “The Cellular Functions of Small GTP-Binding Proteins.” *Science (New York, N.Y.)* 249 (4969): 635–40. http://www.ncbi.nlm.nih.gov/pubmed/2116664.

Han, Guoge, Robert J. Casson, Glyn Chidlow, and John P. M. Wood. 2014. “The Mitochondrial Complex I Inhibitor Rotenone Induces Endoplasmic Reticulum Stress and Activation of GSK-3β in Cultured Rat Retinal Cells.” *Investigative Opthalmology & Visual Science* 55 (9): 5616. doi:10.1167/iovs.14-14371.

Harrigan, George G., and Royston Goodacre, eds. 2003. *Metabolic Profiling: Its Role in Biomarker Discovery and Gene Function Analysis*. Boston, MA: Springer US. doi:10.1007/978-1-4615-0333-0.

Hashiguchi, Kazunari, and Qiu-Mei Zhang-Akiyama. 2009. “Establishment of Human Cell Lines Lacking Mitochondrial DNA.” *Methods in Molecular Biology (Clifton, N.J.)* 554 (January): 383–91. doi:10.1007/978-1-59745-521-3_23.

Hayashi, Genki, and Gino Cortopassi. 2015. “Oxidative Stress in Inherited Mitochondrial Diseases.” *Free Radical Biology & Medicine*, June. doi:10.1016/j.freeradbiomed.2015.05.039.

Hennrich, M. L., and A.-C. Gavin. 2015. “Quantitative Mass Spectrometry of Posttranslational Modifications: Keys to Confidence.” *Science Signaling* 8 (371): re5–re5. doi:10.1126/scisignal.aaa6466.

Heo, Jun Young, Ji Hoon Park, Soung Jung Kim, Kang Sik Seo, Jeong Su Han, Sang Hee Lee, Jin Man Kim, et al. 2012. “DJ-1 Null Dopaminergic Neuronal Cells Exhibit Defects in Mitochondrial Function and Structure: Involvement of Mitochondrial Complex I Assembly.” *PloS One* 7 (3). Public Library of Science: e32629. doi:10.1371/journal.pone.0032629.

Higurashi, Miho, Takashi Ishida, and Kengo Kinoshita. 2008. “Identification of Transient Hub Proteins and the Possible Structural Basis for Their Multiple Interactions.” *Protein Science : A Publication of the Protein Society* 17 (1): 72–78. doi:10.1110/ps.073196308.

Horai, Hisayuki, Masanori Arita, Shigehiko Kanaya, Yoshito Nihei, Tasuku Ikeda, Kazuhiro Suwa, Yuya Ojima, et al. 2010. “MassBank: A Public Repository for Sharing Mass Spectral Data for Life Sciences.” *Journal of Mass Spectrometry : JMS* 45 (7): 703–14. doi:10.1002/jms.1777.

Hu, Chi-Kuo, Margaret Coughlin, and Timothy J Mitchison. 2012. “Midbody Assembly and Its Regulation during Cytokinesis.” *Molecular Biology of the Cell* 23 (6): 1024–34. doi:10.1091/mbc.E11-08-0721.

Huang, Da Wei, Brad T Sherman, and Richard A Lempicki. 2009a. “Bioinformatics Enrichment Tools: Paths toward the Comprehensive Functional Analysis of Large Gene Lists.” *Nucleic Acids Research* 37 (1): 1–13. doi:10.1093/nar/gkn923.

———. 2009b. “Systematic and Integrative Analysis of Large Gene Lists Using

DAVID Bioinformatics Resources." *Nature Protocols* 4 (1): 44–57. doi:10.1038/nprot.2008.211.

Huang, Kaiyao, Dennis R Diener, and Joel L Rosenbaum. 2009. "The Ubiquitin Conjugation System Is Involved in the Disassembly of Cilia and Flagella." *The Journal of Cell Biology* 186 (4): 601–13. doi:10.1083/jcb.200903066.

Humphrey, Sean J., David E. James, and Matthias Mann. 2015. "Protein Phosphorylation: A Major Switch Mechanism for Metabolic Regulation." *Trends in Endocrinology & Metabolism*, October. doi:10.1016/j.tem.2015.09.013.

Huoponen, K, J Vilkki, P Aula, E K Nikoskelainen, and M L Savontaus. 1991. "A New mtDNA Mutation Associated with Leber Hereditary Optic Neuroretinopathy." *American Journal of Human Genetics* 48 (6): 1147–53. http://www.pubmedcentral.nih.gov/articlerender.fcgi?artid=1683111&tool=pmcentrez&rendertype=abstract.

Hurley, James H, and Harald Stenmark. 2011. "Molecular Mechanisms of Ubiquitin-Dependent Membrane Traffic." *Annual Review of Biophysics* 40 (January): 119–42. doi:10.1146/annurev-biophys-042910-155404.

Iesmantavicius, Vytautas, Brian T Weinert, and Chunaram Choudhary. 2014. "Convergence of Ubiquitylation and Phosphorylation Signaling in Rapamycin-Treated Yeast Cells." *Molecular & Cellular Proteomics : MCP* 13 (8): 1979–92. doi:10.1074/mcp.O113.035683.

Inoue, K, D Takai, H Hosaka, S Ito, H Shitara, K Isobe, J B LePecq, E Segal-Bendirdjian, and J Hayashi. 1997. "Isolation and Characterization of Mitochondrial DNA-Less Lines from Various Mammalian Cell Lines by Application of an Anticancer Drug, Ditercalinium." *Biochemical and Biophysical Research Communications* 239 (1): 257–60. http://www.ncbi.nlm.nih.gov/pubmed/9345305.

Iqbal, K, and I Grundke-Iqbal. 1991. "Ubiquitination and Abnormal Phosphorylation of Paired Helical Filaments in Alzheimer's Disease." *Molecular Neurobiology* 5 (2-4): 399–410. http://www.ncbi.nlm.nih.gov/pubmed/1726645.

Jazayeri, M. 2003. “Inducible Expression of a Dominant Negative DNA Polymerase-Gamma Depletes Mitochondrial DNA and Produces a Rho 0 Phenotype.” *Journal of Biological Chemistry* 278 (11): 9823–30. doi:10.1074/jbc.M211730200.

Jazwinski, S Michal. 2013. “The Retrograde Response: When Mitochondrial Quality Control Is Not Enough.” *Biochimica et Biophysica Acta* 1833 (2): 400–409. doi:10.1016/j.bbamcr.2012.02.010.

Jedrychowski, Mark P, Edward L Huttlin, Wilhelm Haas, Mathew E Sowa, Ramin Rad, and Steven P Gygi. 2011. “Evaluation of HCD- and CID-Type Fragmentation within Their Respective Detection Platforms for Murine Phosphoproteomics.” *Molecular & Cellular Proteomics : MCP* 10 (12): M111.009910. doi:10.1074/mcp.M111.009910.

Jiang, S., J. Cai, D. C. Wallace, and D. P. Jones. 1999. “Cytochrome c-Mediated Apoptosis in Cells Lacking Mitochondrial DNA: SIGNALING PATHWAY INVOLVING RELEASE AND CASPASE 3 ACTIVATION IS CONSERVED.” *Journal of Biological Chemistry* 274 (42): 29905–11. doi:10.1074/jbc.274.42.29905.

Johns, D R, M J Neufeld, and R D Park. 1992. “An ND-6 Mitochondrial DNA Mutation Associated with Leber Hereditary Optic Neuropathy.” *Biochemical and Biophysical Research Communications* 187 (3): 1551–57. http://www.ncbi.nlm.nih.gov/pubmed/1417830.

Johnson, Caroline H, and Frank J Gonzalez. 2012. “Challenges and Opportunities of Metabolomics.” *Journal of Cellular Physiology* 227 (8): 2975–81. doi:10.1002/jcp.24002.

Kann, Maricel G. 2007. “Protein Interactions and Disease: Computational Approaches to Uncover the Etiology of Diseases.” *Briefings in Bioinformatics* 8 (5): 333–46. doi:10.1093/bib/bbm031.

Khan, Nahid Akhtar, Periyasamy Govindaraj, Angamuthu Kannan Meena, and Kumarasamy Thangaraj. 2015. “Mitochondrial Disorders: Challenges in Diagnosis & Treatment.” *The Indian Journal of Medical Research* 141 (1): 13–

26. http://www.pubmedcentral.nih.gov/articlerender.fcgi?artid=4405934&tool=pmcentrez&rendertype=abstract.

Khatri, Purvesh, Marina Sirota, and Atul J Butte. 2012. “Ten Years of Pathway Analysis: Current Approaches and Outstanding Challenges.” *PLoS Computational Biology* 8 (2). Public Library of Science: e1002375. doi:10.1371/journal.pcbi.1002375.

King, M P, and G Attardi. 1996. “Isolation of Human Cell Lines Lacking Mitochondrial DNA.” *Methods in Enzymology* 264 (January): 304–13. http://www.ncbi.nlm.nih.gov/pubmed/8965704.

Kirches, E. 2011. “LHON: Mitochondrial Mutations and More.” *Current Genomics* 12 (1): 44–54. doi:10.2174/138920211794520150.

Kitteringham, Neil R., Rosalind E. Jenkins, Catherine S. Lane, Victoria L. Elliott, and B. Kevin Park. 2009. “Multiple Reaction Monitoring for Quantitative Biomarker Analysis in Proteomics and Metabolomics☆.” *Journal of Chromatography B* 877 (13): 1229–39. doi:10.1016/j.jchromb.2008.11.013.

Kölling, R, and C P Hollenberg. 1994. “The ABC-Transporter Ste6 Accumulates in the Plasma Membrane in a Ubiquitinated Form in Endocytosis Mutants.” *The EMBO Journal* 13 (14): 3261–71. http://www.pubmedcentral.nih.gov/articlerender.fcgi?artid=395222&tool=pmcentrez&rendertype=abstract.

Komander, David. 2009. “The Emerging Complexity of Protein Ubiquitination.” *Biochemical Society Transactions* 37 (Pt 5): 937–53. doi:10.1042/BST0370937.

Komander, David, and Michael Rape. 2012. “The Ubiquitin Code.” *Annual Review of Biochemistry* 81 (January). Annual Reviews: 203–29. doi:10.1146/annurev-biochem-060310-170328.

Kozma, R, S Sarner, S Ahmed, and L Lim. 1997. “Rho Family GTPases and Neuronal Growth Cone Remodelling: Relationship between Increased Complexity Induced by Cdc42Hs, Rac1, and Acetylcholine and Collapse Induced by RhoA and

Lysophosphatidic Acid." *Mol. Cell. Biol.* 17 (3): 1201–11. http://mcb.asm.org/content/17/3/1201.abstract?ijkey=447987082ada23782b515088632dc6c0244124f8&keytype2=tf_ipsecsha.

Kraft, Claudine, Anna Deplazes, Marc Sohrmann, and Matthias Peter. 2008. "Mature Ribosomes Are Selectively Degraded upon Starvation by an Autophagy Pathway Requiring the Ubp3p/Bre5p Ubiquitin Protease." *Nature Cell Biology* 10 (5). Nature Publishing Group: 602–10. doi:10.1038/ncb1723.

Krawetz, Stephen. 2008. *Bioinformatics for Systems Biology*. Springer Science & Business Media. https://books.google.com/books?id=s0SxfCuJfOsC&pgis=1.

Kruve, Anneli, Riin Rebane, Karin Kipper, Maarja-Liisa Oldekop, Hanno Evard, Koit Herodes, Pekka Ravio, and Ivo Leito. 2015. "Tutorial Review on Validation of Liquid Chromatography-Mass Spectrometry Methods: Part I." *Analytica Chimica Acta* 870 (April): 29–44. doi:10.1016/j.aca.2015.02.017.

Kuehnbaum, Naomi L, and Philip Britz-McKibbin. 2013. "New Advances in Separation Science for Metabolomics: Resolving Chemical Diversity in a Post-Genomic Era." *Chemical Reviews* 113 (4). American Chemical Society: 2437–68. doi:10.1021/cr300484s.

Kukat, Alexandra, Christian Kukat, Jan Brocher, Ingo Schäfer, Georg Krohne, Ian A Trounce, Gaetano Villani, and Peter Seibel. 2008. "Generation of rho0 Cells Utilizing a Mitochondrially Targeted Restriction Endonuclease and Comparative Analyses." *Nucleic Acids Research* 36 (7): e44. doi:10.1093/nar/gkn124.

Lambert, Adrian J, and Martin D Brand. 2004. "Inhibitors of the Quinone-Binding Site Allow Rapid Superoxide Production from Mitochondrial NADH:ubiquinone Oxidoreductase (complex I)." *The Journal of Biological Chemistry* 279 (38): 39414–20. doi:10.1074/jbc.M406576200.

Lazarou, Michael, David R Thorburn, Michael T Ryan, and Matthew McKenzie. 2009. "Assembly of Mitochondrial Complex I and Defects in Disease." *Biochimica et Biophysica Acta* 1793 (1): 78–88. doi:10.1016/j.bbamcr.2008.04.015.

Lee, Soojin. 2015. "Systems Biology - A Pivotal Research Methodology for

Understanding the Mechanisms of Traditional Medicine." *Journal of Pharmacopuncture* 18 (3): 11–18. doi:10.3831/KPI.2015.18.020.

Lei, Zhentian, David V Huhman, and Lloyd W Sumner. 2011. "Mass Spectrometry Strategies in Metabolomics." *The Journal of Biological Chemistry* 286 (29): 25435–42. doi:10.1074/jbc.R111.238691.

Lev, Nirit, Debby Ickowicz, Eldad Melamed, and Daniel Offen. 2008. "Oxidative Insults Induce DJ-1 Upregulation and Redistribution: Implications for Neuroprotection." *Neurotoxicology* 29 (3): 397–405. doi:10.1016/j.neuro.2008.01.007.

Li, Nianyu, Kathy Ragheb, Gretchen Lawler, Jennie Sturgis, Bartek Rajwa, J Andres Melendez, and J Paul Robinson. 2003. "Mitochondrial Complex I Inhibitor Rotenone Induces Apoptosis through Enhancing Mitochondrial Reactive Oxygen Species Production." *The Journal of Biological Chemistry* 278 (10): 8516–25. doi:10.1074/jbc.M210432200.

Lightowlers, R. N., R. W. Taylor, and D. M. Turnbull. 2015. "Mutations Causing Mitochondrial Disease: What Is New and What Challenges Remain?" *Science* 349 (6255): 1494–99. doi:10.1126/science.aac7516.

Lill, Roland, and Ulrich Mühlenhoff. 2006. "Iron-Sulfur Protein Biogenesis in Eukaryotes: Components and Mechanisms." *Annual Review of Cell and Developmental Biology* 22 (January): 457–86. doi:10.1146/annurev.cellbio.22.010305.104538.

Linnett, P E, and R B Beechey. 1979. "Inhibitors of the ATP Synthethase System." *Methods in Enzymology* 55 (January): 472–518. http://www.ncbi.nlm.nih.gov/pubmed/156854.

Liu, Yichin, Lara Fallon, Hilal A Lashuel, Zhihua Liu, and Peter T Lansbury. 2002. "The UCH-L1 Gene Encodes Two Opposing Enzymatic Activities That Affect Alpha-Synuclein Degradation and Parkinson's Disease Susceptibility." *Cell* 111 (2): 209–18. http://www.ncbi.nlm.nih.gov/pubmed/12408865.

Lommen, Arjen. 2009. "MetAlign: Interface-Driven, Versatile Metabolomics Tool for

Hyphenated Full-Scan Mass Spectrometry Data Preprocessing." *Analytical Chemistry* 81 (8): 3079–86. doi:10.1021/ac900036d.

Lu, Wenyun, Bryson D Bennett, and Joshua D Rabinowitz. 2008. "Analytical Strategies for LC-MS-Based Targeted Metabolomics." *Journal of Chromatography. B, Analytical Technologies in the Biomedical and Life Sciences* 871 (2): 236–42. doi:10.1016/j.jchromb.2008.04.031.

Ma'ayan, Avi. 2011. "Introduction to Network Analysis in Systems Biology." *Science Signaling* 4 (190): tr5. doi:10.1126/scisignal.2001965.

Machnicka, B, R Grochowalska, D M Bogusławska, A F Sikorski, and M C Lecomte. 2012. "Spectrin-Based Skeleton as an Actor in Cell Signaling." *Cellular and Molecular Life Sciences : CMLS* 69 (2): 191–201. doi:10.1007/s00018-011-0804-5.

Maeting, Ines, Georg Schmidt, Hermann Sahm, and K.-Peter Stahmann. 2000. "Role of a Peroxisomal NADP-Specific Isocitrate Dehydrogenase in the Metabolism of the Riboflavin Overproducer Ashbya Gossypii." *Journal of Molecular Catalysis B: Enzymatic* 10 (1-3): 335–43. doi:10.1016/S1381-1177(00)00135-1.

Mailloux, Ryan J. 2015. "Teaching the Fundamentals of Electron Transfer Reactions in Mitochondria and the Production and Detection of Reactive Oxygen Species." *Redox Biology* 4 (January): 381–98. doi:10.1016/j.redox.2015.02.001.

Mandel, John. 2012. *The Statistical Analysis of Experimental Data*. https://books.google.com/books?hl=de&lr=&id=4qHDAgAAQBAJ&pgis=1.

Mannella, Carmen A. 2006. "Structure and Dynamics of the Mitochondrial Inner Membrane Cristae." *Biochimica et Biophysica Acta* 1763 (5-6): 542–48. doi:10.1016/j.bbamcr.2006.04.006.

Marín-García, José. 2012. *Mitochondria and Their Role in Cardiovascular Disease*. Springer Science & Business Media. https://books.google.com/books?hl=de&lr=&id=zNMt-4wsHjEC&pgis=1.

Mayr, Johannes A, Tobias B Haack, Peter Freisinger, Daniela Karall, Christine Makowski, Johannes Koch, René G Feichtinger, et al. 2015. "Spectrum of

Combined Respiratory Chain Defects." *Journal of Inherited Metabolic Disease*, March. doi:10.1007/s10545-015-9831-y.

Mena, Natalia P, Anne Laure Bulteau, Julio Salazar, Etienne C Hirsch, and Marco T Núñez. 2011. "Effect of Mitochondrial Complex I Inhibition on Fe-S Cluster Protein Activity." *Biochemical and Biophysical Research Communications* 409 (2): 241–46. doi:10.1016/j.bbrc.2011.04.137.

Mendes, P, D Camacho, and A de la Fuente. 2005. "Modelling and Simulation for Metabolomics Data Analysis." *Biochemical Society Transactions* 33 (Pt 6): 1427–29. doi:10.1042/BST20051427.

Mick, David U, Thomas D Fox, and Peter Rehling. 2011. "Inventory Control: Cytochrome c Oxidase Assembly Regulates Mitochondrial Translation." *Nature Reviews. Molecular Cell Biology* 12 (1): 14–20. doi:10.1038/nrm3029.

Miranda, Manuel, Kalen R Dionne, Tatiana Sorkina, and Alexander Sorkin. 2007. "Three Ubiquitin Conjugation Sites in the Amino Terminus of the Dopamine Transporter Mediate Protein Kinase C-Dependent Endocytosis of the Transporter." *Molecular Biology of the Cell* 18 (1): 313–23. doi:10.1091/mbc.E06-08-0704.

Miranda, Manuel, and Alexander Sorkin. 2007. "Regulation of Receptors and Transporters by Ubiquitination: New Insights into Surprisingly Similar Mechanisms." *Molecular Interventions* 7 (3). American Society for Pharmacology and Experimental Therapeutics: 157–67. doi:10.1124/mi.7.3.7.

Miranda, Manuel, Christine C Wu, Tatiana Sorkina, Davin R Korstjens, and Alexander Sorkin. 2005. "Enhanced Ubiquitylation and Accelerated Degradation of the Dopamine Transporter Mediated by Protein Kinase C." *The Journal of Biological Chemistry* 280 (42): 35617–24. doi:10.1074/jbc.M506618200.

Mizuno, Emi, Takanobu Iura, Akiko Mukai, Tamotsu Yoshimori, Naomi Kitamura, and Masayuki Komada. 2005. "Regulation of Epidermal Growth Factor Receptor down-Regulation by UBPY-Mediated Deubiquitination at Endosomes." *Molecular Biology of the Cell* 16 (11): 5163–74. doi:10.1091/mbc.E05-06-0560.

Muller, Florian L, Yuhong Liu, Muhammad A Abdul-Ghani, Michael S Lustgarten, Arunabh Bhattacharya, Youngmok C Jang, and Holly Van Remmen. 2008. “High Rates of Superoxide Production in Skeletal-Muscle Mitochondria Respiring on Both Complex I- and Complex II-Linked Substrates.” *The Biochemical Journal* 409 (2): 491–99. doi:10.1042/BJ20071162.

Naz, Shama, Maria Vallejo, Antonia García, and Coral Barbas. 2014. “Method Validation Strategies Involved in Non-Targeted Metabolomics.” *Journal of Chromatography. A* 1353 (August): 99–105. doi:10.1016/j.chroma.2014.04.071.

Neef, Rüdiger, Christian Preisinger, Josephine Sutcliffe, Robert Kopajtich, Erich A Nigg, Thomas U Mayer, and Francis A Barr. 2003. “Phosphorylation of Mitotic Kinesin-like Protein 2 by Polo-like Kinase 1 Is Required for Cytokinesis.” *The Journal of Cell Biology* 162 (5): 863–75. doi:10.1083/jcb.200306009.

New, David C, and Yung H Wong. 2007. “Molecular Mechanisms Mediating the G Protein-Coupled Receptor Regulation of Cell Cycle Progression.” *Journal of Molecular Signaling* 2 (January): 2. doi:10.1186/1750-2187-2-2.

Newman, M.E. J. 2005. “A Measure of Betweenness Centrality Based on Random Walks.” *Social Networks* 27 (1): 39–54. doi:10.1016/j.socnet.2004.11.009.

Noack, Stephan, and Wolfgang Wiechert. 2014. “Quantitative Metabolomics: A Phantom?” *Trends in Biotechnology* 32 (5): 238–44. doi:10.1016/j.tibtech.2014.03.006.

Olsen, Jesper V, Boris Macek, Oliver Lange, Alexander Makarov, Stevan Horning, and Matthias Mann. 2007. “Higher-Energy C-Trap Dissociation for Peptide Modification Analysis.” *Nature Methods* 4 (9): 709–12. doi:10.1038/nmeth1060.

Olsen, Jesper V, Michiel Vermeulen, Anna Santamaria, Chanchal Kumar, Martin L Miller, Lars J Jensen, Florian Gnad, et al. 2010. “Quantitative Phosphoproteomics Reveals Widespread Full Phosphorylation Site Occupancy during Mitosis.” *Science Signaling* 3 (104): ra3. doi:10.1126/scisignal.2000475.

Ong, S.-E. 2002. “Stable Isotope Labeling by Amino Acids in Cell Culture, SILAC, as a Simple and Accurate Approach to Expression Proteomics.” *Molecular &*

Cellular Proteomics 1 (5): 376–86. doi:10.1074/mcp.M200025-MCP200.

Orr, Adam L, Leonardo Vargas, Carolina N Turk, Janine E Baaten, Jason T Matzen, Victoria J Dardov, Stephen J Attle, et al. 2015. "Suppressors of Superoxide Production from Mitochondrial Complex III." *Nature Chemical Biology* 11 (11). Nature Publishing Group, a division of Macmillan Publishers Limited. All Rights Reserved.: 834–36. doi:10.1038/nchembio.1910.

Orr, Adam L., Deepthi Ashok, Melissa R. Sarantos, Tong Shi, Robert E. Hughes, and Martin D. Brand. 2013. "Inhibitors of ROS Production by the Ubiquinone-Binding Site of Mitochondrial Complex I Identified by Chemical Screening." *Free Radical Biology and Medicine* null (null). doi:10.1016/j.freeradbiomed.2013.08.170.

Ouchane, Soufian, Ileana Agalidis, and Chantal Astier. 2002. "Natural Resistance to Inhibitors of the Ubiquinol Cytochrome c Oxidoreductase of Rubrivivax Gelatinosus: Sequence and Functional Analysis of the Cytochrome bc(1) Complex." *Journal of Bacteriology* 184 (14): 3815–22. http://www.pubmedcentral.nih.gov/articlerender.fcgi?artid=135180&tool=pmcentrez&rendertype=abstract.

Owusu-Ansah, Edward, Amir Yavari, Sudip Mandal, and Utpal Banerjee. 2008. "Distinct Mitochondrial Retrograde Signals Control the G1-S Cell Cycle Checkpoint." *Nature Genetics* 40 (3). Nature Publishing Group: 356–61. doi:10.1038/ng.2007.50.

Pandey, Suwarna, Suhel Parvez, Iqbal Sayeed, Rizwanul Haque, Bilal Bin-Hafeez, and Sheikh Raisuddin. 2003. "Biomarkers of Oxidative Stress: A Comparative Study of River Yamuna Fish Wallago Attu (Bl. & Schn.)." *The Science of the Total Environment* 309 (1-3): 105–15. doi:10.1016/S0048-9697(03)00006-8.

Patti, Gary J, Oscar Yanes, and Gary Siuzdak. 2012. "Innovation: Metabolomics: The Apogee of the Omics Trilogy." *Nature Reviews. Molecular Cell Biology* 13 (4): 263–69. doi:10.1038/nrm3314.

Pence, Harry E., and Antony Williams. 2010. "ChemSpider: An Online Chemical

Information Resource." *Journal of Chemical Education* 87 (11). American Chemical Society: 1123–24. doi:10.1021/ed100697w.

Perry, RH, RG Cooks, and RJ. Noll. 2008. "Orbitrap Mass Spectrometry: Instrumentation, Ion Motion and Applications. - PubMed - NCBI." *Mass Spectrometry Reviews*. doi:10.1002/mas.20186.

Querec, Troy D, Rama S Akondy, Eva K Lee, Weiping Cao, Helder I Nakaya, Dirk Teuwen, Ali Pirani, et al. 2009. "Systems Biology Approach Predicts Immunogenicity of the Yellow Fever Vaccine in Humans." *Nature Immunology* 10 (1). Nature Publishing Group: 116–25. doi:10.1038/ni.1688.

Raemaekers, Tim, Katharina Ribbeck, Joel Beaudouin, Wim Annaert, Mark Van Camp, Ingrid Stockmans, Nico Smets, Roger Bouillon, Jan Ellenberg, and Geert Carmeliet. 2003. "NuSAP, a Novel Microtubule-Associated Protein Involved in Mitotic Spindle Organization." *The Journal of Cell Biology* 162 (6): 1017–29. doi:10.1083/jcb.200302129.

Rahmatallah, Y, F Emmert-Streib, and G Glazko. 2012. "Gene Set Analysis for Self-Contained Tests: Complex Null and Specific Alternative Hypotheses." *Bioinformatics (Oxford, England)* 28 (23): 3073–80. doi:10.1093/bioinformatics/bts579.

Rappsilber, Juri, Ursula Ryder, Angus I Lamond, and Matthias Mann. 2002. "Large-Scale Proteomic Analysis of the Human Spliceosome." *Genome Research* 12 (8): 1231–45. doi:10.1101/gr.473902.

Richter, C. 1992. "Reactive Oxygen and DNA Damage in Mitochondria." *Mutation Research* 275 (3-6): 249–55. http://www.ncbi.nlm.nih.gov/pubmed/1383767.

Ridley, Anne J., Hugh F. Paterson, Caroline L. Johnston, Dagmar Diekmann, and Alan Hall. 1992. "The Small GTP-Binding Protein Rac Regulates Growth Factor-Induced Membrane Ruffling." *Cell* 70 (3): 401–10. doi:10.1016/0092-8674(92)90164-8.

Ritchie, Marylyn D., Emily R. Holzinger, Ruowang Li, Sarah A. Pendergrass, and Dokyoon Kim. 2015. "Methods of Integrating Data to Uncover Genotype–

phenotype Interactions." *Nature Reviews Genetics* 16 (2). Nature Publishing Group, a division of Macmillan Publishers Limited. All Rights Reserved.: 85–97. doi:10.1038/nrg3868.

Rojo, David, Coral Barbas, and Francisco J Rupérez. 2012. "LC-MS Metabolomics of Polar Compounds." *Bioanalysis* 4 (10): 1235–43. doi:10.4155/bio.12.100.

Rommelaere, Guillaume, Sébastien Michel, Ludovic Mercy, Antoine Fattaccioli, Catherine Demazy, Noelle Ninane, Andrée Houbion, Patricia Renard, and Thierry Arnould. 2011. "Hypersensitivity of mtDNA-Depleted Cells to Staurosporine-Induced Apoptosis: Roles of Bcl-2 Downregulation and Cathepsin B." *American Journal of Physiology. Cell Physiology* 300 (5): C1090–1106. doi:10.1152/ajpcell.00037.2010.

Roshak, A K, E A Capper, C Imburgia, J Fornwald, G Scott, and L A Marshall. 2000. "The Human Polo-like Kinase, PLK, Regulates cdc2/cyclin B through Phosphorylation and Activation of the cdc25C Phosphatase." *Cellular Signalling* 12 (6): 405–11. http://www.ncbi.nlm.nih.gov/pubmed/11202906.

Ross, Philip L, Yulin N Huang, Jason N Marchese, Brian Williamson, Kenneth Parker, Stephen Hattan, Nikita Khainovski, et al. 2004. "Multiplexed Protein Quantitation in Saccharomyces Cerevisiae Using Amine-Reactive Isobaric Tagging Reagents." *Molecular & Cellular Proteomics : MCP* 3 (12): 1154–69. doi:10.1074/mcp.M400129-MCP200.

Rouault, Tracey A. 2012. "Biogenesis of Iron-Sulfur Clusters in Mammalian Cells: New Insights and Relevance to Human Disease." *Disease Models & Mechanisms* 5 (2): 155–64. doi:10.1242/dmm.009019.

Saha, Prasenjit Prasad, Shubhi Srivastava, Praveen Kumar S K, Devanjan Sinha, and Patrick D'Silva. 2015. "Mapping Key Residues of ISD11 Critical for NFS1-ISD11 Subcomplex Stability: IMPLICATIONS IN THE DEVELOPMENT OF MITOCHONDRIAL DISORDER, COXPD19." *The Journal of Biological Chemistry* 290 (43): 25876–90. doi:10.1074/jbc.M115.678508.

Schaefer, Andrew M, Robert McFarland, Emma L Blakely, Langping He, Roger G

Whittaker, Robert W Taylor, Patrick F Chinnery, and Douglass M Turnbull. 2008. "Prevalence of Mitochondrial DNA Disease in Adults." *Annals of Neurology* 63 (1): 35–39. doi:10.1002/ana.21217.

Schapira, Anthony H V. 2012. "Mitochondrial Diseases." *Lancet (London, England)* 379 (9828): 1825–34. doi:10.1016/S0140-6736(11)61305-6.

Schubert, Susanna, Sandra Heller, Birgit Löffler, Ingo Schäfer, Martina Seibel, Gaetano Villani, and Peter Seibel. 2015. "Generation of Rho Zero Cells: Visualization and Quantification of the mtDNA Depletion Process." *International Journal of Molecular Sciences* 16 (5): 9850–65. doi:10.3390/ijms16059850.

Schürmann, Andreas, Veronika Dvorak, Claudio Crüzer, Patrick Butcher, and Anton Kaufmann. 2009. "False-Positive Liquid Chromatography/tandem Mass Spectrometric Confirmation of Sebuthylazine Residues Using the Identification Points System according to EU Directive 2002/657/EC due to a Biogenic Insecticide in Tarragon." *Rapid Communications in Mass Spectrometry : RCM* 23 (8): 1196–1200. doi:10.1002/rcm.3982.

Scola, Gustavo, Helena K. Kim, L. Trevor Young, Mirian Salvador, and Ana C. Andreazza. 2014. "Lithium Reduces the Effects of Rotenone-Induced Complex I Dysfunction on DNA Methylation and Hydroxymethylation in Rat Cortical Primary Neurons." *Psychopharmacology* 231 (21): 4189–98. doi:10.1007/s00213-014-3565-7.

Secades, J J. 2011. "Citicoline: Pharmacological and Clinical Review, 2010 Update." *Revista de Neurologia* 52 Suppl 2 (March): S1–62. http://www.ncbi.nlm.nih.gov/pubmed/21432836.

Seo, Arnold Y, Anna-Maria Joseph, Debapriya Dutta, Judy C Y Hwang, John P Aris, and Christiaan Leeuwenburgh. 2010. "New Insights into the Role of Mitochondria in Aging: Mitochondrial Dynamics and More." *Journal of Cell Science* 123 (Pt 15): 2533–42. doi:10.1242/jcs.070490.

Seok, Junhee, H Shaw Warren, Alex G Cuenca, Michael N Mindrinos, Henry V Baker, Weihong Xu, Daniel R Richards, et al. 2013. "Genomic Responses in Mouse

Models Poorly Mimic Human Inflammatory Diseases." *Proceedings of the National Academy of Sciences of the United States of America* 110 (9): 3507–12. doi:10.1073/pnas.1222878110.

Shannon, Paul, Andrew Markiel, Owen Ozier, Nitin S Baliga, Jonathan T Wang, Daniel Ramage, Nada Amin, Benno Schwikowski, and Trey Ideker. 2003. "Cytoscape: A Software Environment for Integrated Models of Biomolecular Interaction Networks." *Genome Research* 13 (11): 2498–2504. doi:10.1101/gr.1239303.

Smith, Bradley N, Nicola Ticozzi, Claudia Fallini, Athina Soragia Gkazi, Simon Topp, Kevin P Kenna, Emma L Scotter, et al. 2014. "Exome-Wide Rare Variant Analysis Identifies TUBA4A Mutations Associated with Familial ALS." *Neuron* 84 (2): 324–31. doi:10.1016/j.neuron.2014.09.027.

Smith, Christopher P, and Peter E Thorsness. 2005. "Formation of an Energized Inner Membrane in Mitochondria with a Gamma-Deficient F1-ATPase." *Eukaryotic Cell* 4 (12): 2078–86. doi:10.1128/EC.4.12.2078-2086.2005.

Smith, Colin A, Grace O'Maille, Elizabeth J Want, Chuan Qin, Sunia A Trauger, Theodore R Brandon, Darlene E Custodio, Ruben Abagyan, and Gary Siuzdak. 2005. "METLIN: A Metabolite Mass Spectral Database." *Therapeutic Drug Monitoring* 27 (6): 747–51. http://www.ncbi.nlm.nih.gov/pubmed/16404815.

Smith, Colin A, Elizabeth J Want, Grace O'Maille, Ruben Abagyan, and Gary Siuzdak. 2006. "XCMS: Processing Mass Spectrometry Data for Metabolite Profiling Using Nonlinear Peak Alignment, Matching, and Identification." *Analytical Chemistry* 78 (3): 779–87. doi:10.1021/ac051437y.

Sorkina, Tatiana, Brian R Hoover, Nancy R Zahniser, and Alexander Sorkin. 2005. "Constitutive and Protein Kinase C-Induced Internalization of the Dopamine Transporter Is Mediated by a Clathrin-Dependent Mechanism." *Traffic (Copenhagen, Denmark)* 6 (2): 157–70. doi:10.1111/j.1600-0854.2005.00259.x.

Soundararajan, Rama, David Pearce, Rebecca P Hughey, and Thomas R Kleyman. 2010. "Role of Epithelial Sodium Channels and Their Regulators in Hypertension." *The Journal of Biological Chemistry* 285 (40): 30363–69.

doi:10.1074/jbc.R110.155341.

Spence, Jean, Rayappa Reddy Gali, Gunnar Dittmar, Fred Sherman, Michael Karin, and Daniel Finley. 2000. “Cell Cycle–Regulated Modification of the Ribosome by a Variant Multiubiquitin Chain.” *Cell* 102 (1): 67–76. doi:10.1016/S0092-8674(00)00011-8.

Srivastava, Pallavi, and Dulal Panda. 2007. “Rotenone Inhibits Mammalian Cell Proliferation by Inhibiting Microtubule Assembly through Tubulin Binding.” *The FEBS Journal* 274 (18): 4788–4801. doi:10.1111/j.1742-4658.2007.06004.x.

Starita, L. M., Y. Machida, S. Sankaran, J. E. Elias, K. Griffin, B. P. Schlegel, S. P. Gygi, and J. D. Parvin. 2004. “BRCA1-Dependent Ubiquitination of -Tubulin Regulates Centrosome Number.” *Molecular and Cellular Biology* 24 (19): 8457–66. doi:10.1128/MCB.24.19.8457-8466.2004.

Steen, Hanno, and Matthias Mann. 2004. “The ABC’s (and XYZ's) of Peptide Sequencing.” *Nature Reviews. Molecular Cell Biology* 5 (9). Nature Publishing Group: 699–711. doi:10.1038/nrm1468.

Subramanian, Aravind, Pablo Tamayo, Vamsi K Mootha, Sayan Mukherjee, Benjamin L Ebert, Michael A Gillette, Amanda Paulovich, et al. 2005. “Gene Set Enrichment Analysis: A Knowledge-Based Approach for Interpreting Genome-Wide Expression Profiles.” *Proceedings of the National Academy of Sciences of the United States of America* 102 (43): 15545–50. doi:10.1073/pnas.0506580102.

Svinkina, Tanya, Hongbo Gu, Jeffrey C. Silva, Philipp Mertins, Jana Qiao, Shaunt Fereshetian, Jacob D. Jaffe, Eric Kuhn, Namrata D. Udeshi, and Steven A. Carr. 2015. “Deep, Quantitative Coverage of the Lysine Acetylome Using Novel Anti-Acetyl-Lysine Antibodies and an Optimized Proteomic Workflow.” *Molecular & Cellular Proteomics*, May, mcp.O114.047555. doi:10.1074/mcp.O114.047555.

Syka, John E P, Joshua J Coon, Melanie J Schroeder, Jeffrey Shabanowitz, and Donald F Hunt. 2004. “Peptide and Protein Sequence Analysis by Electron Transfer Dissociation Mass Spectrometry.” *Proceedings of the National Academy of Sciences of the United States of America* 101 (26): 9528–33.

doi:10.1073/pnas.0402700101.

Sylvester, James E, Nathan Fischel-Ghodsian, Edward B Mougey, and Thomas W O'brien. 2004. "Mitochondrial Ribosomal Proteins: Candidate Genes for Mitochondrial Disease." *Genetics in Medicine* 6 (2). The American College of Medical Genetics: 73–80. doi:10.1097/01.GIM.0000117333.21213.17.

Thapa, Mamata, Ananth Bommakanti, Md Shamsuzzaman, Brian Gregory, Leigh Samsel, Janice M Zengel, and Lasse Lindahl. 2013. "Repressed Synthesis of Ribosomal Proteins Generates Protein-Specific Cell Cycle and Morphological Phenotypes." *Molecular Biology of the Cell* 24 (23): 3620–33. doi:10.1091/mbc.E13-02-0097.

Thompson, Winston E, João Ramalho-Santos, and Peter Sutovsky. 2003. "Ubiquitination of Prohibitin in Mammalian Sperm Mitochondria: Possible Roles in the Regulation of Mitochondrial Inheritance and Sperm Quality Control." *Biology of Reproduction* 69 (1): 254–60. doi:10.1095/biolreprod.102.010975.

Tischfield, Max A, Hagit N Baris, Chen Wu, Guenther Rudolph, Lionel Van Maldergem, Wei He, Wai-Man Chan, et al. 2010. "Human TUBB3 Mutations Perturb Microtubule Dynamics, Kinesin Interactions, and Axon Guidance." *Cell* 140 (1): 74–87. doi:10.1016/j.cell.2009.12.011.

Tsang, William Y, and Bernard D Lemire. 2002. "Stable Heteroplasmy but Differential Inheritance of a Large Mitochondrial DNA Deletion in Nematodes." *Biochemistry and Cell Biology = Biochimie et Biologie Cellulaire* 80 (5): 645–54. http://www.ncbi.nlm.nih.gov/pubmed/12440704.

Tuppen, Helen A L, Emma L Blakely, Douglass M Turnbull, and Robert W Taylor. 2010. "Mitochondrial DNA Mutations and Human Disease." *Biochimica et Biophysica Acta* 1797 (2): 113–28. doi:10.1016/j.bbabio.2009.09.005.

Tusher, V G, R Tibshirani, and G Chu. 2001. "Significance Analysis of Microarrays Applied to the Ionizing Radiation Response." *Proceedings of the National Academy of Sciences of the United States of America* 98 (9): 5116–21. doi:10.1073/pnas.091062498.

Tzoulis, Charalampos, and Laurence A Bindoff. 2012. “Acute Mitochondrial Encephalopathy Reflects Neuronal Energy Failure Irrespective of Which Genome the Genetic Defect Affects.” *Brain : A Journal of Neurology* 135 (Pt 12): 3627–34. doi:10.1093/brain/aws223.

Van Aelst, L., and C. D’Souza-Schorey. 1997. “Rho GTPases and Signaling Networks.” *Genes & Development* 11 (18): 2295–2322. doi:10.1101/gad.11.18.2295.

Vance, Jean E. 2014. “MAM (mitochondria-Associated Membranes) in Mammalian Cells: Lipids and Beyond.” *Biochimica et Biophysica Acta* 1841 (4): 595–609. doi:10.1016/j.bbalip.2013.11.014.

Veuthey, J.-L., D. Guillarme, P.J. Schoenmakers, Sara Forcisi, Franco Moritz, Basem Kanawati, Dimitrios Tziotis, Rainer Lehmann, and Philippe Schmitt-Kopplin. 2013. “Liquid Chromatography–mass Spectrometry in Metabolomics Research: Mass Analyzers in Ultra High Pressure Liquid Chromatography Coupling.” *Journal of Chromatography A* 1292: 51–65. http://www.sciencedirect.com/science/article/pii/S0021967313005955.

Viscomi, Carlo, Emanuela Bottani, and Massimo Zeviani. 2015. “Emerging Concepts in the Therapy of Mitochondrial Disease.” *Biochimica et Biophysica Acta* 1847 (6-7): 544–57. doi:10.1016/j.bbabio.2015.03.001.

Vogel, Rutger O, Jan A M Smeitink, and Leo G J Nijtmans. 2007. “Human Mitochondrial Complex I Assembly: A Dynamic and Versatile Process.” *Biochimica et Biophysica Acta* 1767 (10): 1215–27. doi:10.1016/j.bbabio.2007.07.008.

von Kleist-Retzow, Jürgen-Christoph, Hue-Tran Hornig-Do, Matthias Schauen, Sabrina Eckertz, Tuan Anh Duong Dinh, Frank Stassen, Nadine Lottmann, et al. 2007. “Impaired Mitochondrial Ca2+ Homeostasis in Respiratory Chain-Deficient Cells but Efficient Compensation of Energetic Disadvantage by Enhanced Anaerobic Glycolysis due to Low ATP Steady State Levels.” *Experimental Cell Research* 313 (14): 3076–89. doi:10.1016/j.yexcr.2007.04.015.

Wallace, D C, G Singh, M T Lott, J A Hodge, T G Schurr, A M Lezza, L J Elsas, and E K Nikoskelainen. 1988. “Mitochondrial DNA Mutation Associated with Leber’s Hereditary Optic Neuropathy.” *Science (New York, N.Y.)* 242 (4884): 1427–30. http://www.ncbi.nlm.nih.gov/pubmed/3201231.

Wallace, Douglas C. 2005. “The Mitochondrial Genome in Human Adaptive Radiation and Disease: On the Road to Therapeutics and Performance Enhancement.” *Gene* 354 (July): 169–80. doi:10.1016/j.gene.2005.05.001.

———. 2010. “Mitochondrial DNA Mutations in Disease and Aging.” *Environmental and Molecular Mutagenesis* 51 (5): 440–50. doi:10.1002/em.20586.

Walther, Tobias C, and Matthias Mann. 2010. “Mass Spectrometry-Based Proteomics in Cell Biology.” *The Journal of Cell Biology* 190 (4): 491–500. doi:10.1083/jcb.201004052.

Wang, Yang, Shuying Liu, Yuanjia Hu, Peng Li, and Jian-Bo Wan. 2015. “Current State of the Art of Mass Spectrometry-Based Metabolomics Studies – a Review Focusing on Wide Coverage, High Throughput and Easy Identification.” *RSC Adv.* 5 (96). Royal Society of Chemistry: 78728–37. doi:10.1039/C5RA14058G.

Wells, J Mitchell, and Scott A McLuckey. 2005. “Collision-Induced Dissociation (CID) of Peptides and Proteins.” *Methods in Enzymology* 402 (January): 148–85. doi:10.1016/S0076-6879(05)02005-7.

Wiesner, Rudolf J., J.Caspar Rüegg, and Ingo Morano. 1992. “Counting Target Molecules by Exponential Polymerase Chain Reaction: Copy Number of Mitochondrial DNA in Rat Tissues.” *Biochemical and Biophysical Research Communications* 183 (2): 553–59. doi:10.1016/0006-291X(92)90517-O.

Wishart, David S, Timothy Jewison, An Chi Guo, Michael Wilson, Craig Knox, Yifeng Liu, Yannick Djoumbou, et al. 2013. “HMDB 3.0--The Human Metabolome Database in 2013.” *Nucleic Acids Research* 41 (Database issue): D801–7. doi:10.1093/nar/gks1065.

Wiśniewski, Jacek R, Alexandre Zougman, and Matthias Mann. 2009. “Combination of FASP and StageTip-Based Fractionation Allows in-Depth Analysis of the

Hippocampal Membrane Proteome." *Journal of Proteome Research* 8 (12). American Chemical Society: 5674–78. doi:10.1021/pr900748n.

Wittig, Ilka, Bjoern Meyer, Heinrich Heide, Mirco Steger, Lea Bleier, Zibiernisha Wumaier, Michael Karas, and Hermann Schägger. 2010. "Assembly and Oligomerization of Human ATP Synthase Lacking Mitochondrial Subunits a and A6L." *Biochimica et Biophysica Acta* 1797 (6-7): 1004–11. doi:10.1016/j.bbabio.2010.02.021.

Wojtovich, Andrew P, C Owen Smith, Cole M Haynes, Keith W Nehrke, and Paul S Brookes. 2013. "Physiological Consequences of Complex II Inhibition for Aging, Disease, and the mKATP Channel." *Biochimica et Biophysica Acta* 1827 (5): 598–611. doi:10.1016/j.bbabio.2012.12.007.

Wolff, M. M., and W. E. Stephens. 1953. "A Pulsed Mass Spectrometer with Time Dispersion." *Review of Scientific Instruments* 24 (8). AIP Publishing: 616. doi:10.1063/1.1770801.

Worthylake, R A, and K Burridge. 2001. "Leukocyte Transendothelial Migration: Orchestrating the Underlying Molecular Machinery." *Current Opinion in Cell Biology* 13 (5): 569–77. http://www.ncbi.nlm.nih.gov/pubmed/11544025.

Wu, Huifeng, Andrew D Southam, Adam Hines, and Mark R Viant. 2008. "High-Throughput Tissue Extraction Protocol for NMR- and MS-Based Metabolomics." *Analytical Biochemistry* 372 (2): 204–12. doi:10.1016/j.ab.2007.10.002.

Xue, Shifeng, and Maria Barna. 2012. "Specialized Ribosomes: A New Frontier in Gene Regulation and Organismal Biology." *Nature Reviews. Molecular Cell Biology* 13 (6). Nature Publishing Group, a division of Macmillan Publishers Limited. All Rights Reserved.: 355–69. doi:10.1038/nrm3359.

Yamada, T, and J Carlsson. 1975. "Regulation of Lactate Dehydrogenase and Change of Fermentation Products in Streptococci." *J. Bacteriol.* 124 (1): 55–61. http://jb.asm.org/content/124/1/55.short.

Yan, Zhixiang, and Ru Yan. 2015. "Increase the Accessibility and Scale of Targeted Metabolomics: Construction of a Human Urinary Metabolome-Wide Multiple

Reaction Monitoring Library Using Directly-Coupled Reversed-Phase and Hydrophilic Interaction Chromatography." *Analytica Chimica Acta* 894 (September): 65–75. doi:10.1016/j.aca.2015.08.056.

Yasuda, Ryohei, Hiroyuki Noji, Kazuhiko Kinosita, and Masasuke Yoshida. 1998. "F1-ATPase Is a Highly Efficient Molecular Motor That Rotates with Discrete 120° Steps." *Cell* 93 (7): 1117–24. doi:10.1016/S0092-8674(00)81456-7.

Yuan, Juping, Frank Eckerdt, Jürgen Bereiter-Hahn, Elisabeth Kurunci-Csacsko, Manfred Kaufmann, and Klaus Strebhardt. 2002. "Cooperative Phosphorylation Including the Activity of Polo-like Kinase 1 Regulates the Subcellular Localization of Cyclin B1." *Oncogene* 21 (54): 8282–92. doi:10.1038/sj.onc.1206011.

Zeviani, Massimo, and Stefano Di Donato. 2004. "Mitochondrial Disorders." *Brain : A Journal of Neurology* 127 (Pt 10): 2153–72. doi:10.1093/brain/awh259.

Zhang, Guo-Fang, Sushabhan Sadhukhan, Gregory P. Tochtrop, and Henri Brunengraber. 2011. "Metabolomics, Pathway Regulation, and Pathway Discovery." *Journal of Biological Chemistry* 286 (27): 23631–35. doi:10.1074/jbc.R110.171405.

Zhang, Yan Victoria, and Alan Rockwood. 2015. "Impact of Automation on Mass Spectrometry." *Clinica Chimica Acta; International Journal of Clinical Chemistry*, September. doi:10.1016/j.cca.2015.08.027.

Zheng, J, and V D Ramirez. 2000. "Inhibition of Mitochondrial Proton F0F1-ATPase/ATP Synthase by Polyphenolic Phytochemicals." *British Journal of Pharmacology* 130 (5): 1115–23. doi:10.1038/sj.bjp.0703397.

Zubarev, Roman A., Neil L. Kelleher, and Fred W. McLafferty. 1998. "Electron Capture Dissociation of Multiply Charged Protein Cations. A Nonergodic Process." *Journal of the American Chemical Society* 120 (13). American Chemical Society: 3265–66. doi:10.1021/ja973478k.

List of Figures

List of Tables

Appendix

Table S1: List of all metabolites with masses, MS conditions and MRM ion ratios.

Table S2: List of protein groups and LFQ intensities identified in every replicate of rotenone treated and control cells.

Table S3: Phosphorylated (STY) sites with n=1-4 values of ρ^0 versus 143B.TK$^-$ cells and cut-off settings according to the methods part.

Table S4: DiGly (K) sites with n=1-4 values of ρ^0 versus 143B.TK$^-$ cells and cut-off settings according to the methods part.

Table S5: List of protein groups with 4 valid values of ρ^0 versus 143B.TK$^-$ cells.

Table S6: List of identified metabolites with at least 2 transitions and 3 measured values per condition of rotenone treated versus control cells.

Table S7: List of identified metabolites in ρ^0 versus parental cells.

List of Publications

Aretz, Ina, and David Meierhofer. 2016. “Advantages and Pitfalls of Mass Spectrometry Based Metabolome Profiling in Systems Biology.” *International Journal of Molecular Sciences* 17 (5). Multidisciplinary Digital Publishing Institute: 632. doi:10.3390/ijms17050632.

Aretz, Ina, Christopher Hardt, Ilka Wittig, and David Meierhofer. 2016. “An Impaired Respiratory Electron Chain Triggers down-Regulation of the Energy Metabolism and de-Ubiquitination of Solute Carrier Amino Acid Transporters.” *Molecular & Cellular Proteomics* 15 (5): mcp.M115.053181. doi:10.1074/mcp.M115.053181.

Gielisch, Ina, and David Meierhofer. 2015. “Metabolome and Proteome Profiling of Complex I Deficiency Induced by Rotenone.” *Journal of Proteome Research* 14 (1): 224–35. doi:10.1021/pr500894v.